Republic of Iraq
Ministry of Higher Education and Scientific Research
University of Babylon
Collage of Materials Engineering
Department of Metallurgical Engineering

Ceramic -to - Metal Joining for Bio-Medical Applications

A Dissertation
Submitted to the Council of the College of Materials Engineering / University of Babylon in Partial Fulfillment of the Requirements for the Degree of Doctor of Philosophy in Materials Engineering / Metallurgical Engineering

Sarah Muhi Jawad

(B.Sc.n Materials Engineering 2012)
(M.Sc Metallurgical Engineering 2015)

Supervised by
Prof. Dr. Ahmed O. Al- Roubaiy (Ph.D.)
Prof. Dr. Saad H Al-shafaie (Ph.D.)

2022 A.D **1443 A.H**

وزاره التعليم العالي والبحث العلمي
جامعة بابل
كلية هندسة المواد
قسم هندسة المعادن

وصلات سيراميكية ـ معدنية للتطبيقات الحياتية

أطروحة

مقدمة إلى قسم هندسة المعادن في كلية هندسة المواد / جامعة بابل
كجزء من متطلبات نيل درجة الدكتوراه في علوم في هندسة معادن

من قبل
ساره محي جواد
(بكالوريوس هندسة مواد ٢٠١٢)
(ماجستير هندسة مواد ٢٠١٥)

بإشراف
أ . د. احمد عود ة جاسم الربيعي
أ . د. سعد حميد الشافعي

١٤٤٣ ه ٢٠٢٢ م

Supervisor's certificate

We certify this dissertation entitled,

" ***Ceramic -to - Metal Joining for Bio-Medical Applications "***

had been carried out under our supervision at the University of Babylon / College of Materials Engineering / Department of Metallurgical Engineering in partial fulfillment of the requirements for the degree of Doctor of Philosophy in Materials
Engineering / Metallurgical Engineering.

Signature:
Name: Professor
Ahmed O. Al- Roubaiy
Date: / / 2022

Signature:
Name: Professor
Saad H Al-shafaie
Date: / / 2022

DEDICATION

To my father & mother
For being my first teachers
To my lovely husband
To my family for supporting me all the way
To my friends with respect.

Sarah Muhi Jawad
2022

Acknowledgments

First of all, I would like to express my gratitude to ALLAH for show me the path.
I would like to thank my supervisors, Dr. Ahmed O. Al-Roubaiy and Dr. Saad H Al-shafaie for their unwavering support and guidance in this research.
I would like also to extend my gratitude to the Dean of the Materials Engineering College, Head Metallurgy Engineering Department and all the staff for their great efforts
I wish to express my deepest thanks to the staff and laboratories of the Metallurgical Department of the Materials Engineering College/University of Babylon.
I greatly thankful to all our well-wishers, classmates, friends and family for their inspiration and help.

Sarah Muhi Jawad
2022

بسم الله الرحمن الرحيم

وَفَوْقَ كُلِّ ذِي عِلْمٍ عَلِيمٌ

صدق الله العلي العظيم

(سورة يوسف/الآية ٧٦)

Abstract

Metal to ceramic joints has great benefits especially in engineering and biomedical applications. Ceramic exhibited mechanical and physical properties different from metal especially in thermal expansion coefficient (CTE). This research based on manufacturing Ag-Cu-Ti and Ag-Cu-Ti-Co eutectic alloys by using melt spinning technology and use them in joining process of ZrO_2 with Ti6Al4V by brazing. Firstly, The Ag-Cu-Ti alloy was prepared by melt spinning technology with high rotating brass disk to get high cooling rate which can cause amorphous structure in the alloy. In order to increase the cooling rate of the prepared alloy some dry ice added on the disk. The minimum cooling degree of the disk was -3 ℃. The brazing processes were done by different temperatures (850,875, 900 and 925 ℃) for 20 minutes. In order to study the effect of brazing temperatures on microstructures and also on mechanical properties of joint, some mechanical and microstructure test were done on the prepared samples like single shear test, microhardness test and biocompatibility tests.

The amorphous structure of the prepared alloys increased with increasing the cooling rate due to the high strain in the crystal lattice of the alloy. Present of titanium in the filler alloy caused discoloration of ZrO_2 because of its reaction with oxygen. The discoloration effect increases as temperature or brazing time increases. The SEM images of the prepared joints showed 3 different regions along the specimen (diffusion zone, brazing zone and interlayer between ZrO_2 and filler alloy). Each region characterized by phases differs from other regions which gave it a special property. The shear strength of the prepared joints increased as the brazing temperature increased until 875 ℃ then gradually decrease. The maximum shear strength of Ti6Al4V/ Filler 1/ ZrO_2 was 20.4 Mpa and its was 22.1 Mpa for Ti6Al4V/ Filler 2/ ZrO_2 joints. The microhardness of the prepared joints in the joining region

increased as the brazing temperature increased. The maximum microhardness of Ti6Al4V/ Filler 1/ ZrO_2 in the joining region was 220 Hv for samples brazed at 925 °C while its was 245 Hv for Ti6Al4V/ Filler 2/ ZrO_2 samples prepared at same conditions.

Histopathological Test Results showed that normal muscle fibers underneath the test specimen after the implantation process. The blood rest for urea, Creatinine, Albumin, Alanine Aminotransferase enzyme, Aspartate Aminotransferase enzyme and Alkaline Phosphatase enzymes confirm they were in normal level. The biocompatibility tests (histopathological and blood tests) in the vivo (rabbit body) showed that the both types of prepared specimens are biocompatible.

الخلاصة

الوصلات السيراميكية المعدنية أصبحت ذات اهميه كبيره خاصه في المجالات الهندسية والتطبيقات الحياتية. تمتلك المواد السيراميكية خواص فيزيائية وميكانيكية تختلف بشكل كبير عن المواد المعدنية خاصة في معامل التمدد الحراري (CTE) بينما يمتلك التيتانيوم و سبائكه خواص معينة جعلته مؤهلا للاستخدام في التطبيقات الحياتية داخل الجسم ومن اهم هذه السبائك هي سبيكة Ti6Al4V . المواد السيراميكية وبشكل خاص الزركونيا تظهر خواص متانه ومقاومه كسر عالية وكما يمكن اعتبارها موصلات ايونية حيده في درجات الحرارة العالية.

نظريا فان أجزاء من التراكيب المعقدة المكونة من السيراميك والمعدن يمكن ان تصنع باستخدام ثلاثة تقنيات: أولا الربط الميكانيكي، ثم الربط الغير المباشر عن طريق ال عمليتي brazing و soldering بالإضافة الى اللحام بالطريقة مباشره الربط بالحالة الصلبة والسائلة . على سبيل المقارنة بين الطريقة المباشرة وغير المباشرة فانه الربط بالالتصاق فان الاسطح يجب ان تكون قريبه من بعضها البعض حتى تكون ربط قوي يتغلب على الاجهادات المتبقية بعد عملية اللحام خاصة عند لحام المواد ذات الاختلاف الكبير في معامل التمدد الحراري.

ان من اهم التطبيقات الحياتية للوصلات السيراميكية المعدنية زوارع الركبة، الزوارع ثنائية القناة والتي تشمل منظم ضربات القلب ومنظم رجفان القلب ومنظم الحركة العصبي والعضلي متعدد القنوات وزوارع الاذن.

خلال هذا البحث تم تحضير سبيكة فضه -نحاس – تيتانيوم بالإضافة الى سبيكة أخرى تتضمن إضافة عنصر الكوبلت للمجموعة سابقة الذكر بواسطة تقنية المنصهر الدوار ولغرض معرفة إمكانية تحضير سبائك ذات تراكيب عشوائية خلال هذه الطريقة تم إضافة كمية من الثلج على القرص الدوار للجهاز حيث تم الحصول على سبيكة ذات تركيب عشوائي اكثر من السبيكة الاعتيادية ثم تم استخدام السبيكة الناتجة كماده مساعد للربط واستخدامها في عملية لحام الزركونيا على سبيكة التيتانيوم. جرت عملية الربط في درجات مختلفة هي (850,875, 900 and 925 °C)

وخلال مده 20 دقيقه. ولغرض دراسة تأثير دراجات الحرارة على كل من خواص البنية المجهرية والخواص الميكانيكية جرى فحص الوصلات الناتجة بواسطة اجهزه خاصة بالإضافة الى فحص مقاومة الكسر للوصلات وكذلك فحص مقدار التوافقية الحياتية للوصلات عن طريق زراعتها في جسم الارنب لدراسة سلوكها التأكل ومدى تأثيرها على الأفعال الحياتية للجسم.

وقد اظهرت النتائج المتحصلة ان مقدار العشوائية في السبيكة يزداد مع زيادة معدل التبريد. ان وجود عنصر التيتانيوم في معدن اللحام سوف يؤدي الى تغيير لون الزركونيا نتيجة لتفاعله معها وكلما زادت حراره اللحام او الوقت الخاصة بالعملية كلما زاد هذا التاثير .

اظهرت نتائج فحص البنية المجهرية ثلاثة مناطق مميزه في الوصلات الناتجة وهي منطقة الانتشار ومنطقه اللحام ومنطقه السطح الفاصل بين الزركونيا والمعدن المالئ ولكل منطقة اكوار تختلف عن المنطقة الأخرى وبالتوالي خواص مختلفة بين المناطق.

نتائج فحص مقاومة القص للوصلات الناتجة بينت ان مقاومة القص ترتفع مع زيادة درجه الحرارة حتى حراره 875 ثم تبدء بالانخفاض حيث كانت اعلى مقاومه هي 20.4 ميغا باسكال للوصلات الملحومة بالمعدن المالئ من دون كوبلت ولكن كانت اعلى قيمة لهذه المقاومة في حالة المعدن المالئ مع إضافة الكوبلت حوالي 22.1 ميغا باسكال حيث ان وجود الكوبلت يساعد على زياده انتشارية المعدن المالئ وبالتالي تراكيب اكثر تجانسا واعلى مقاومة.

وكذلك الحال بالنسبة لفحص الصلادة حيث ان صلادة الوصلات الناتجة ازدادت مع زيادة الحرارة لكلا النوعين من الوصلات المحضرة.

بينت نتائج فحص الزراعة للوصلات في جسم الارنب ان كلا النوعين ذات توافقية حياتية عالية ونتائج تفاعلها مع الجسم لا تسبب حساسية او سرطان.

Abstract

metal to ceramic joints has great benefits especially in engineering and biomedical applications. Ceramic exhibited mechanical and physical properties different from metal especially in thermal expansion coefficient (CTE). Titanium and its alloys exhibited suitable properties made it fit to use in biomedical applications. pure titanium and Ti6Al4V are the most used in implants. Zirconia exhibits evaluated strength and fracture toughness and it is also a good in biomedical application at elevated temperatures.

The parts of hybrid metal to ceramic that used for medicinal applications may be joined through three methods. The mechanical joining by essential part feature. directly joining through resources of the solid or the liquid phase bonding. indirectly bonding through mean of the brazing and the soldering with filler metal. For understanding a consistent direct and the indirect joint; a close contact among the parts is required. The interface between parts essential be talented to conciliated residual stresses because of CTEs difference and produced by temperatures differences through service.

The biomedical applications of ceramic / metal joints include: knee prosthesis and feedthroughs. Ceramic/metal feedthroughs which can be used as implantable devices involve implantable pacemaker, cardioverter defibrillator, multi-channel neuromuscular stimulator, and cochlear implants.

This research based on manufacturing Ag-Cu-Ti and Ag-Cu-Ti-Co eutectic alloys by using melt spinning technology and use it in joining process of ZrO_2 with Ti6Al4V by brazing. Firstly, Ag-Cu-Ti alloy prepared by melt spinning technology with high rotating brass disk to get high cooling rate which can cause amorphous structure in the alloy. In order to increase the cooling rate of the prepared alloy some

dry ice added on the disk. The minimum cooling degree of the disk was -3 ℃. The prepared alloys used in joining process of ZrO_2 with Ti6Al4V by brazing. The brazing processes done by different temperatures (850, 875, 900 and 925 ℃) for 20 minutes. In order to study the effect of brazing temperatures on microstructures and also on mechanical properties of joint, some mechanical and microstructure test done on the prepared specimens like single shear test, microhardness test, biocompatibility tests.

The amorphous structure of the prepared alloys increased with increasing the cooling rate due to high strain in the crystal lattice of the alloy. present of Titanium in the filler alloy caused discoloration of ZrO_2 due because of react it with Oxygen. The discoloration effect increases as temperature or brazing time increased. The SEM images to the prepared joints showed 3 different regions along the specimen (diffusion zone, brazing zone and interlayer between ZrO_2 and filler alloy). Each region characterized by phases different from other regions which gave it a special property. The shear strength of the prepared joints increased as the brazing temperature increase until 875 ℃ then gradually decrease. The maximum shear strength of Ti6Al4V/ Filler 1/ ZrO_2 was 20.4 Mpa and its was 22.1 Mpa for Ti6Al4V/ Filler 2/ ZrO_2 joints. The microhardness of the prepared joints in the joining region increased as the brazing temperature increased. The maximum microhardness of Ti6Al4V/ Filler 1/ ZrO_2 in the joining region was 220 Hv for specimens brazed at 925 ℃ while its was 245 Hv for Ti6Al4V/ Filler 2/ ZrO_2 specimens prepared at same conditions.

Histopathological Test Results showed that normal muscle fibers underneath the test specimen after the implantation process . The blood rest for urea ,Creatinine , Albumin, ALT Alanine Aminotransferase enzyme , AST Aspartate Aminotransferase enzyme and ALP Alkaline Phosphatase enzymes confirm they

were in normal level. The biocompatibility tests (histopathological and blood tests) in the vivo (rabbit body) showed that the both types of prepared specimens are biocompatible.

List of contents

List of contents

List of Figures

List of Figures

List of Figures

List of Figures

List of abbreviation and symbols

abbreviation	Definition
AWS	American Welding Society
CTE	coefficient of thermal expansion
CVD	Chemical vapor deposition
PVD	Physical l vapor deposition
IMCs	intermetallic compounds
HAZ	Heat effected zone
YTZP	Yttria tetragonal zirconia polycrystalline
MgPSZ	magnesia partially stabilized zirconia
PSZ	partially stabilized zirconia
FES	functional electrical stimulation
ALT	(Alanine Aminotransferase enzyme)
AST	Aspartate Aminotransferase enzyme
ALP	Alkaline Phosphatase enzyme

List of Tables

List of Tables

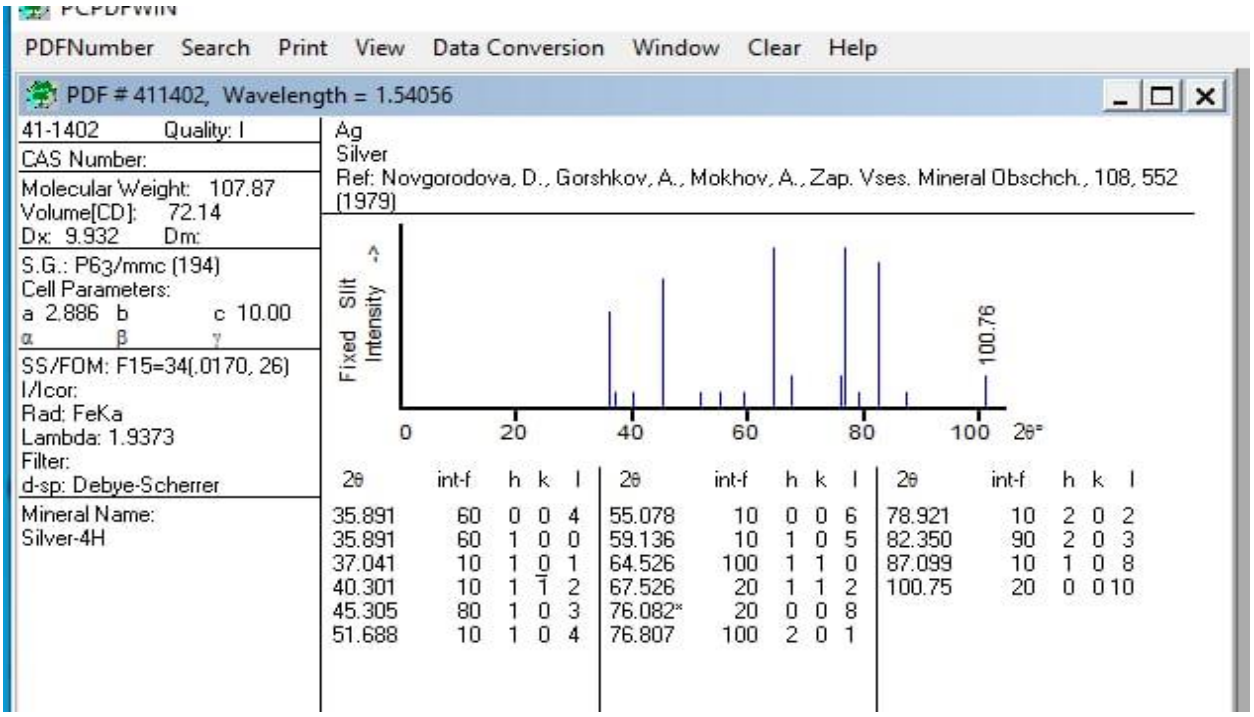

XRD – charts for silver element

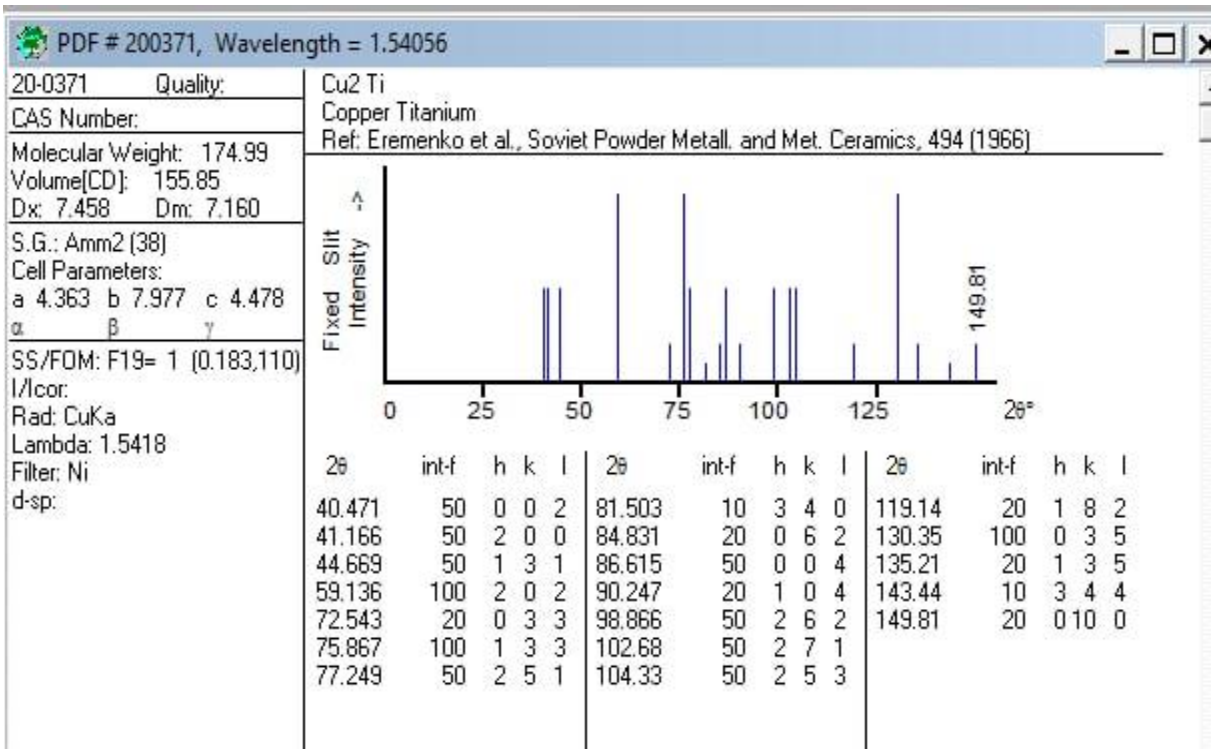

XRD charts for Cu_2 Ti phase

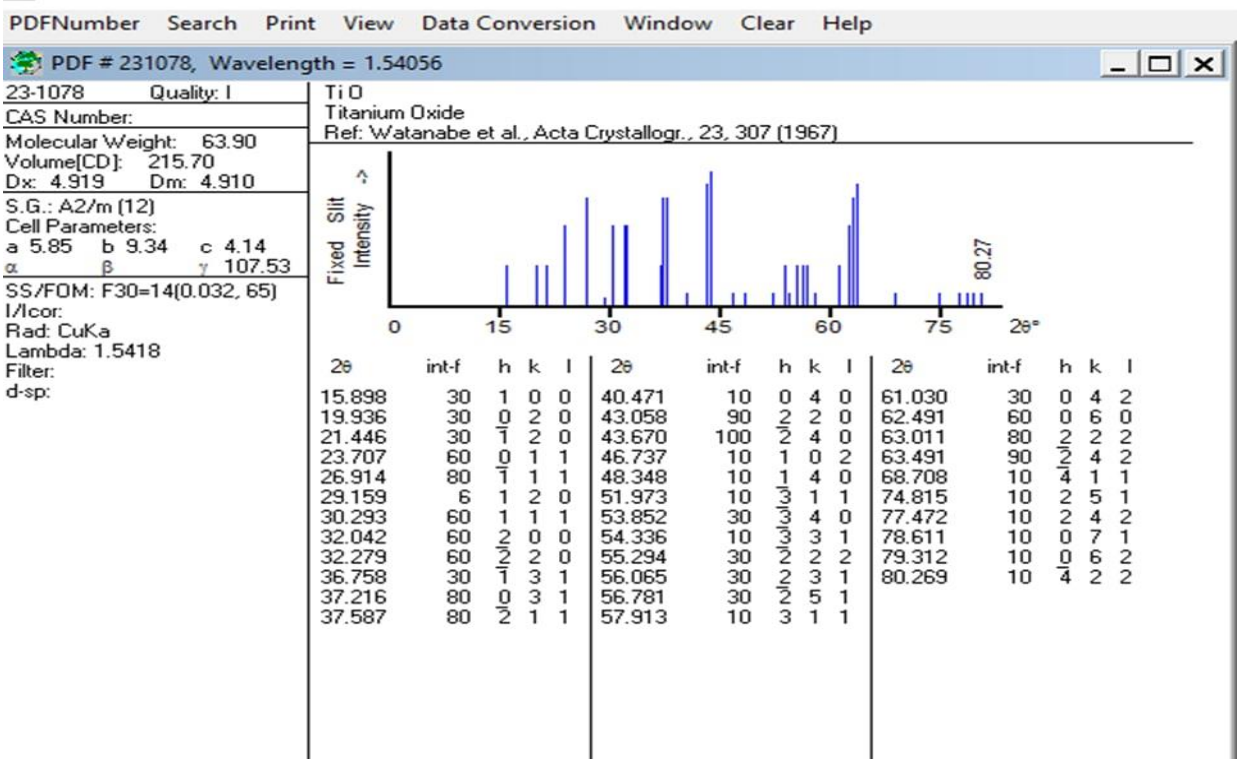

XRD charts for TiO phase

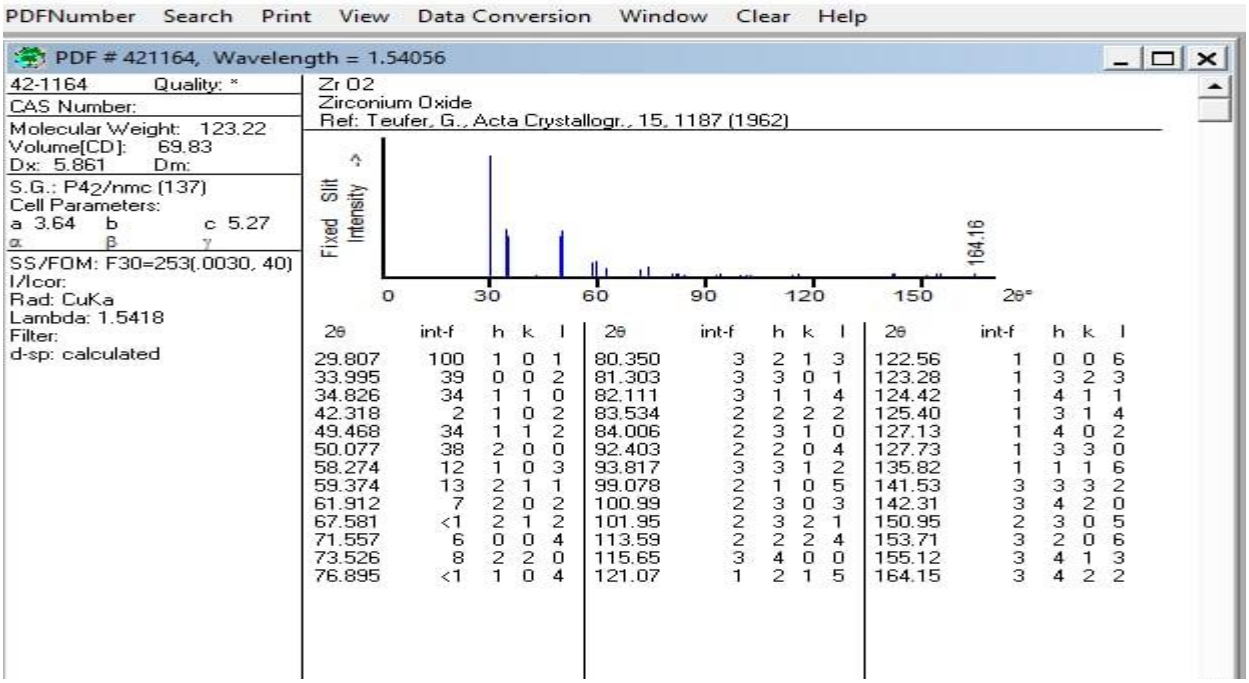

XRD charts for ZrO_2 phase

Appendix

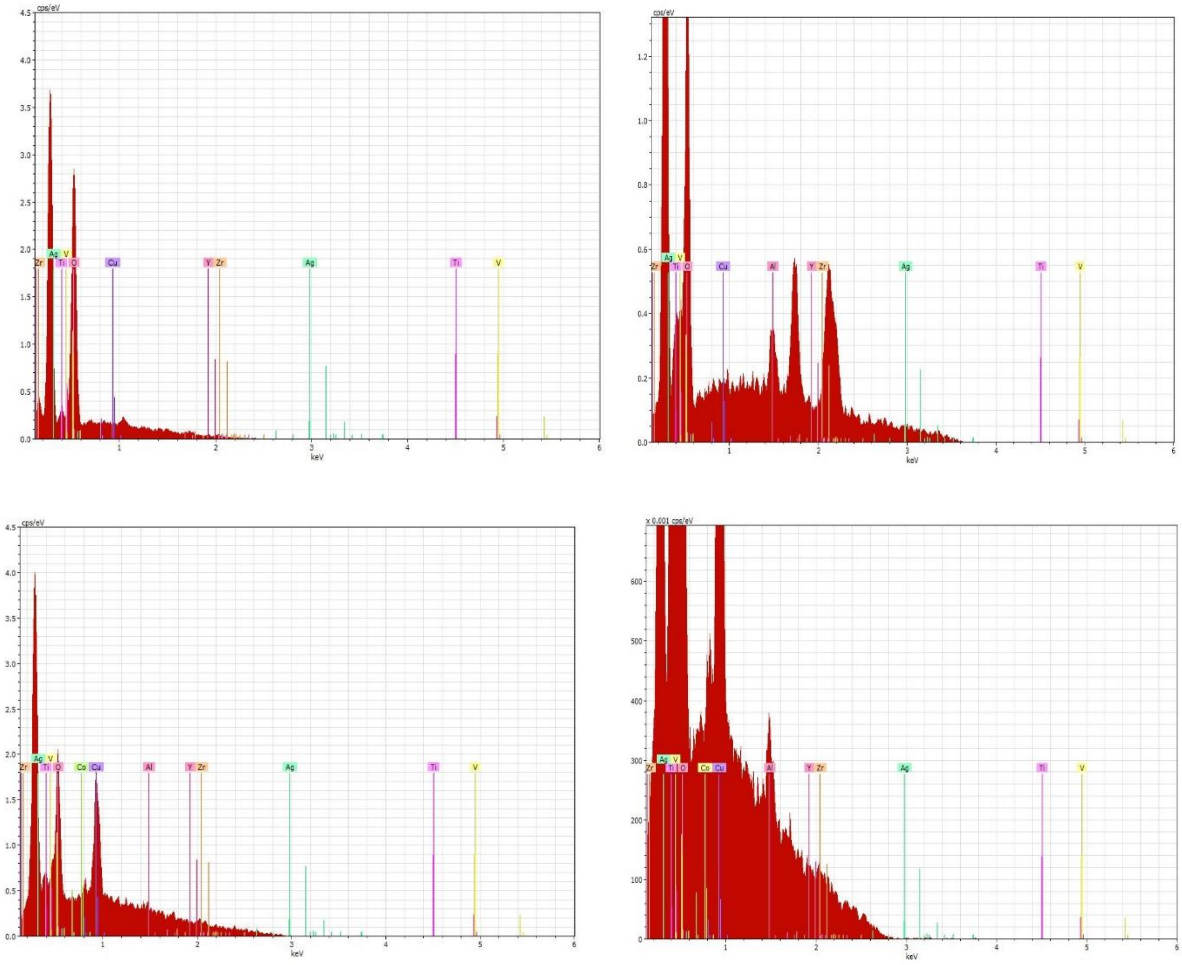

EDS curves for tested joints

Chapter One (Introduction)

1.1 General View

The American Welding Society (AWS) defines brazing process such as a collection of joining processes which produce the combination of material through raise them temperature to temperatures of the brazing process with presence of metal act as active filler metal which has liquidus temperatures higher than 450ºC and lower the solidus temperature for base materials. The brazing filler metal spread between the faying surfaces which are fitted closely by capillary action and joining them together. Brazing temperature can be defined as the temperature in which a material is heated to allow the brazing filler material to spread and wet the base metals and procedure a brazed joint [1].

Actually, the physically and chemically processes through brazing process might be fairly similar to both kinds of bonding process. The important difference is in choice of materials. The difference in the materials will cause some difference in phenomena through the heating bonding cooling arrangement of the processes[2].

Stringent demandants are made of materials properties for both traditional and for the progressive applications. In a case of the single material can't meet as demands normally . Metals, have ductility with high thermals and electrical conductivity, every so often can't resist high temperature or corrosion environments, and expand with rising temperature. Otherwise, ceramic, good brittle insulators, hard, and wear resistant and quite low thermally expansion .The composite component could be made by joining ceramic and metal that have the wanted properties of each material to encounter the increasing requirements. The technology needed bonding ceramic and metal which are very dissimilar materials, efficiently ,

dependably, and economically is case of high demands. Numerous joining technologies recognized effectively[3][4].

Even effective joint formation doesn't pledge mechanical reliability of the joint. The characteristic differences in physical properties among ceramics and metals make it difficult to discovery effective processes to join which keeps in detail and complete strength and flexibility. Two important factors limited the success of the joint, coefficient of thermal expansion (CTE) mismatch and natural of interface bond. The thermally residual stresses formed through joint in cooling step due to mismatch of CTE and difference in mechanical properties between ceramics and metals. This may cause a huge effect on the strength of the joint[5]

Metal-ceramic joining become an important industrial step. The joining processes developments permit using of ceramics as a combination with metals by using many devices like electronic devices. New joining devices and new approaches on the traditional methods are developed to improve the joints characteristics through improve reliability and interfaces capable of with-standing high temperature resistant with reduce the residual stresses[6]

The achievement of biomaterials through human body depends on many factors like material properties like design, and biocompatibility of the used material. Extra factors consist of technique that used by surgeons, the healthy and conditions of patient and also the patient activities. The biomedical applications of ceramics to metals joints include: - knee prosthesis and feedthrough [7]. Applications of ceramics to metals feedthrough for implantable medical devices involved implantable pacemakers , cardioverter defibrillators , implantable multichannel neuromuscular stimulators, and cochlear implant[8, 9] Figure (1-1) showed the main ceramic – metal joints as biomedical devices.

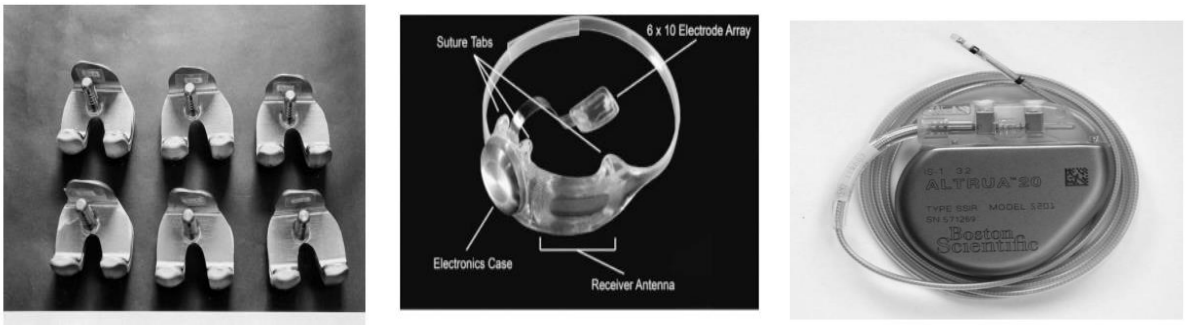

a b c

Figure (1-1) A- Semi-finished metal–ceramic knee prostheses before final grinding and polishing[7], B - Argus II internal design, showing the array of electrodes and the electronics casing[10],C- The lead and header of a single channel chamber pacemaker comprise a significant portion of the system volume. Leadless BIONs obviate this requirement[11].

Biocompatibility includes the degree of accept to the artificial implants through the surrounding tissue and through whole body. Biocompatible material doesn't annoy the surrounding structure, doesn't aggravate an irregular response, doesn't inflame sensitive or any immunologic reactions, and doesn't result of cancer. Other characteristic that might be important in the function of the implantable device manufactured by biomaterial involve:

(1) Corrosion and mechanical properties of the material like its strength, its stiffness and the fatigue resistance.

(2) The optical property of the used material if it will used as implants in the eyes, skin or teeth.

(3) the material density, the ability to manufacture, and the engineering design [12].

Zirconia shows high strength and good fracture strength, especially in temperatures under 300°C and it's as well a expectable ionic conductor at high temperatures. therefore, Zirconia could be created in application extending from

wires deep drawing dies, cutting instruments and machining tools, ending with the oxygen sensors and fuel cell**.** Zirconia shows 3 well defined polymorph: - monoclinic one, tetragonal one, and cubic one. As most ceramics like zirconia usually difficult and expensive to be manufacture into big and or multipart shaping component. Hereafter, joining is documented like a main permitting technology to the future commercial used of all kind's ceramics, as well as zirconia. The procedures which used to joining the ceramics are well recognized, the most popular method consist of mechanically attachment, adhesives process and brazing[13, 14].

Subsequent to the emergence of titanium like a wonder metal in the 1950s. The titanium manufacturing has established a wide range of alloy with different compositions[14]. Titanium as pure element or as alloys have a great attractive metallic material for biomedical applications. Ti6Al4V become the chief biomedical titanium alloys for using as a long periods implant. Biomedical titanium alloys which have high biocompatibility have been development[15].

1.2 The Aim of the Search

The aims of the search are preparing of Ag-Cu-Ti and Ag-Cu-Ti-Co alloys by using melt spinning technology and study the ability of this technology to prepare amorphous alloys by increase the cooling rate. used the prepared alloys as a filler metal in joining process of dissimilar materials (ZrO2 and Ti6Al4V) instead of used the ready filler. Additionally, minimize the cost of that joint (by using Ag-Cu alloy instead of pure gold). Then study ability of using these joints as implants by study the biocompatibility in rabbit body. Then, study the effect of Cobalt addition to the filler alloy on the mechanical properties of the joints.

(Theoretical Background and Literature Survey)

Ceramic – Metal Joining Process and Joining Evaluation

2.1 Introduction

In recent years, great efforts have been focused on joining ceramics to metals to establish processes for a wide range of industrial uses. Several important problems, however, still remain unsolved. Among them,how to obtain atomic bonds at ceramic/metal interfaces and how to compensate for residual stress due to thermal expansion mismatch between two constituents are two of the most serious ones[16].

2.2 Joining Techniques

Uniform ceramics, composites and metals, which can't be Components completed in one part should be joined. Through using joining technologies material hybrids are as well possible. Ceramic to metal joining's increase the application spectrum extremely. Through joining of simple numerals parts complex shapes for specific applications could be comprehended [3] .Ceramics and metals could be joined by mechanical, direct and indirect processes [7, 4,17]

2.2.1 Mechanical Joining

Mechanical joining among metals and ceramics could be achieved by several methods, similar interlocking, press fitting, clamping, fastening and basic threading. Just in case of fastening, the possible damages because of inherent ceramic brittleness might arise. These damages might derive from bearing and holding loads and must limited by assuming large contact area (bolt heads , nuts and washers). In addition to compliant interlayers (metal liners, sleeves and inserts). Besides, holes for studs, pins and fasteners are difficult to be machined in ceramics, owing to

cutting-tool wear and possible ceramics chipping and cracking; preferably, they should be integrally molded and fired-in; in any case, generous fillets have to be provided. Moreover, since compressive stresses are better tolerated by ceramics than tensile ones, design should avoid complex states-of-stress (e.g. bending and deviated compression) leading to dangerous situations. Finally, large differences between CTEs of metals and ceramics should be accurately considered to reduce the effects of thermal loading due to autoclave sterilization process[7]

2.2.2 Direct Joining

Direct joining - achieved by pressing together very flat mating surfaces to achieve diffusion bonding, as in the joining of sapphire to niobium during the fabrication of high-pressure sodium lamps. Experimental work on fusion welding using electron beam, laser, and imaging arc techniques has also met with some success with high melting point systems[18].

2.2.3 Diffusion Bonding

When a ceramic and a metal are to be directly joined with no intermediate material at sub solidus temperatures, the mating materials typically are prepared to extremely high surface finishes (Often < 1-micron surface finish quality). This will maximize the surface area of contact in an attempt to compensate for the inability of solids to conform to another surface as readily as a liquid under fair wetting action. When the mated materials are caused to join by heating such an assembly for an extended period of time at a temperature below either material's melting point or solidus temperature, this is referred to as diffusion bonding. In order to assist diffusion, an applied pressure normal to the bond surface is often introduced [19][20]

2.2.4 Fusion Welding

Fusion Welding is a direct joining method based on the localized melting of the metallic component. Techniques that employ localized heating, such as electron beam or arc-welding are often not suitable for joining dissimilar materials. The high heat generated creates a localized molten region which fuses the surrounding materials together on cold down. This requires an acceptable fracture toughness and thermal shock resistance which brittle material, such as ceramics and intermetallic do not generally possess [21].

2.2.5 Indirect Joining

Indirect bonding - the most common method of achieving high integrity joints using a wide range of intermediate bonding materials such as organic adhesives, glasses or glass-ceramics, oxide mixtures, including cements and mortars, or metal. Metal intermediates are used as solid-state diffusion bonding agents or as brazes with or without pretreatment of the ceramic surfaces to render them wettable[18].

2.2.5.1 Adhesive Joining

Adhesive bonding is used to join metallic and ceramic materials and is a technique used for medical devices both in plastic and in metals. The surfaces being joined are not melted although they may be heated. When two materials are joined together using adhesive bonding, those two materials are called the adherents, or substrates. The material that forms the bond between them is called the adhesive[7]. In adhesive bonding, materials are joined with the aid of a substance capable of holding those materials together by surface attachment attraction forces. This attachment relies on a combination of varying degrees of microscopic mechanical locking and chemical bonding through primary or (usually more importantly)

secondary atomic or molecular forces. The substance used to cause the attachment is called an adhesive, which is usually, but not always, added to the parts to be joined at the joint mating or faying surfaces. Depending on the nature of the adhesive and the substrate being joined, adhesive bonding usually causes little or no disruption of the microstructure of the parts being joined but may cause varying degrees of chemical alteration or disruption. Because attachment occurs over the surfaces of the joint, loads are spread, and stress concentrations are minimized. The greatest shortcoming of adhesive bonding is susceptibility of the adhesive to environmental degradation[22].

2.2.5.2 Brazing

Designers and engineers have many options to choose from when considering how to join metals to nonmetals for structural, electrical, and packaging applications. These options could include mechanical means of fastening such as screws, bolts, rivets and other fasteners, or an elevated-temperature means such as soldering or brazing. Metal-ceramic brazing is particularly useful for fabricating high-reliability devices such as those used in high-voltage applications or requiring hermetically sealed joints [23].

It is a well-known fact that ceramics are poorly wetted by brazing alloys. This poor wettability of ceramics is due to the ionic and covalent bonding in their lattice due to which the electron movement is restricted. There are two approaches to overcome the poor wetting characteristic of ceramic materials: Metallization of the ceramic or active metal brazing[18, 24].

2.3 Metallization

Ceramic/metal brazing and metallization are intimately related, since metallized ceramics can be brazed to metals without active filler alloys at reduced

costs. The choice of a suitable metallization technique should take into account the base materials involved and microstructural characteristics of the ceramic (such as presence of intergranular glassy phases) as well as availability of equipment and intended purpose of the joint[6].

To promote wetting, inherently different materials should be made similar. The problem is to join two dissimilar un-compatible surfaces, one ceramic, and the other metallic. To make them compatible, two approaches can be adopted: (a) to oxidize the metallic surface; in this way, the ceramic being an oxide as well, an oxide to an oxide can be joined; and (b) to cover the ceramic surface with a metallic layer; in so doing, we can join a metal to a metal. Metallizing can be accomplished through sintered metal powder technique, titanium hydride powder activation or refractory-metal salt process. Other methods for ceramic metallization may consist in metal–glass surface powder sintering, CVD, PVD, sublimation (vacuum metallizing), sputtering, ion plating and plasma spraying [7, 9, 25].

The following are a few of the advantages for using thin-film metallization coatings:

1- They have a proven brazing practice history and are forgiving when used

with standard filler metals.

2- Versatility. A wide range of metal choices exist for the engineer or designer that can be deposited to address special applications or environments.

3- Another important advantage is the speed, which can often be less than a few hours total, that simple geometries can be prepared for brazing.

The primary disadvantages of thin film metallization coatings are as follows:

1-Specialized equipment is required to apply the coatings.

2- Intricate masking may become necessary to prevent the deposition of metal in unwanted locations.

3- Ceramic geometric constraints, which may prohibit the proper positioning of the ceramic member or hinder the application of uniform coating thicknesses, of most thin-film deposition chambers [23]. Silver has maximum metallization in elements, copper has the maximum surface energy to bonding , while Titanium has great active with Zirconia for this reason this alloy used as filler alloy.

2.4 Active Filler Metal Brazing

Another approach, called active brazing, consists in using a filler (brazing agent) containing an active metal which reacts with the ceramic. Although brittle micro-structures containing intermetallic compounds may be created at the interface, limiting its capability to accommodate CTEs mismatch, active brazing can presently be considered one of the most promising techniques for structurally joining metallic and ceramic parts of medical devices [7, 9, 25].

The following points are suggested when one designs a filler metal for joining ceramic to ceramic or ceramic to metal:

• The selected active element should have a high free energy of reaction with the ceramic and a strong segregation on the ceramic/metal interface.

• The lower limit of active-element content in the filler metal should ensure good wetting of the ceramic by the filler metal, while the upper limit should be such that there is no brittle dispersed phase in the filler metal.

• The brazing temperature and time should be sufficient to ensure interface reaction of the filler metal with the ceramic[25].

There are many advantages to using an active filler metal brazing process for certain brazing applications. These include the following:

1- The number of required steps to make metal-ceramic brazes are reduced and greatly simplified;

2- There are a variety of commercially available filler metal compositions for use in a wide range of processing temperatures and service conditions;

3- Specialized metallization equipment and the associated time-consuming metallization processes are eliminated.

There are, however, several disadvantages of using an active brazing process over a conventional metallization and subsequent standard brazing process. The primary disadvantages are as follows:

1- Active brazing processes require more stringent atmospheric control.

2- Not all braze joint geometries are compatible with active brazing processes.

3-Processing equipment capable of adequate atmospheric control can be a limiting factor, placing size constraints on brazed assemblies[23].

Active filler alloys for direct ceramic/metal brazing should depict some essential features in order to improve interfacial microstructure, such as:
1. Melting point or melting range compatible with those of the base materials;
2. Moderated fluidity at the brazing temperature, promoting capillarity and uniform distribution over the joint but preventing infiltration into sintered base materials (both metals and ceramics).

3. Homogeneous composition and stability to minimize constituent separation or segregation upon melting and solidification (brazing cycle);

4. Thermodynamic compatibility with the base metal surfaces promoting wetting; 5. Limited trend to brittle phase formation (usually intermetallic) and 6. Compatibility with the working temperature, mechanical loading, environment, and intended life span for the joint[6].

2.5 Factors Influencing Dissimilar Metals joining

The main important parameters that affect the characteristics of the dissimilar welded joint and lead to its failure happen when any variation occurs in the following factors[26] :

A. Weld Metals

The solidification properties of the dissimilar weld are affected via several factors, e.g., the base metals composition, their relative dilution and mutual solubility, and filler metals (when utilized). The mutual solubility between the dissimilar metals influences the intermetallic compounds (IMCs) microstructural composition, which is responsible for determining the joint characteristics, for instance, the ductility, corrosion and sensitivity of the crack. Therefore, it's significant to evaluate the metals' phase diagram to show if the mutual solubility presents in the welding fusion of these metals [27].

B. Melting Temperature

The temperature of melting is an important parameter that is considered when dissimilar metals are welded, particularly in the fusion welding case. The metal solidification and contraction with a high temperature of melting generates stresses in the metal having a lower point of melting because it's weak and incompletely solidified. The problem of differences in the melting temperature of the base metals can be solved by using the filler metal buttering having an intermediate temperature of melting among the base metals [27, 28].

C. The Thermal Conductivity

The heat balance can be achieved by the preheating process for the base metal having a high thermal conductivity for controlling the base metal heat loss as well as reducing the rate of the cooling of the (HAZ)[27].

D. The Coefficient of Thermal Expansion

The high differences in the coefficient of thermal expansion between the dissimilar metals cause a compressive stress in one metal and a tensile stress in other by the process of cooling. When joints are operated at the elevated temperature at cyclic modes, this becomes critical during the welding, the weld metal having the tensile stress can subject to hot cracking or when the stresses are not relieved in service; it undergoes the cold cracking[27].

E. Dilution

When the filler metal was used to join dissimilar metals, the alloy with the base metal should be able to produce weld metal with continuous, ductile matrix, phase, and it should also be able to accept dilution (alloying) by base metal without producing a crack sensitive microstructure[27].

2.6 The Mechanism of Brazing

Since the brazing process is joining the materials without fusion of the base metal, thus it is necessary to explain the mechanism of joining[29].

1.Adhesion

If two various materials or metals (A and B) are needed to be joined together, the free energy variation calls the operation of the adhesion. This is provided by the expression of Young-Dupree for the liquid contacting the surface of a solid body, as shown in Figure (2-1)[25, 30]

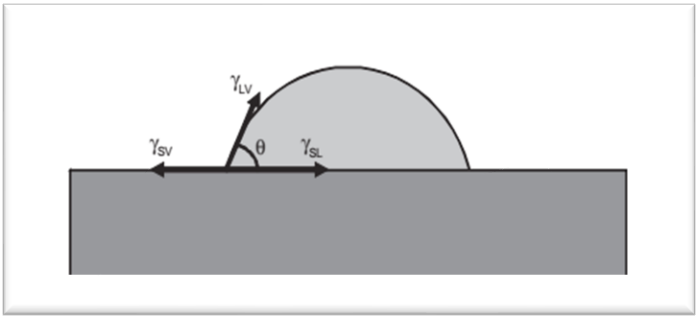

Figure (2-1): Equilibrium shape of a liquid sessile drop formed on a solid surface in the presence of a vapor. γ_{SV}, γ_{LV}, and γ_{SL} are the respective energies along the solid-liquid, solid-vapor, and liquid-vapor interfaces and θ is the contact angle formed by the sessile drop at the position noted in the figure[31].

The work of adhesion can be obtained by equation (2.1) to measure the attraction between different materials[25]

$$W_{adh} = \gamma_S + \gamma_{l/v} + \gamma_{s/l} \quad \text{……..} \quad (2\text{-}1)$$

Where :

$\mathcal{W}_{adh}$: The energy of adhesion for a liquid contacting a solid surface.

γ_s: Free energy of a solid surface (J/m^2).

$\gamma_{s/l}$: Free energy of a solid-liquid interface (J/m^2).

$\gamma_{l/v}$: Free energy of a liquid in balance with the liquid vapor (J/m^2).

2.Wetting

It can be concluded that wetting is the ability of the molten filler metal to adhere to the surface of a metal in the solid state and, when cooled below its solidus temperature, to make a strong bond with that metal. [25, 32].

It is widely accepted that joining by brazing is possible if the liquid braze wets the solids to be joined. The most frequently used criterion to quantify this condition is a contact angle lower than 90°[2]. Ceramic brazing relies on the ability of a filler metal or alloy to wet the ceramic surface, which is often hindered by the covalent

nature and the low surface energy of the ceramics. There are two basic approaches to encourage wetting: the modification of the ceramic surface and the modification of the braze itself. (see Figure 2-2), which is often hindered by the covalent nature and the low surface energy of the ceramics[31]

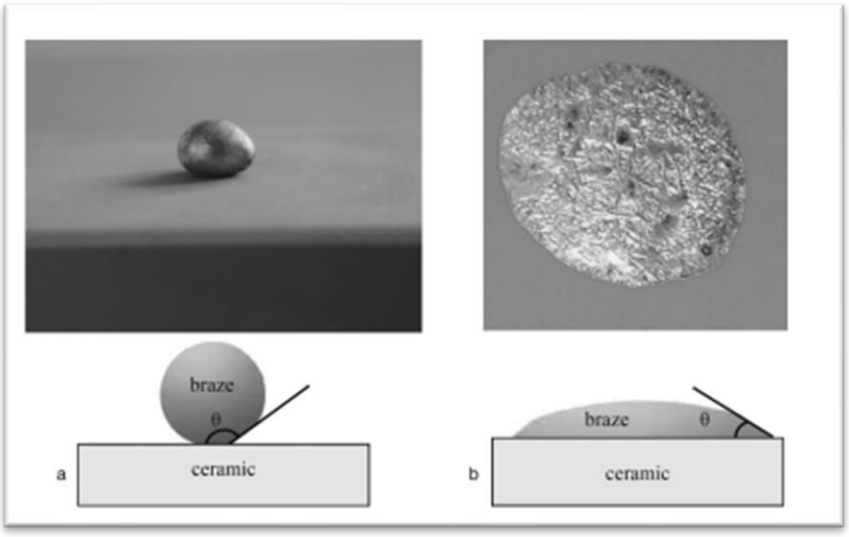

Figure 2-2. Two wetting experiments showing (a) poor and (b) good wetting[31].

3.Capillary Action (Capillary Flow)

The capillary flow of a molten brazing alloy relies on its ability for wetting the base materials. Additionally, it was obtained by the relationship between the liquid and solid phases as shown in Figure (2-2) [33]. The wetting angle measurement permits first to obtain the ability of materials for brazing and then to predict the brazed joints' characteristics, as depicted in Figure (2-3) [25]

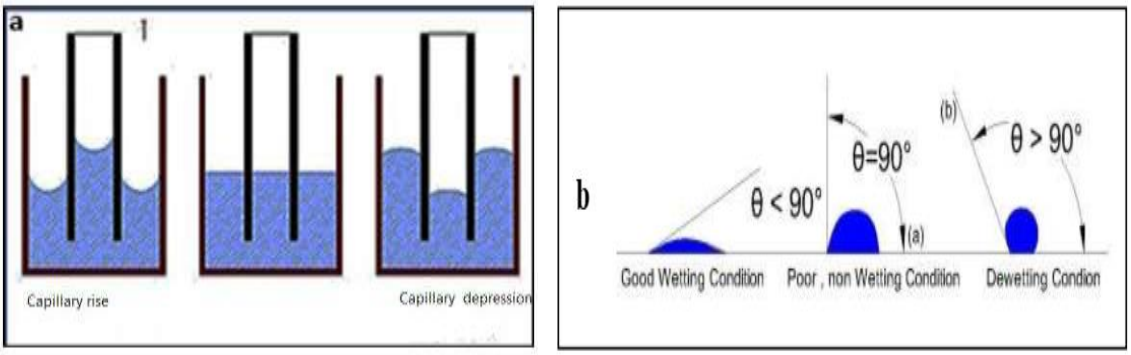

Figure (2-3): (a) The Corresponding Behavior of Liquids in Vertical Capillaries: (b) The Drops Distribution of Three Various Liquids with Different Wetting Characteristics[30].

The flow average velocity is the velocity (V) between the horizontal level and parallel surfaces and it is mathematically written as [27]:

$$V = \frac{d\gamma_{l/v}}{6\eta\, s}\, cos\theta \qquad \ldots\ldots\ldots\ldots\ldots\ldots \qquad (2\text{-}2)$$

Where:

$\gamma_{l/v}$ is the free energy of the liquid surface in the balance with the liquid vapor.

θ is the angle of contact (radian or degree).

η is the molten alloy viscosity (N/m^2. s).

S is the distance by which the filler metal has moved (m).

The time (t) required for the filler metal for completing the distances is stated as [34]:

$$t = \frac{3s}{dg\cos\theta} \qquad \ldots\ldots\ldots\ldots\ldots\ldots \qquad (2\text{-}3)$$

The same relations can be applied to the capillary paths that are either at right angles or inclined to the horizontal level. For these states, a peak height, H,

will exist, and the melted filler shall rise to it. That is provided by using the following expression [34]:

$$H = \frac{2\gamma \cos\theta}{d\rho g} \quad \ldots\ldots\ldots\ldots\ldots\ldots\ldots\ldots \quad (2\text{-}4)$$

Where:

d = The joint gap dimension (m).

g = The acceleration due to gravity (m/s^2)

ρ = The density of filler metal (kg/m^3)

The liquids and solids surface energies and their compositions are suggested to be constant. Nevertheless, the interactions occur if [35]:

1- The alloy is between the base metal and liquid.

2- The base material diffusion occurs within the filler.

3- The filler metal diffusion occurs within the base metal grains.

4-The filler penetration is along the boundary of grain.

5- The intermetallic constituents are formed.

4.The Diffusion Process

This process makes a coalescence of materials through heating to proper temperatures and utilizing metallic filler in the liquid form. This filler may spread via the capillary attraction. Also, this filler diffuses into the base material to a range that the joint characteristics vary to become near the base material properties. Also, the pressure can or cannot be exerted [36].

In a good brazing process, the base material thin layer surface is partially alloyed by brazing the filler metal. The metal atoms' migration, which is significant for such processes, is called the diffusion. Correspondingly, the

development of the transformation regions is also named the diffusion regions, as manifested in Figure (2-4)[37].

The brazed joint consistency is depended on the diffusion zone formation. For providing the generation of such regions, the brazing alloy atoms must be introduced into the structure of the metal atom of the base material. Obviously, not the whole metal atoms display similar capabilities to achieve such needs for the solid solution development. For the bigger discrepancies in atomic fields, the least magnitude of atoms should be introduced with a possibility for slowing down their moving capability. In order to fulfill the optimal consistency, the filler metal must reach the liquid phase within 5-10 seconds to ensure the generation of the enough depth of the diffusion region [38].

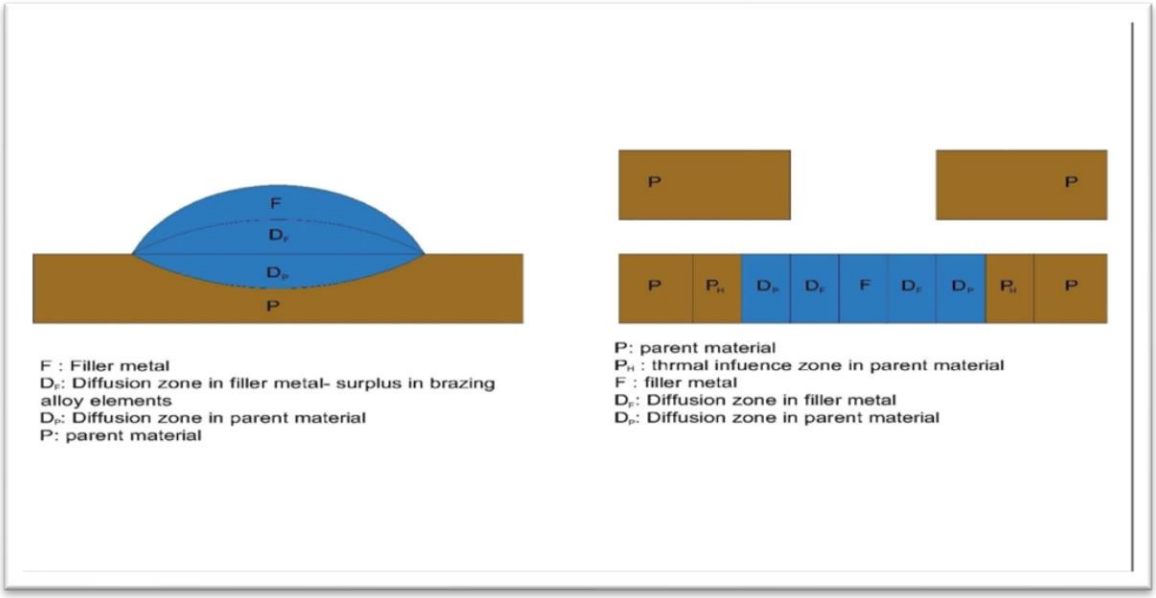

Figure (2-4): The diffusion zone [39].

2.7 of the Brazing Process

In order to produce satisfactory brazed joints, a careful and intelligent appraisal of the following elements is required [25].

1. Filler metal flow
2. Base metal characteristics
3. Preparation of the surface
4. Temperature and time
5. Joint design and clearance
6. Heating source and rate

1-Filler metal flow

Flow is promoted via the capillary attraction that in turn caused by the influences of the surface energy effect. Therefore, it's apparent that the high surface tension of liquid, low viscosity and a low angle of contact are demanded. The flow is considered the filler characteristic that obtains the distance that the filler will move away from its primary place owing to the effect of forces of capillary [25]

Filler metals are available as rod, ribbon, powder, paste, creams, wire, sheet, and preforms (stamped shapes, washers, rings, or shaped wires) shaped to fit a particular part. Depending on the joint design, heating method, and level of automation, the filler metal can be preplaced before the heating cycle starts or face fed after the work is heated. High-production brazing, such as furnace, flame, or induction brazing, which typically involves a high level of automation, usually requires preplacement of the filler metal[25].

For active brazing, powder metallurgy may be used to develop new brazing filler compositions with an optimized amount of the active element. It is expected

that the increased amount of active element should improve the wetting of the melted filler material on the ceramic, and therefore increase the strength of the bond. The interaction of all these effects has to be taken into account when determining the optimum content of the active element for maximum joint strength, as shown in Figure 2.5 [31].

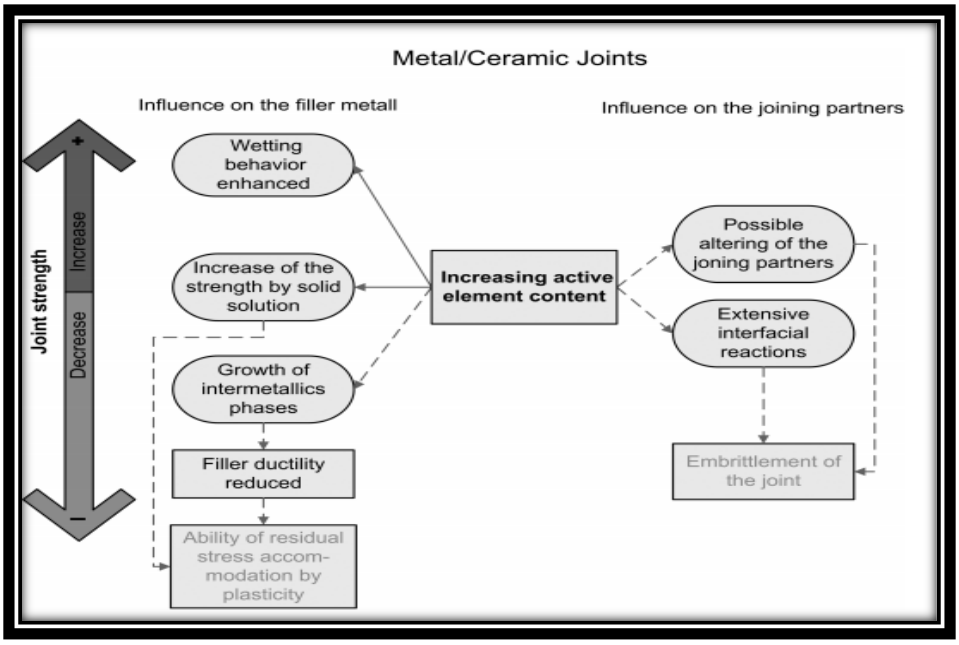

Figure (2-5) The influence of the active element on the joint strength: complex interactions[31]

2-Base metal characteristics

There are several metallurgical features that impact on the brazed joints behavior, some instances require certain methods. Including among these base–metal effects are alloying elements, carbide precipitation, stress cracking, hydrogen, sulfur, and oxide stability. In addition, the influence of the cycle of brazing upon base material and eventual strength of the joint are regarded [25]

3-Preparation of the surface

A successful process of brazing is principally associated with the cleanliness of base material surfaces to be joined. Thus, cleaning of such surfaces from the contaminants and oxides is needed and is too significant, since their existence avoids the action of capillary and thus avoids the brazing [40].

4-Temperature and Time

The brazing filler temperature possesses a significant influence upon the wetting operation, since the alloying effect and wetting are improved due to rise of temperature. Of course, the temperature must be greater than brazing filler melting temperature and less than the parent metal melting point [43].

Usually, the lowest satisfactory brazing temperatures are preferred to (a) economize on heat energy required, (b) minimize the heat effect on the base metal (annealing, grain growth, or warpage, for example), (c) minimize base metal/filler-metal interactions, and (d) increase the life of fixtures, jigs, or other tools. Higher brazing temperatures may be desirable to (a) use a higher-melting but more economical or otherwise superior filler metal; (b) combine annealing, stress relief, or heat treatment of the base metal with brazing; (c) permit subsequent processing at elevated temperatures; (d) promote base-metal interactions in order to modify the filler metal (this technique is usually used to increase the remelt temperature of the joint); (e) more effectively remove surface contaminants and oxides with vacuum brazing; and (f) avoid stress cracking.

The time at brazing temperature also affects the wetting action, particularly with respect to the distance the filler metal can creep. If the filler metal has a tendency to creep, the distance generally increases with time. The alloying action

between the filler metal and parent metal is, of course, a function of both temperature and time. In general, for production work, both temperature and time are kept at a minimum consistent with good quality[25].

5-Joint Design and Clearance

There are many kinds of brazed joints, the operation of choosing the joints kind is affected by the loading stress need and other service needs, like appearance, the tightness of pressure and electrical conductivity. The clearance between the base metal faces needed to be joined is called a gap or fit up; such distance is desirable to become too short. Since the greater capillary performance occurs by narrower clearance, through this manner, the filler material is exerted inside the gap by the capillary effect. A rigid, sound and strong joint is provided by the clearance with a close fit [41].

Lap joints, which are the most common type of brazed joint, are usually as strong as or stronger than the base materials being joined as long as (a) the faying surfaces overlap for a distance equal to at least 3 times the thickness of the thinner of the two members being joined, and (b) the clearance between the two parts (joint thickness) is kept to approximately 0.075 mm (0.003 in.) or less at braze temperature. Figure (2-6) shows good and bad butt-joint and lap-joint designs. Butt joints are usually used where strength requirements may not be critical or where the use of a lap joint would be objectionable[25].

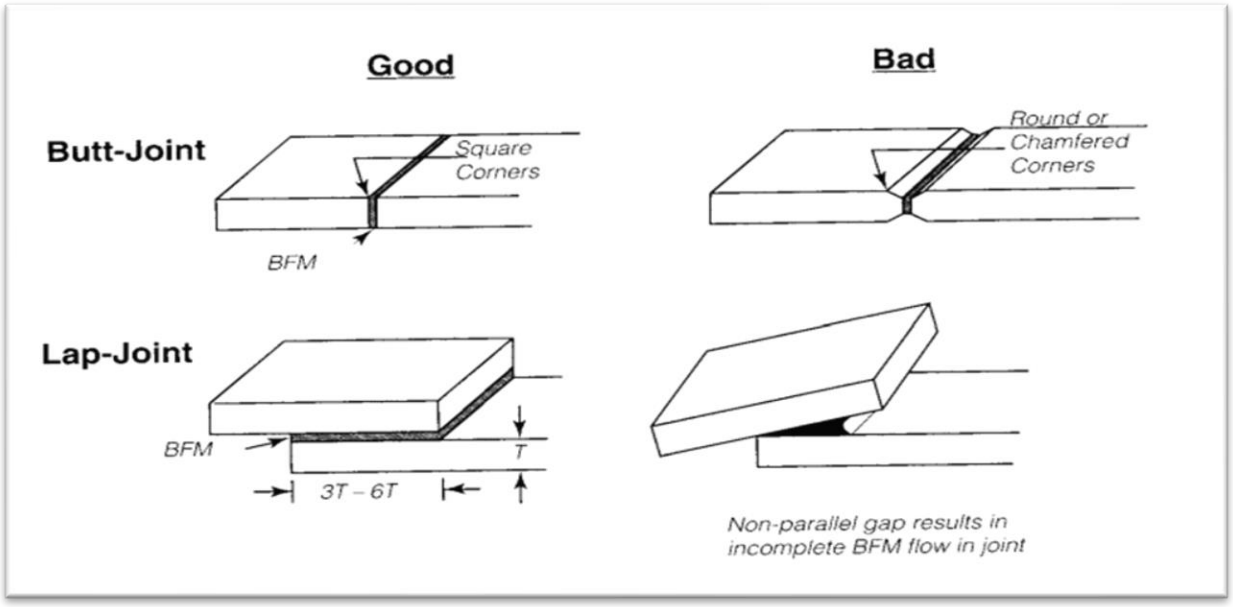

figure (2-6) Comparison of some good and bad ways to assemble lap and butt joints. BFM, brazing filler metal. T, thickness[23]

6-Heating Source and Rate

Many factors must be considered before the selection of the heating method, such as the size and value of individual assemblies, the numbers required, the rate of production, the rate of heating, the differential thermal gradients, and the cooling rate. All these factors have an effect on dimensional stability, distortion, and metallurgical structure [25]

2.9 Pure Ti and Ti6Al4V for Biomedical Applications

Attempts to use titanium for implant fabrication dates to the late 1930s. It was found that titanium was tolerated in cat femurs, as was stainless steel and Vitallium® (CoCrMo alloy). Titanium's lightness (see Table 2-1) and good mechanochemical properties are salient features for implant application[12].

Table 2-1 Specific Gravities of Some Metallic Implant Alloys[12]

Alloys	Density (g/cm^3)
Ti and its alloys	4.5
316 Stainless steel	7.9
CoCrMo	8.3
CoNiCrMo	9.2
NiTi	6.7

Titanium and its alloys offer unique advantages over steels in medicine, predominantly, low weight and high corrosion resistance. While there are 38 grades of titanium and its alloys, approximately five of those grades constitute almost 80 % of the production in the USA and a majority of that is Ti6Al4V (ASTM Grade 5; Type III)[42] .as shown in table (2-2)

Table (2-2) Chemical Compositions of Ti and Its Alloy [41]

Element	Grade 1	Grade 2	Grade 3	Grade 4	Ti6Al4V[a]
Nitrogen	0.03	0.03	0.05	0.05	0.05
Carbon	0.10	0.10	0.10	0.10	0.08
Hydrogen	0.015	0.015	0.015	0.015	0.0125
Iron	0.20	0.30	0.30	0.50	0.25
Oxygen	0.18	0.25	0.35	0.40	0.13
Titanium			Balance		

Pure titanium and α + β type Ti–6Al–4V ELI (extra low interstitials) alloys are currently used widely as structural biomaterials. These alloys are used for making instruments for replacing failed hard tissues such as artificial hip joints, dental implants, etc. because they have excellent specific strength and corrosion resistance, no allergic problems and the greatest biocompatibility among the metallic

biomaterials. They occupy almost all market of titanium biomaterials[43, 44] a in figure (2-7)

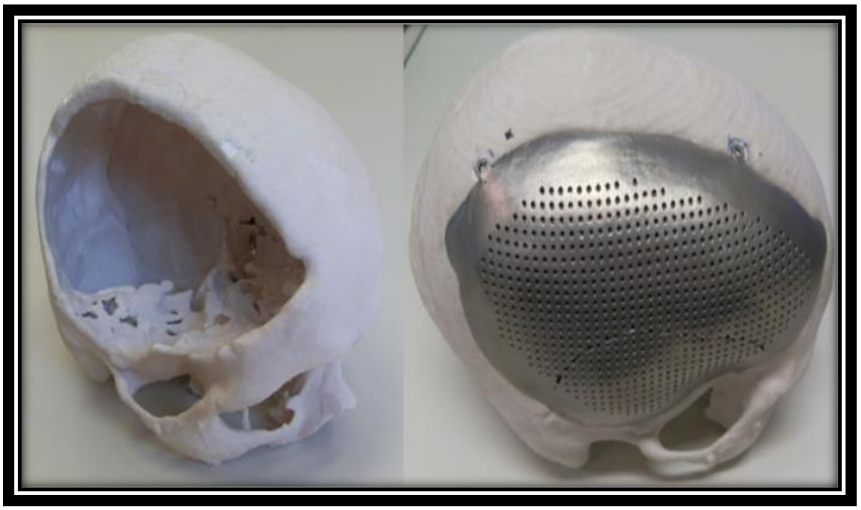

Figure (2-7): Bio model and customized implant for craniofacial reconstruction surgery[45].

However, other new titanium alloys for biomedical applications have been registered in ASTM standardizations after pure titanium and Ti–6Al–4V ELI being registered. Very recently, other new titanium alloys for biomedical applications such as β type (Ti–15Mo) have been registered in ASTM standardizations. β type (Ti–35Nb–7Zr–5Ta and α + β type Ti–3Al–2.5V) are on the way to being registered in ASTM standardizations. Nowadays, both α + β type4) and β type5(titanium alloys composed of non-toxic and non-allergic elements are being developed energetically[44].

Titanium and its alloys have two allotropic phases, low temperature hexagonal α phase and high temperature body centered cubic β phase. This transformation from α to β is known as the β-trans vs temperature[12, 46] as in figure (2-8).

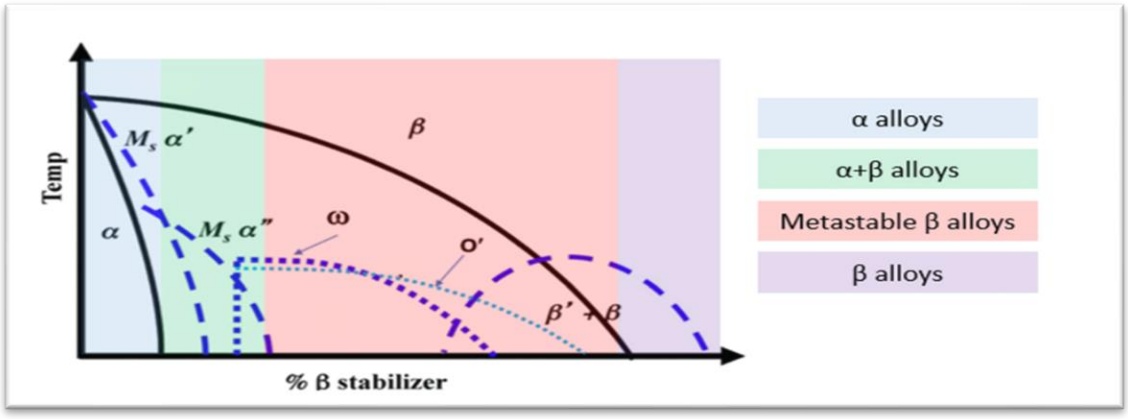

a

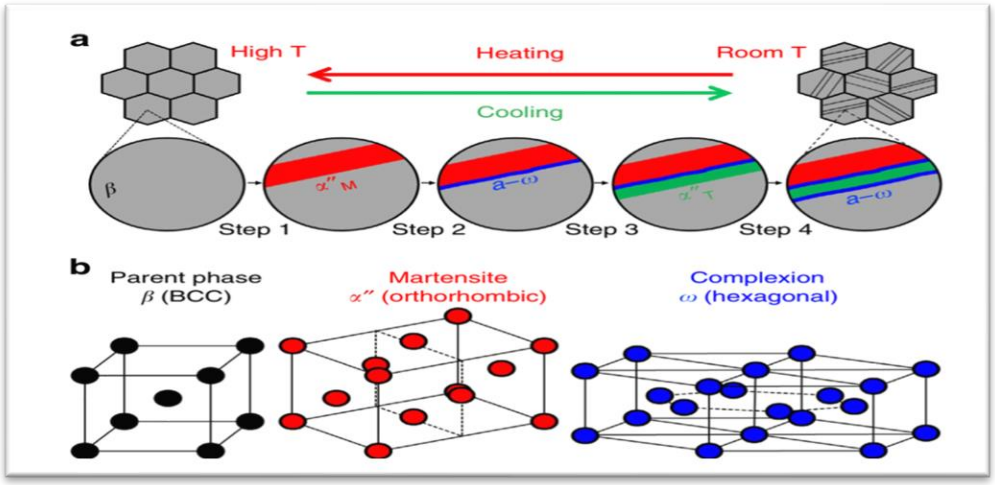

b

Figure 2-8 : a- phase diagram illustrating equilibrium and non-equilibrium phases observed in titanium alloys[47], b-Schematic explanation of α-, (α +β)-, and β-type titanium alloys based on crystal structure[48].

The α-phase in titanium is characterized by the hexagonal close-packed (HCP) unit cell. These alloys are characterized by good strength, toughness, creep resistance, and weldability[42].The alloying additions to titanium tend to stabilize the alpha or beta phase. The alpha phase is stabilized at higher temperatures, by elements called alpha stabilizers, such as aluminum, tin and zirconium[45].

β-type titanium alloys are becoming more popular in orthopedic applications as their lower modulus is believed to reduce the effect of stress-shielding on the bone as well as exhibit an increased fracture toughness as compared to an alpha-beta alloy of equivalent aging. Generally, β-type titanium alloys have good ductility, relatively low strength, low modulus, and excellent uniaxial formability. The ability to harden the alloy is easily controlled during the cooling process enabling the alloy to be better designed to the spinal biomechanical environment. These properties also suggest β-type titanium alloys as effective metals in spinal applications given the metal can be formed at room temperature without appreciable cold-work hardening[42]. while the beta phase is stabilized by beta stabilizers at lower temperatures, such as vanadium, molybdenum, niobium, chromium, iron and manganese[45].

Ti–6Al–4V belongs to a type of α–β duplex titanium alloys, since their microstructure can be tailored to provide either high toughness at ambient temperature or high creep resistance at elevated temperatures. It is one of the most important titanium alloys for aerospace, turbine engines and biomedical applications owing to their highly desirable performance characteristics, such as high strength-to-weight ratio, low density, and corrosion resistance[46].As shown in figure (2-9)

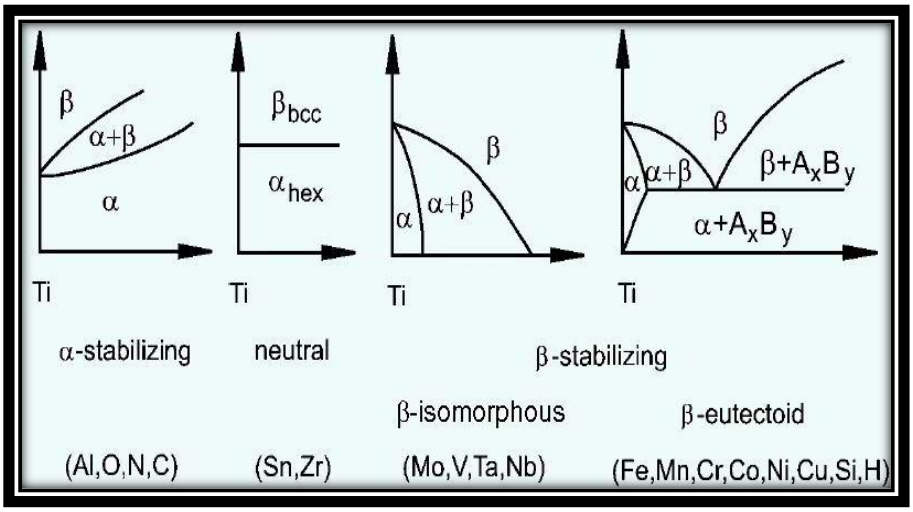

Figure (2-9) : illustrated the effect of alloying elements on stabilizing Titanium phases [48].

depending on the type of implant, a low young's modulus can sometimes prove detrimental. For example, when applying a β-type titanium alloy, with a low young's modulus, to spinal fixation devices, the amount of spring back in the device should ideally be as small as possible in order to improve spring back in the device should ideally be as small as possible in order to improve its handling ability during operations. This degree of spring back is considered to be related to the young's modulus, with a lower young's modulus correlating to a larger spring back. To put it more simply, a higher young's modulus is more desirable for surgeons, whereas a lower young's modulus is more desirable for patients. Consequently, in developing spinal fixation devices, it is necessary to satisfy the competing requirements of both the surgeon and the patient[42].

If the Young's modulus of an implant is higher than that of the cortical bone, then the load is preferentially transferred to the implant. This phenomenon is referred to as stress shielding, and it is especially true in the case of load-bearing implants, such as those used for replacing failed hard tissue (cortical bone). When stress shielding occurs, it results in bone resorption and poor bone remodeling, which are the leading causes of implant loosening and refracture of the bone after implant extraction. As previously mentioned, the Young's moduli of β-type titanium alloys are typically smaller than those of the other metallic biomaterials, such as stainless steels and Co–Cr alloys, as well as those of α- and (α + β)-type titanium alloys[42, 46,49].

2.10 Zirconia for Biomedical Application

Zirconia is a material that also has been around for decades. It is made up of oxygen anions that are not set in a hexagonally structured close-packed arrangement but, more or less, in a square pattern. Zirconia was known for decades for its use in highly reactive glass furnaces. It had limited use until the last quarter of the 20th century because of the destructive nature of the reversible phase transformation to

and from tetragonal to monoclinic. Zirconia has also become a synthetic gem quality replacement for diamond in its cubic form[50].

Zirconia exhibits high strength and fracture toughness, particularly at temperatures below ~300℃(K_{IC} 15–20 MPa $m^{1/2}$) and it is also a good ionic conductor at elevated temperatures. For these reasons, zirconia can be found in applications ranging from wire drawing dies, cutting and machining tools, to oxygen sensors and fuel cell [13].Zirconium forms inorganic (zirconium dioxide) and organometallic (zirconide dichloride) compounds. Five isotopes occur naturally, three of which are stable as shown in figure (2-10). Zirconium dioxide is called zirconia, which is often used in aerospace or as cutting tool in the watch industry[51].

ZrO_2 has three polymorphs: cubic, c-ZrO_2, tetragonal, t-ZrO_2, and monoclinic, m-ZrO2. At room temperature, the monoclinic structure is the stable phase. Upon cooling from the melting point, zirconia shows two kinds of solid–solid phase transformation, namely, cubic–tetragonal (c–t) and tetragonal–monoclinic (t–m). The t–m transformation occurs with a volume expansion and a shear distortion parallel to the basal plane of t-ZrO_2. These two characteristics can be used to increase both the strength and the toughness of zirconia. In fact, ZrO_2-based ceramics exhibit various outstanding properties that are closely related to the t–m phase transformation; for example, the volume change and the shear strain developed by the t–m transformation of metastable tetragonal particles act against the opening of a crack, and therefore increase the resistance of the ceramic to crack propagation. This mechanism significantly extends the reliability and lifetime of ZrO_2 derived materials and leads to the high fracture toughness of tetragonal zirconia[52].

The tetragonal– monoclinic transformation is of great importance, since the zirconia undergoes a relatively large volume increase (3–5%), likened to that of martensite formation when quenching steel. The stresses induced can be sufficient

to crack the zirconia on cooling from the firing temperature; however, additions of certain metal oxides (such as MgO, CaO and Y_2O_3) and appropriate heat treatment can overcome this volume increase. These additives decrease the transformation temperature, allowing the zirconia to be cooled to room temperature - retaining a (meta) stable cubic phase over the entire temperature range. Materials adjusted in such a way are termed fully stabilized zirconia (FSZ). These materials are used in sensors and fuel cells. Still better mechanical properties are achieved with partially stabilized zirconia (PSZ), where a precipitation of very small (50–100 nm) particles of metastable tetragonal phase are induced into the cubic matrix by thermal treatment. The resultant properties are a result of transformation toughening, where the volume change of the tetragonal to monoclinic transformation improves both toughness and strength[13].

Yttria tetragonal zirconia polycrystalline (YTZP) ceramic and magnesia partially stabilized zirconia (MgPSZ) are both types of zirconia. As discussed earlier, zirconia goes through a set of phase transformations when it is heated and cooled. Though they do so differently, yttria and magnesia promote toughness in zirconia through control of the transformation from tetragonal to monoclinic zirconia within the material. In YTZP, the whole zirconia microstructure is designed to be made up of small tetragonal zirconia crystals. If a crack forms, there is a stress region emanating from the crack front that leads the crack as it moves through a solid. When the crack front moves through a region of YTZP, it causes the tetragonal zirconia within the crack front zone to martensitic ally transform to the monoclinic phase. This change is accompanied by an increase in volume and so causes a compression in front of the crack tip. This compressive stress is similar to pushing the crack together so that the stress is used to slow down or stop the crack. Different to YTZP, the MgPSZ microstructure is made up mostly of large cubic zirconia crystals. In this

particular type of zirconia, the large, stabilized cubic grains of zirconia have transformable tetragonal seeds embedded within the larger crystal. When a crack front approaches, the seeds inside the grain transform creating a compressive stress to the material [50].

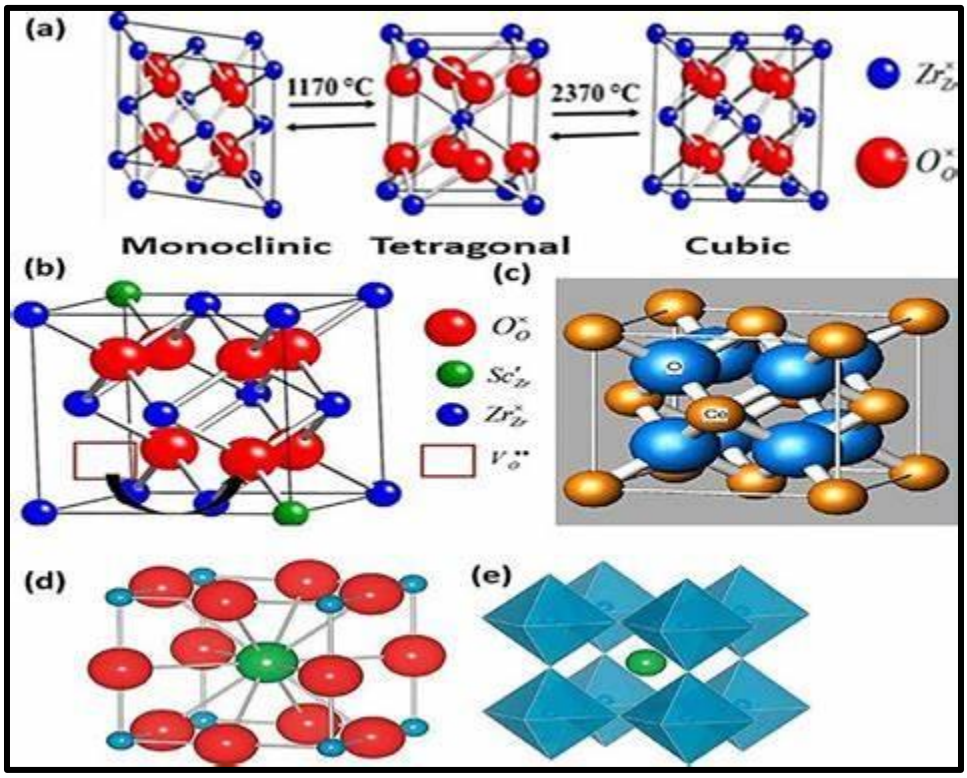

Figure 2-10 Crystal structures of zirconia polymorphs: (a) monoclinic, (b)tetragonal, (c) cubic, (d) brookite and (e) cotunnite[53].

Moreover, YTZP has some other eloquent characteristics:

a. Electrical neutral.

b. Low thermal conductivity.

c. High resistance to high temperature.

d. High thermal shock resistance.

e. Chemical stability.

Due to all these criteria, zirconia is an excellent material for medical and dental applications. In comparison to titanium, zirconia showed no induction of any adverse reaction or global toxic effect in vitro. Tests were performed on fibroblasts, lymphocytes, monocytes, macrophages, connective tissues, immunologic and bone tissues as in Table 2-3 [51].

Table 2-3 : Biological comparison titanium versus zirconia[51].

	Titanium	Zirconia
Ion release	Yes	No
Toxicity	Low	No
Plaque adhesion	Low	Very low

2.11 Ag – Cu Filler Metal

Bonding of ceramic materials to metals is a recent hot topic in various engineering applications, including heat exchangers, connectors, capacitors, thermoelectric, solar cells, and complex structural joints. It is always a practical challenge to bond these ceramic materials directly due to a wide difference in physicochemical and mechanical properties of ceramics and metals that imposes a great challenge in micro joining operations. For this purpose, various popular brazing fillers are already developed where the most popular ones are eutectic Ag-Cu or Ag-Cu-Ti alloys as reported in the past. However, with regard to complex geometry, the thickness of IMCs, and cost, each filler is unique and has limitations of its own[54].

The equilibrium phases of the Ag-Cu system are (1) liquid, L, with no miscibility gaps; (2) (Ag), a Ag-rich phase, fcc solid solution, with a maximum solubility of 14.1 at. % Cu; and (3) (Cu), a Cu-rich phase, fcc solid solution, with a

maximum solid solubility of 4.9 at.% Ag, resulting in a eutectic equilibrium, as shown in the assessed phase diagram Figure(2-11).summarizes the invariant reactions in the Ag-Cu system. The Ag-Cu system with its limited solid solubilities is a unique system in that it violates the Hume-Rothery rules of solid solubility[55].

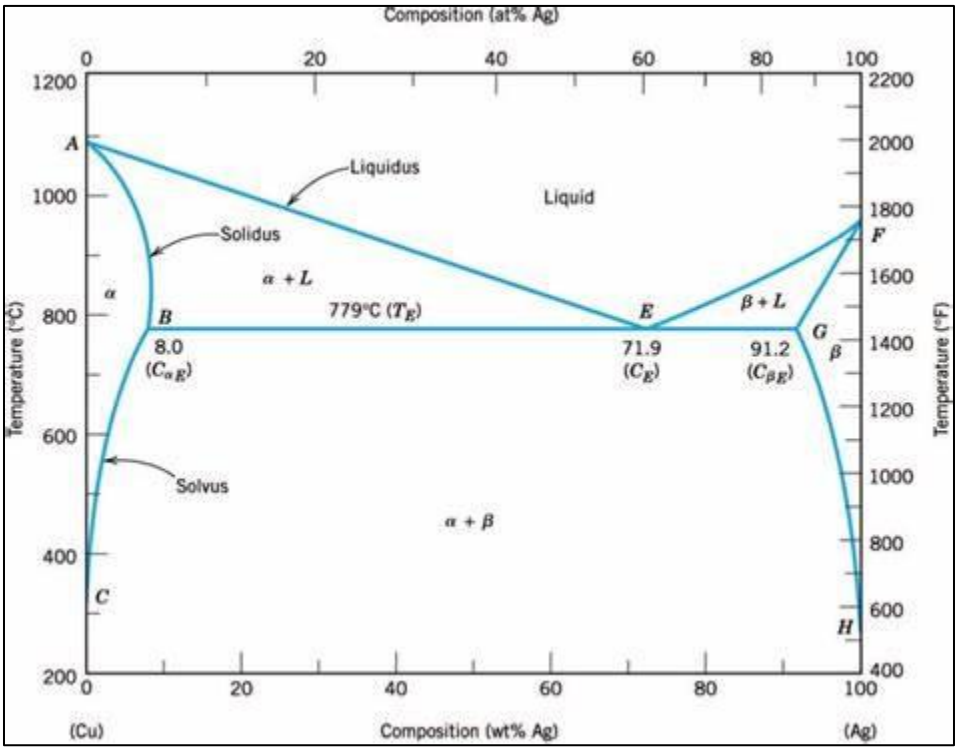

Figure (2- 11) : illustrated Ag-Cu phase diagram [55]

Silver brazing alloys consist of alloys of silver, copper, zinc and sometimes also cadmium. They flow easily, with low working temperatures of 600-800°C. They can be used with all heating methods, and for almost all materials except aluminum and magnesium alloys[20].

Ag-Cu eutectic can be found commercially with a few weight percent of titanium intimately dispersed into or alloyed with it that can be placed between two or more properly fixtured materials in a similar manner as with conventional metal/metal brazing. Here, however, steps must be made to melt this paste or preform in flowing inert gas (e.g., Ar, He but generally not including Nz) or mild

vacuum « 0.1 mile-torr) at temperatures that are 10-20 degrees centigrade above the braze matrix solidus temperature. This is necessary to provide a high temperature condition in which bonding to the ceramic is not prevented through competing reaction between the active metal and any potentially reactive atmosphere. Care must also be taken that vacuum/temperature conditions do not exceed volatility restrictions of the metallurgical species present[19].

In the case of zirconia brazing, the addition of Ti to silver–copper alloys promote low contact angles and hence wetting. However, during this process the active element titanium, reacts with the zirconia, depleting the surface region of oxygen. This has the effect of darkening the zirconia in the region of the interface as in figure (2-12). At the braze–ceramic interface, the PSZ has turned from cream to black. The graduation in color becomes lighter as the distance from the joint increases. The darkening effect is influenced by a number of potential factors including: dwell time at temperature; final dwell temperature; the substrate to which the PSZ is being joined; and the percentage of Ti in the braze alloy[13].

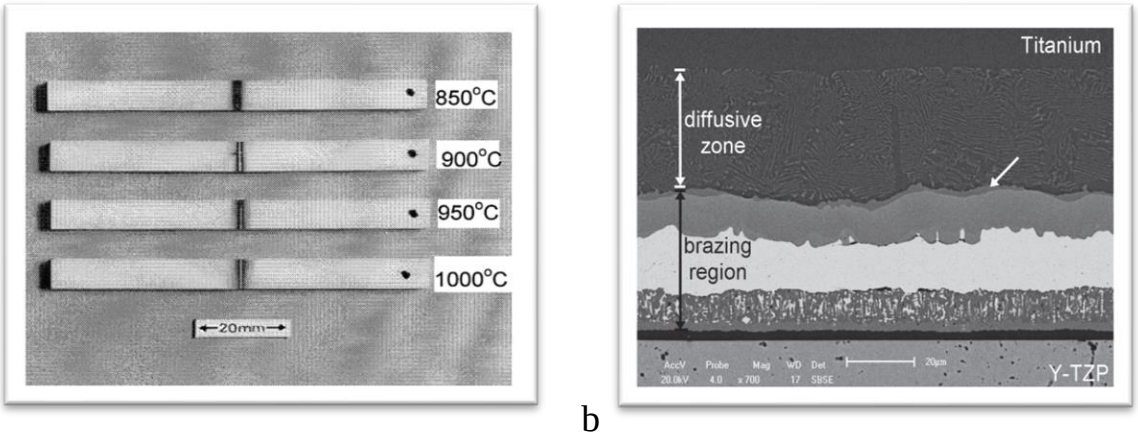

a b

Figure (2-12).a- Discoloration of PSZ brazed for 5 min at temperatures of 850, 900, 950 and 1000°C using Cusil ABA[13] ,b- SEM image at the Y-TZP/Ag-28Cu/Ti joint interface: diffusive zone and intermetallic layer (see the white arrow); and a dark reaction sublayer on the ceramic surface [56].

It was suggested that copper has a strong tendency to rapid formation of intermetallic with titanium, and Ag is the less active element of Ag-Cu filler alloys with low diffusivity through the CuTi layer; however, the presence of Ag can remarkably increase the activity of filler alloys to promote interfacial reactions with technically stable ceramics. Other elements such as V, Cr, Zr, V, Nb, Ta and Hf can also be considered chemically active in braze alloys composition – especially Ti, which can make chemical interactions (dissolution, interdiffusion and/or product formation reaction) at the ceramic/metal interfaces to enhance wetting on the ceramic surface[56].

2.12 Rapid Solidification

New materials and methods of production are crucial in the emerging high technology industries for manufacture of products from electronic devices to superconducting, machinery parts and also in more traditional areas, such as the automotive, bio applications, aerospace and plastic industries [74].

Metallic glasses are alloys having amorphous or glassy structures. Oxide, glasses, liquids and glassy polymers are well-known amorphous materials. However, metallic glasses are relatively new class of amorphous materials, since liquid metals and alloys crystallize so rapidly on cooling that until 1960 that the first metallic glass, Au80Si20, was obtained by so called melt spinning, capable of achieving rates of 10^6 K/sec. A “time temperature transformation” (TTT) diagram is a quantitative way to envision the thermal tolerances required to produce Bulk Metallic Glasses (BMGs) during solidification processing. Figure (2-13) shows a TTT diagram representative BMGs exhibiting the classic C-shaped curve. The familiar silicate glasses are transparent containing silica are brittle and electrical insulators. In comparison, metallic glasses containing primarily metallic elements

and are metallic conductors and ductile. Some show ferromagnetism and superconducting behavior [75].

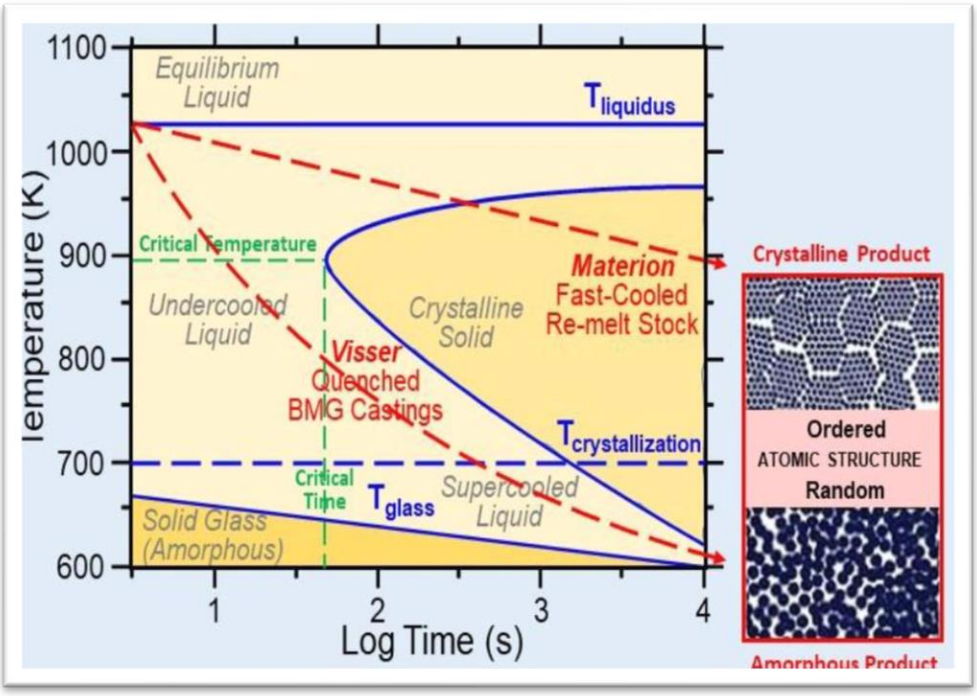

Figure(2-13). TTT diagram representative of BMG(Bulk Metallic Glass) alloys [76].

Schematic sketches of the atomic arrangements and its pair distribution function in a gas, liquid, glass and crystal are shown in Figure (2-14). In the gaseous state, the state is distributed randomly and are totally uncorrelated. However, the atom does not mutually approach within the atomic diameter a, in both the liquid and glassy states, the atoms are randomly distributed in a nearly close-packed structure. There exists a high degree of local correlation. The atomic configuration in the glassy state has more rigid packing compared with that of the liquid state. The essential aspect with which the amorphous solid structure differs with respect to that of crystalline solid is the absence of long-range order. There is no translational periodicity [77]

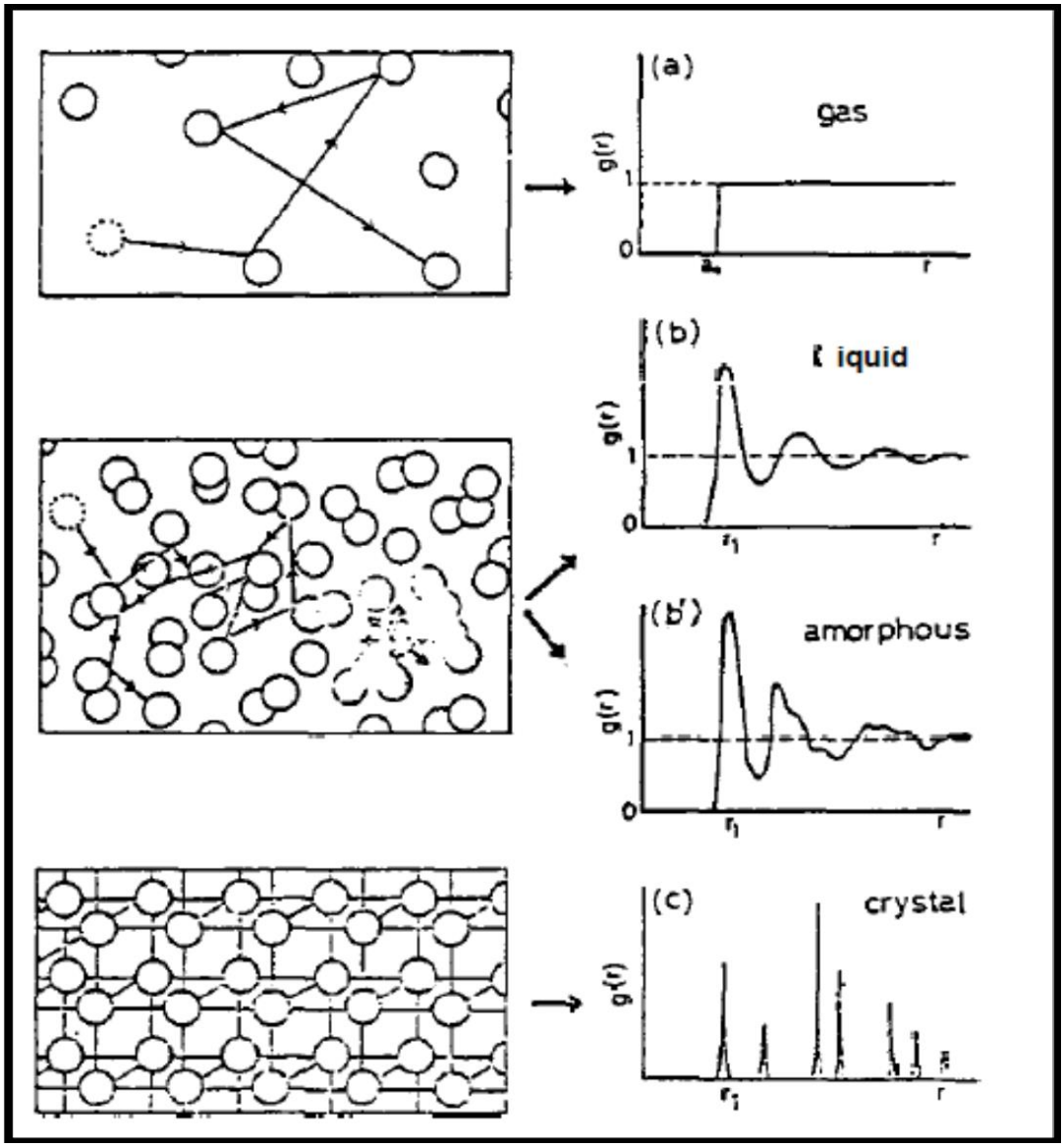

Figure 2.14. Schematic Sketches of The Atomic Configuration and Its Pair Distribution Function G(R) In A Gas, Liquid, Glass and Crystal [77].

The principal uses of metallic glasses were derived from their increased corrosion resistance, wear resistance and reduced eddy current lasses in ferromagnetic ribbons as compared to that of normal crystalline alloys. There was a gradual growth within the elemental base is such there are quite a dozen of distinct metals for the basis of bulk metallic glasses. They exhibit for the first time the opportunity of the find out about of the properties of the glassy and the supercooled

liquid states on a temporal and spatial scale previously regarded impossible. A totally unexpected result was that on devitrification they produced nanocrystals, paving the way for bulk nanostructured materials. Some of them gave rise to quasicrystals, again leading to bulk nano quasicrystal line materials [78].

Amorphous alloys are a class of metal alloys that, unlike ordinary metals, they don't have a long-range crystalline structure and don't grain boundaries, and the atoms are randomly and tightly packed. Because their structure resembles that of glasses, these alloys are also called metallic glasses These materials are now available in bulk quantities, as well as wire, ribbon, strip, and powder, and continue to be investigated as an important and emerging material system[79].

2.13 Shear Strength of Ceramic /Metal Joints

Ideally, the mechanical strength of a ceramic/metal joint component should be higher than those of its constituents. The joint should fail at one of the base materials. In reality, joints fail at lower strengths, either because of the interfacial strength is inherently lower or because of residual stresses which lower the strength of the ceramic counterpart. Effective joining should grant strength levels compatible to the demand of the intend application along with maximum reliability[6].

The bond strength values obtained also depend on the testing technique chosen. Bend test values are generally higher than tensile test values for joints and for brittle ceramic materials. The shear stress test is one of the simplest techniques. However, the shear stress at the interface is not simple shear and it always contains a component of tensile stress that originates from a bending moment, which cannot be neglected. The influence of a slight change of the push position and the fixing condition on the stress distribution is very important. Therefore, the shear test is not

recommended for the common evaluation method. Bending and tensile test has almost the same stress distributions as those derived from[5].

Joint strength is mainly determined by:

1-Joining process and related parameters. The strength of brazed joints, in particular, depend on the quality of the metallized layer (when present), filler alloy, and brazing cycle.

2-Intrinsic properties (Young modulus and coefficient of thermal expansion) and characteristics (roughness and toughness of the ceramic) of the base materials, especially the ceramic for its brittle nature

3-Joint type (planar or fitted) and geometry (cylindrical or rectangular).

However, a fundamental aspect on ceramic/metal mechanical strength is the composition and microstructure of the interface. The presence of intermetallic (usually brittle) along with the thickness and morphology of reaction layers can drastically enhance or dwindle the strength of the joint. The presence of organic material or impurity particles either on the surfaces to be joined on the filler alloy (for brazing) is deleterious to the interfacial microstructure. Joining defects are created. These areas of joining discontinuities increase local stresses and promote crack nucleation and growth Figure (2-15). In particular, ceramics are quite susceptible to the presence of microcracks and areas of high local stresses. Upon cooling, the ceramic is often submitted to tensile stresses capable of growing existent cracks and nucleating new ones[6].

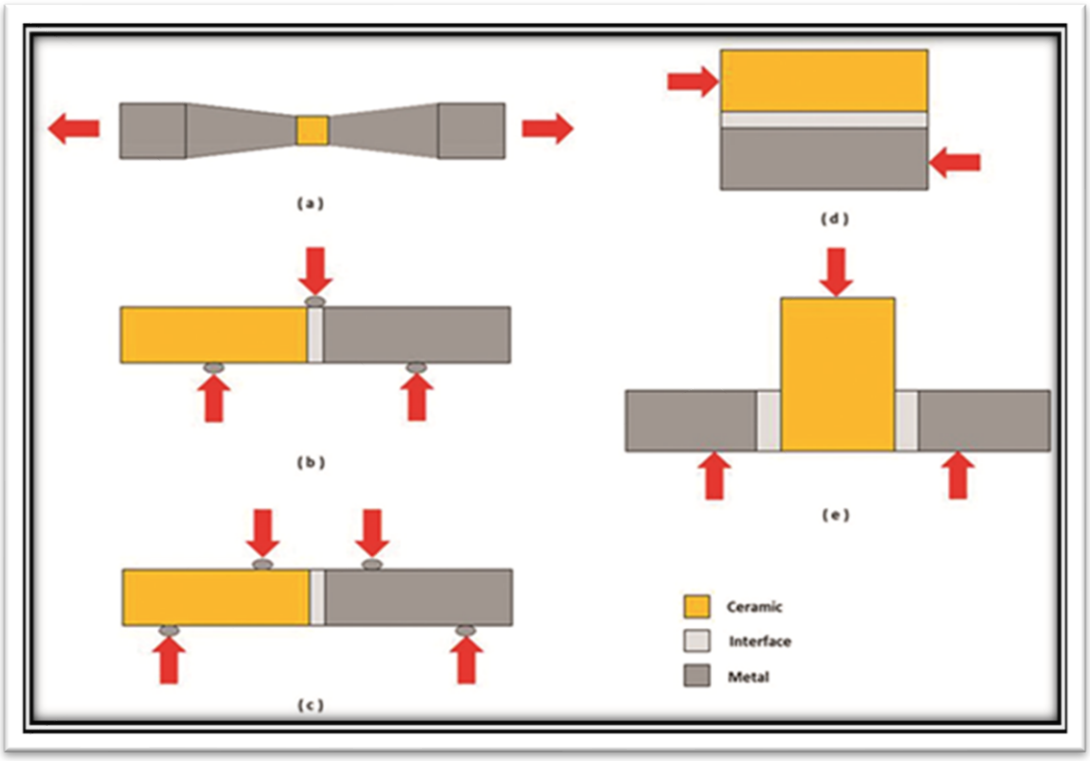

Figure (2-15): Sample geometry for mechanical tests of joined specimens. (a) tensile; b) 3-point bending, (c) 4-point bending, (d) plain shear and (e) shear on ring/cylinder[5].

2.14 Biomedical Applications of Ceramic/Metal joints (Feedthrough)

Once the ceramic part is formed, it must be hermetically joined to the housing material to form feedthroughs, windows or seals. In a feedthrough, one or more metal pins are also joined to the ceramic body to create conductive paths between the outside and the inside of the package; the ceramic body is then joined to the metal housing of the implant Figure (2-16) [80,81].

Figure 2-16: The original Alumina/Ti feedthrough. Here, an alumina feedthrough is brazed to a titanium housing, with a titanium pin brazed inside it [80].

A-Implantable Cardiac Pacemaker

The pacemaker unit delivers an electrical pulse with the proper intensity to the proper location to stimulate the heart at a desired rate. The pacemaker unit is usually implanted in the pectoral region, with the lead running through the right subclavian vein to the internal surface of the heart. A pacemaker is programmed by means of a programmer, a computer with a special user interface for data entry and display, and with special software to communicate with the pacemaker [82].

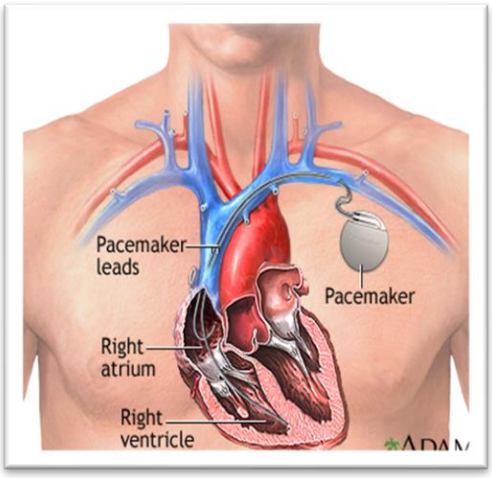

Figure (2-17) Overview of symbiotic pacemaker system. illustration of symbiotic cardiac pacemaker system[83].

B-Cochlear Implants, Cis

The over-arching goal of a cochlear implant is to use electric stimulation safely to provide or restore functional hearing. Figure (2-18) shows graphically a typical modern cochlear implant system .where the electrical impulses are interpreted as sound[84]

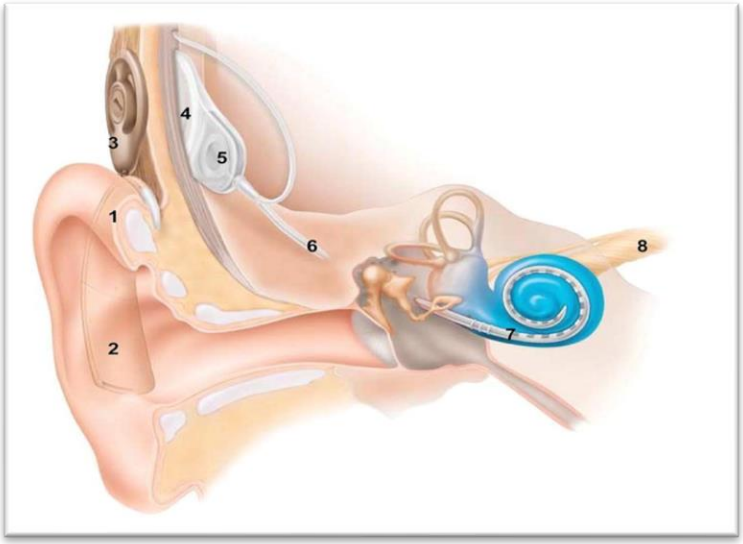

Figure 2-18 A typical modern cochlear implant system that converts sound to electric impulses delivered to the auditory nerve[84]

C-Retinal Implants

The principle underlying all retinal implants is the replacement of rod and cone photoreceptor function in patients with outer retinal degenerations. At present, only patients with a history of functional vision that has been reduced to light perception are candidates for retinal implants, In principle, however, they may use in the future to restore vision in only those retinal areas where it has been lost due to, for example, macular degeneration[85].

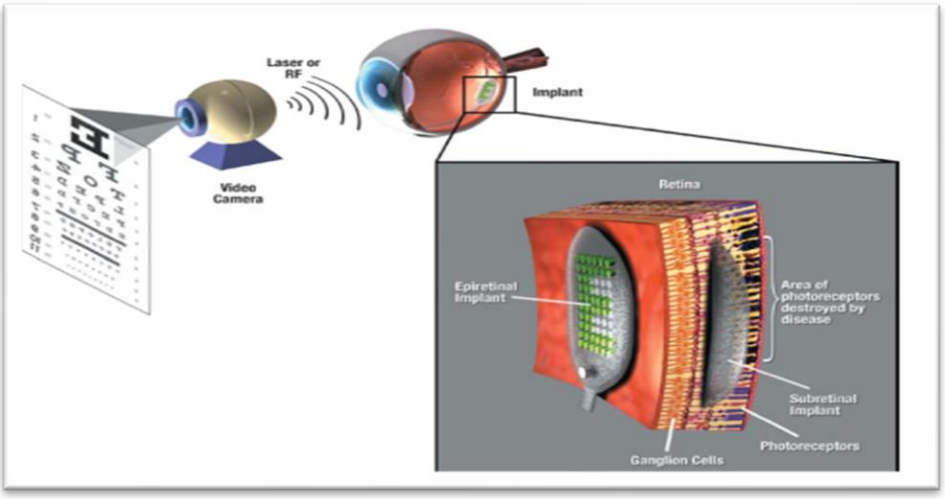

Figure (2-19) A retinal prosthesis will convert light to an electrical signal with an image acquisition and processing system. The information will be transmitted to an implant positioned somewhere in the eye. The implant will have the necessary subsystems to receive the signal and produce an artificial stimulus signal at the retina. The stimulus will be delivered by an electrode array. The electrode array will be positioned on the surface of the retina or underneath the retina (electrode array not shown for subretinal implant)[86].

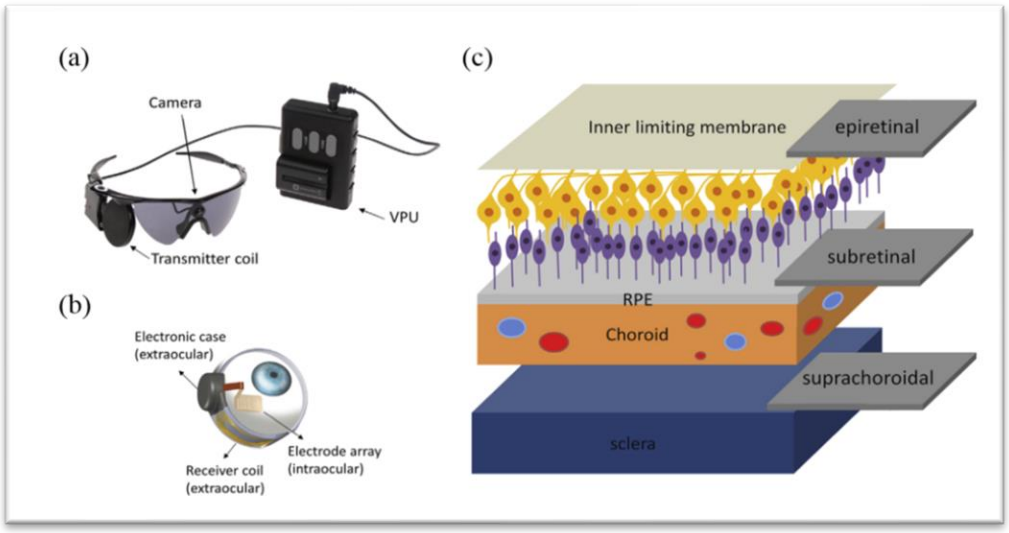

Figure (2-20) :(a) External and (b) implant part of the Argus II system; (c) illustration of the implantation sites of the visual cortex, epiretinal, subretinal, and supra-choroidal prostheses[87]

D-Functional Electrical Stimulation (FES)

Many neurological and orthopedic disorders reduce or eliminate voluntary recruitment of muscles. Such loss degrades the ability to perform motor tasks or to maintain muscles, connective tissues, and metabolic systems that depend on muscle activity for their function and integrity[88].

The BION (Bionic Neuron) is a single channel implantable neurostimulator that combines the current implanted device technology and microelectronics with a novel system design to yield a general-purpose single-channel neurostimulator that can be delivered by injection[11]. Figure (2-21) shows types of BIONS.

Figure (2-21) :A/ Photograph depicting three neuromuscular microstimulators (BIONs) in different packages [9, 88] , B/The functional electrical stimulation device including two cuffs, a foot switch, and a control unit[89]

2.15 Literature Survey

Many researchers have developed to investigate brazed joint between metal and ceramic for biomedical applications. The following section briefly browses some researchers work in order to compete and support current work.

C. Peytour and et al. , 1990 [57] studied of the possibility of brazing AI_20_3 Ti6A14V wt. by using (Cu-40Ag-5Ti wt. %) as filler alloy. Then, compared the results with joint of Zirconia (3 mol % Y_20_3) with Ti6A14V wt. with same filler. Brazing was achieved by heating sample for 5minutes in a vacuum furnace (about $2 \times 10^{-5}\ torr$) at temperature 870°C. Afterward a 5minutes hold on this temperatures, then the samples been cooled to room temperature in cooling time about (3 – 4) hours . The samples were characterized through TEM, and also by XRD. The Tensile test was carried out in room temperature. the conclusions, ZrO_2 / Ti6A14V joints showed interfacial phases that are show great similarity to the experiential in AI_20_3 /Ti6A14V joints. Nevertheless, the obtained tensile strengths of the produced samples by using ZrO_2 ceramic are higher (varied from 150 to 50MPa) also All specimens failed in joint areas that are near to PSZ inter-faces . the fracture had propagated into the zirconia.

R. N. CORREIA and et al. , 1998[58] prepared ZrO_2/ Ti /ZrO_2 , ZrO_2/Pt/Ti /ZrO_2 and ZrO_2/ Pt/ Ti6Al4V /ZrO_2 by brazing by using diffusion bonding with stance of an inert atmospheres at temperatures varied between (1162 to1494°C) . ZrO_2-Pt-Ti joints extant a complex layer arrangement which by lower temperatures could be defined on the fact of the Pt to Ti binary system, but near the ceramics where a Pt-rich and Zr-rich layer formulae. Higher temperatures cause a Ti_2O_3 oxide layer to form on these junctions. When Titanium is substituted with Ti-6Al-4V alloy in Pt-containing joints. A presence of liquids at lower joining temperature and a faster

growth of an oxide layers, already of nominal compositions, are the primary implications. The fracture route at direct ZrO_2/Ti joints runs by the metal, but in joints wherein Pt is present, it runs via the interface among the ceramics and the Pt-rich and Zr-rich layers.

Guangqiang Jiang and et al. 2005 [59] prepared biocompatible ceramic-to-metal seal like BION micro stimulator from 3 mol % yttria-stabilized tetragonal zirconia poly crystal (3Y-TZP) and a Ti-6Al-4V titanium alloy brazed by (TiNi)clad with 0.050 mm thickness as braze filler with a laminar structure consisted from 3 layers (Ni-Ti-Ni). The SEM test with EDS analysis, the x- ray detraction XRD test, and also electrochemical analysis are done on the prepared joints. Tissue investigation indicated thin fibrinoid encapsulation of both the micro - stimulators and also no histological damages to the neighboring nerve after necropsy and histological assessment through a pathologist, confirming acceptable biocompatibility.

O. Smorygo et al. 2007 [60] Zirconia with yttria (3Y-PSZ) and pure titanium joints were made by active brazing process in vacuum environment by using the (63 Ag35.25 Cu1.75 Ti (wt.%)) like filler alloy at brazing temperature ranged from 840 to 870 °C below different contact load. The joints microstructures and the fracture surface observation and the quantitative elements analysis were done by SEM supported by XRD and EDS analysis. the results showed that the Brazing conditions didn't affect clearly on the joints mechanical strength. nevertheless, a remarkable change occurs on the inter-layer.

Yuhua Liu , et al. 2011 [61] prepared ZrO_2-3 mol. %Y_2O_3 to Ti6Al4V joints by using a Ti_{47}-Zr_{28}-Cu_{14}-Ni_{11} (at.%) as filler alloy in amorphous ribbon at temperatures ranged from 1123 to 1273 K under high vacuum atmosphere . The microstructures and shear strengths of the prepared joints were studied in relation to brazing temperatures. the resulting phases in the microstructure involve ZrO_2 phase

, the TiO phase ,the TiO_2 phase , the Cu_2Ti_4O phase and also Ni_2Ti_4O- *alfa*-Ti phase. As the brazing temperature increase, the thickness of produced inter layers- layer reduce also. The shear strength to the prepared joints didn't affect by thickness of the produced phases.

Y.H. Liu and et al. , 2013 [62] studied the possibility of joining Ceramic ZrO_2 and Ti6Al4V alloy through using a Ti_{33}-Zr_{17}-Cu_{50} (at.%) as amorphous filler alloy at brazing temperature ranged from (1123 to 1273) K in high vacuum atmosphere. The resulting phases in the microstructure included ZrO_2 phase- the Cu_2Ti_4O phase - the $(Ti,Zr)_2Cu$ phase – the TiO phase -the Ti_2O phase -the $CuTi_2$ phase ,the $(Ti,Zr)_2Cu$ phase- the $CuTi_2$ phase and alsoTi6Al4V phase . when the brazing temperature increased the thickness weakens the shear strength also increased , even increasing the brazing cooling will increase the thickness of these inter – layers. The maximum obtained shear strength to the prepared joints was 162 MPs for joint prepared at 1173 K which heating for 10 minutes. While the fracture happened in a region near to ZrO_2 side.

J. Cao et al. 2013 [63] by using brazing method to produce ZrO2 to Ti6Al4V joints through use NiCrSiB with amorphous structure as filler alloy. The brazing process done at brazing temperature ranged from (950 to 1050 ℃) with heating rate for (20 ℃/min). the brazing time was 10 min under vacuum atmosphere. The microstructure analysis and phases done by SEM and XRD analysis. The formed phases include Ti_2Ni phase, TiO phase the $Ti5Si_2$ phase and also β-Ti phase. The maximum shear strength was 284.6 Mpa to samples brazed at 1025 °C with brazing time of 10 min.

Jean S. Pimenta et al. , 2013 [64] pure Titanium joined to ZrO2 with Yttria (Y-TZP) prepared by using two kind of filler alloys, firstly Ag-28Cu alloy and Au-18Ni alloy. The brazing process done at temperatures ranged from 700 to 750 ℃ for socking time of 10 minutes. At ambient temperatures, the helium (He) gas leakage

detection study was run at the ceramic to metal contact. With eutectic AgCu filler, strong connections were created that revealed an inter-metallic layer and a darkening reaction layer at the ceramic surfaces; titanium (Ti) diffusion was effective for external chemical inter-actions among individual components. 3-point flexure testing was also used to evaluate brazing joints.

Jicai Feng, et al. 2015 By employing inactive AgCu used as filler metal, a junction of ZrO2 ceramic and TiAl alloy was created. The AgCu as foil was sandwiched between ZrO2 and Ti-Al samples, and a little pressure was used to guarantee that graphite blocks had tight surface contact. by using vacuum furnace, the brazing trials were done at temperature ranged from (860 to 940 °C) while the brazing temperatures were ranged from 5 to 30 minutes. The impact of brazing temperatures on the micro-structure and mechanical characteristics of ZrO2/Ti-Al junctions was studied. The microstructure evolution of ZrO2/Ti-Al joints is greatly influenced by Ti and Al dissolved from Ti-Al substrate, and the process is explored. When brazed at 880 °C for 10 minutes, the highest mean shear strength achieved 48.4 MPa.

Xiangyu Dai, et al. , 2015 [66] ZrO_2 ceramic and TC4(**Ti-6Al-4V**) alloy effectively brazed by using AgCu alloy as filler metal. SEM, XRD, and TEM were used to examine the interfacial micro-structure of the prepared joints. TiO and Cu3Ti3O inter- layers formed in the joints after brazing process. Nanoindentation was used to determine the hardness value and the strength to the reaction phases, as well as their plastic deformability. After brazed at temperature of 870 °C for 10 minutes, the greatest shear strength that obtained was 52.2 MPa was attained.

Ashutosh Sharma et al. ,2016 [67] produced and compared the strength of joints that consisted from (ZrO_2-Ti6Al4) which brazed by using AgCuSnTi (Ag-35 wt. %Cu while Sn and Ti were added in minute concentrations (1 wt.%)). The brazing

process was done at a temperature (750 ℃) for brazing time of (30 minutes) by using high vacuum furnace under about (5×10^{-6} Torr) atmosphere. The joint's compressive strengths were tested at 1477 MPa, which is nearly 5 times more than that of conventional dental cements. The high von Mises stresses value were also validated by a finite element study. The compressive stresses in the specimens were found to be localized towards the Ti6Al4V position, which corresponded to the location of the fractured specimen in real life. These findings point to extraordinarily high compressive strength for ZrO2/Ti6Al4V joints filled with AgCuSnTi.

Chun Li , et al. , 2019 [68] prepared a hybrid joints consists of ZrO2 and Ti6Al4V also . The Zirconia ceramic was partially stabilized with Yttria (3 mol% YSZ). The brazing process done at 870 ℃ for 10 minutes as brazing time with 10 ℃/min as heating rate. The initially parts (metal and ceramic) jointed by Ag-28Cu alloy and also Ag-21Cu-4.5Ti (wt.%) as filler alloy . SEM, XRD, and TEM were used to examine the interfacial micro-structure of the prepared joints. The resulting brazing seam is mostly composed of Ag solid solution (Ag(s,s)) phase and also Cu phase as solid solution (Cu(s,s)),in addition to fine Ti3Cu3O secondary phases, that has been proven to be effective in releasing thermal stress. The maximum strength obtained from the prepared specimens was 95.6 MPa, in which 83.1% upper than that for the joints that brazed without inter-layers.

Changan Zhang, et al. , 2020 [69] a joints consists of ZrO2 as ceramic part with Ti6Al4V as a metallic part. The joining process occurs by Ultrasonic assisted brazing. the brazing temperature was 700 ℃ for 10 minutes in air atmosphere. (Aluminum – 5 silicon wt.%) alloy used as filler alloy. SEM, XRD, and TEM were used to examine the interfacial micro-structure of the prepared joints. The resulting phases appeared in the micro structure were $Ti(Al,Si)_3$ phase and also $Ti_7Al_5Si_{12}$

phase. The joint's average shearing strength peaked at 90.68 MPa, with two major categories of shear strength.

Weibing Guo, et al. 2020 [70] First principles calculations were used to investigate the interface bonding process Titanium element with ZrO2. The interfacial bonding processes were investigated utilizing work of adhesion principal , electrical behavior, and the energies of the interface on two types of interfaces having varied termination and mounting sequences. The results demonstrate that Titanium and Oxygen create a strong ionic covalent connection at the Exterminated contact, When ZrO2 is brazed with Ag- Ti as filler metal, the contact tends to generate TiO compounds.

Yuzhen Lei, et al. , 2020 [71] achieved a joints consists of metallic part (pure Titanium) joined with ceramic part (ZrO_2). These two parts jointed by using the gold (Au) as filler metal. The brazing process done at 1150 ℃ for 10 minutes under vacuum atmosphere. SEM, XRD, and also EDS were used to examine the interfacial micro-structure of the prepared joints. The resulting phases appeared in the micro structure were Ti_2Au phase, the TiAu phase, the $TiAu_2$ phase, the $TiAu_4$ phase. The maximum shear strength was 35 Mpa for Ti/ Au/ ZrO_2 joint that prepared through this search. on the interface of both $TiAu_2$ and TiAu4 reaction layers, fractures began to form and spread.

Ashutosh Sharma and Byungmin Ahn , 2020 [54] achieved a joints consists of metallic part (Ti6Al4V) joined with ceramic part (ZrO_2). These two parts jointed by using the Ag-Cui Ti (Ag +28Cu +2 Ti% wt.) as filler metal then add CeO2 as reinforcement additives with (0.03 , 0.05 and 0.1 % wt.) to Ag-Cu filler. The parts was in lap -joint shape. The brazing process done at 950 ℃ for 10 minutes under vacuum atmosphere. The maximum shear strength was 22.3 Mpa for ZrO2/ Ti joint that joining by Ag-Cu-Ti filler with 0.05 % wt. of CeO_2 .

Sung Woo Park and et al. ,2020 [72] prepared joint of Zirconia with Ti-3Al-2.5V alloy using amorphous $Zr_{54}Ti_{22}Ni_{16}Cu_8$ as active filler alloy. Ti/graphene/ZrO2 blocks were jointed in a graphite dies at temperature 1200 ^{0}C for time of 60 minutes under vacuum atmosphere about 10^{-2} Pa and also under 10 Mpa as mechanical pressure applied through hydraulic graphitic head. In order to compatriots, a pure Titanium with ZrO2 initial materials were jointed through using same processes at 1200 ^{0}C. the brazing process done at temperature ranged as (800 ◦C - 860 ◦C). the highest strength was (186 Mpa) obtained for specimens brazed at 860 ℃.

Yong Xian, et al. , 2020 [73] 3 mol% Y_2O_3-stabilized zirconia (3Y-TZP) discs with Titanium discs was joined by Graphene Nano-platelets (GNPs) as joining agent with diameter average(5–10 μm) and also (3–10 nm) thickness inside graphitic dies at 1200 ℃ for time about 60 minutes below high vacuum about (10^{-2}) Pa and some pressure about (10 Mpa) through hydraulic graphitic heads. Then, compared with direct Ti-ZrO_2 joints that prepared by same steps at 1200 ℃. The strength of the Ti/graphene/ ZrO_2 prepared joints been increased by (48.5 ± 7.0 Mpa) despite of no new phases formed in the joints. Carbon diffusion limits the available interstitial and vacancies for Titanium, Oxygen, and Zirconium diffusions, delaying inter-diffusion among Ti and ZrO2 and creating a favored diffusion bonding to improve Ti-ZrO2 joint strength.

2.12.1 Summary of Literature Survey

Table 2-4 illustrated the summery of literature survey

Reference no.	Used base materials	Brazing process conditions	Tests
[57]	$AI_2 0_3$, ZrO2, Ti6A14V (Cu-40Ag-5Ti) as filler	5min,vacuum furnace ,870°C	TEM, XRD. and Tensile test
[58]	ZrO_2/ Ti /ZrO_2 , ZrO_2/Pt/Ti /ZrO_2 and ZrO_2/ Pt/ Ti6Al4V /ZrO_2	(1162 to1494°C)	SEM
[59]	(3Y-TZP) , Ti6Al4V , (TiNi) clad		Biocompatibility
[60]	(3Y-PSZ),pure titanium, (63 Ag35.25 Cu1.75 Ti)	Vacuum , 840 to 870 °C	SEM ,XRD and EDS
[61]	ZrO_2-3 mol. %Y_2O_3 to Ti6Al4V by using a Ti_{47}-Zr_{28}-Cu_{14}-Ni_{11} (at.%)	1123 to 1273 K under high vacuum	microstructures and shear strengths
[62]	ZrO_2 and Ti6Al4V alloy through using a Ti_{33}-Zr_{17}-Cu_{50} (at.%) as amorphous filler	(1123 to 1273), 10 minutes	SEM, XRD, shear strength
[63]	ZrO2 to Ti6Al4V NiCrSiB with amorphous structure as filler alloy.	brazing temperature ranged from (950 to 1050 ℃) with heating rate for (20 ℃/min). the brazing time was 10 min under vacuum atmosphere.	The microstructure analysis and phases done by SEM and XRD analysis.
[64]	pure Titanium , ZrO2 with Yttria (Y-TZP) , Ag-28Cu alloy and Au-18Ni alloy.	700 to 750 ℃ for socking time of 10 minutes.	SEM, XRD, shear strength
[65]	ZrO2 , TiAl alloy ,AgCu as foil	(860 to 940 °C) , 5 to 30 minutes.	Impact , SEM

		vacuum furnace,	
[66]	ZrO_2,**Ti-6Al-4V**) ,AgCu alloy as filler metal.	(1123 to 1273), 10 minutes	SEM, XRD, and TEM
[67]	(ZrO_2-Ti6Al4) which brazed by using AgCuSnTi (Ag-35 wt. %Cu while Sn and Ti were added in minute concentrations	(750 ℃) for brazing time of(30minutes) by using high vacuum furnace	compressive strengths
[68]	ZrO2, Ti6Al4V, Ag-28Cu, Ag-21Cu-4.5Ti	870 ℃ for 10 minutes	SEM, XRD, and TEM
[69]	ZrO2, Ti6Al4V by direct joining	700 ℃ for 10 minutes in air atmosphere.	SEM, XRD, and TEM
[70]	Titanium, ZrO2	(1162 to1494°C)	SEM, shear strength
[71]	Titanium, ZrO_2 , ,(Au) as filler metal.	1150 ℃ for 10 minutes under vacuum atmosphere.	SEM, XRD, and also EDS, shear strength
[54]	Ti6Al4V, ZrO_2 Ag-Cui Ti (Ag +28Cu +2 Ti% wt.) as filler metal then add CeO2 as reinforcement additives with (0.03, 0.05 and 0.1 % wt.)	at 950 ℃ for 10 minutes under vacuum atmosphere	Shear strength
[72]	Zirconia, Ti-3Al-2.5V$Zr_{54}Ti_{22}Ni_{16}Cu_8$ as active filler	1200 ^{0}C for time of 60 minutes under vacuum atmosphere	SEM, shear strength
[73]	(3Y-TZP) discs, Titanium discs, Graphene	1200 ℃ for time about 60 minutes	Shear strength

Chapter Three

Experimental Part

3.1 Introduction

In the current chapter, materials which were utilized and the essential experimental steps and procedures that have been achieved in the preparation of alloys and sample specimens for tests will be explained. This chapter also exhibited the sequential order of all operation as well as tests that were done in order to reach reliable results**.** The layout of experimental work is shown in figure (3-1).

3.2 Materials

3.2.1 Metals

The used metal is Titanium rod (Ti6Al4V ELI) from TOTSRIOS A TIMET Company with 10 mm diameter and 850 mm long cut up by wire cut machining by (DK7720, Germany) in training and workshop center in University of Technology into two deferent lengths (15mm and 7mm). The specimens were ground on a series of emery papers (silica carbide papers) with (400, 600, 800 and 1000) then cleaned by degreasing in acetone bath using ultrasonic vibration container and then dried by passing warm air over them.

3.2.2 Ceramic

The cylindrical ceramic specimens (diameter 10mm and 15mm length) used in this investigation were provided by Khorasan Science and Technology Park (KSTP)-Iran who manufactured it from a polycrystalline -Zirconia and Yttria. The chemical composition and purity illustrated in table (3-1)

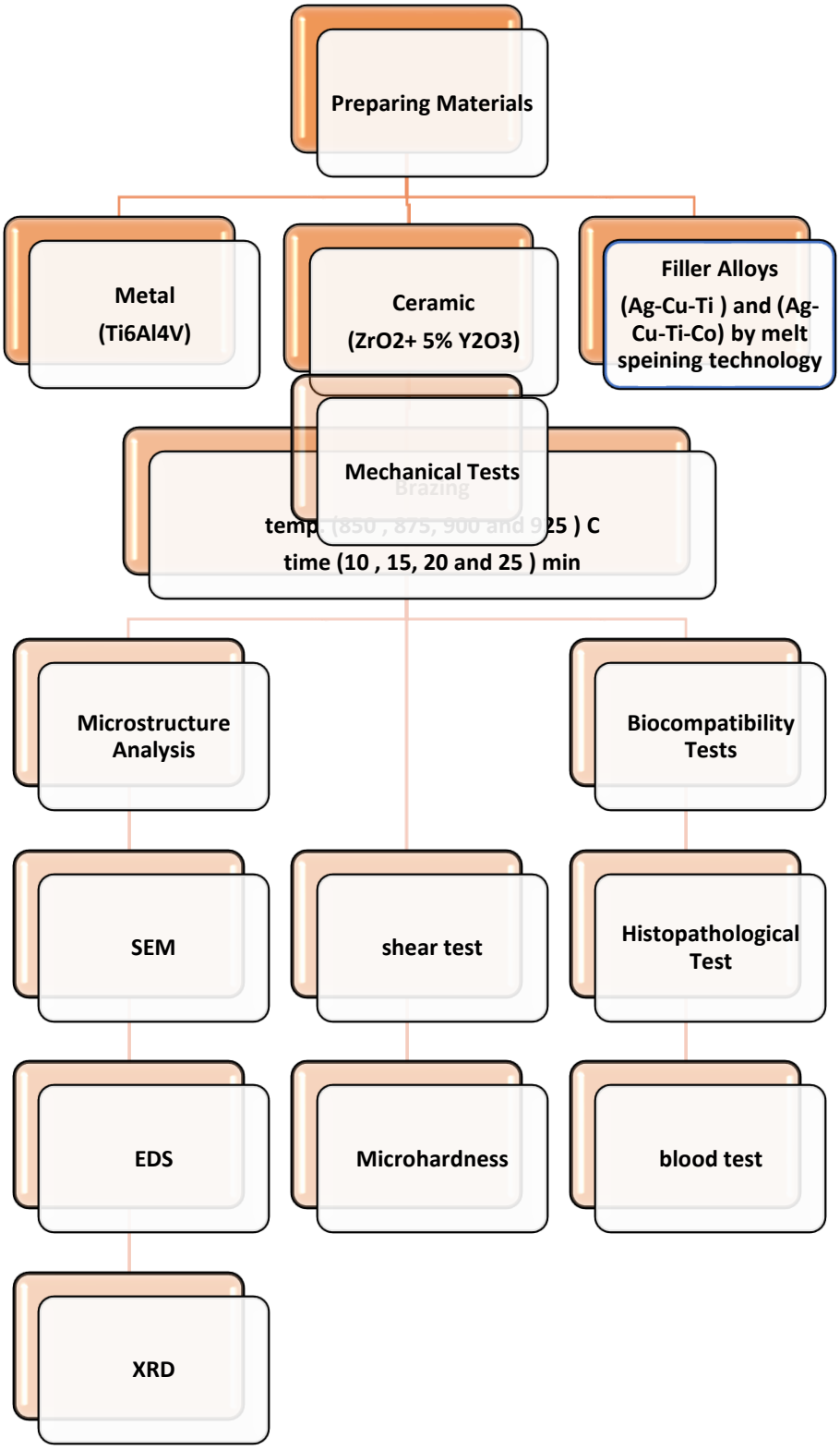

figure 3-1 : Experimental work layout

Table 3-1 : the chemical composition of used ceramic

Material	Formula	Purity	wt. %
Zirconia	ZrO_2	99.8	95
Yttria	Y_2O_3	99.9	5

The ceramic specimens were prepared with following presager[65]:

1. Calculation of dimensional change in sintering temperature with considering the production conditions of the specimens.
2. Design and manufacturing the mold according to final dimensions of the samples by using tool steel.
3. Preparation of Yttria stabilized Zirconia powders (PSZ)(95% wt. ZrO2 + 5% wt. Yttria) with (1-5) µm grain size.
4. Pressing homogenized powders using 5-ton load for 5 second by hydraulic compressor as shown in figure 3-2 B.
5. Sintering specimens at temperature of 1550 C^0 for 1 hour. Figure (3-2) exhibit the sintered specimens.
6. The ceramic specimens then degreased in acetone bath using ultrasonic vibration container (for 15 minutes) and finally dried by passing warm air.

Figure 3-2 : The prepared ceramics specimens

3.2.3 Filler Metal Alloys

The used metallic filler alloys prepared by melt spinning technique as following procedure:

The elements of the alloy (Silver as the main constituent, Coper, Titanium in addition to Cobalt) have been melted by mean of electrical furnace, the melting process was done in an inert atmosphere via pumping argon (Ar) gas with (99.999 % wt. purity of gas). The alloys have been casted composed of (68.8 % wt. Ag+ 26.7 %wt. Cu+ 4.5% wt. Ti) and (68.8 % wt. Ag+ 26% wt. Cu+ 4.5%wt. Ti + 0.7% wt. Co). Casting operation is done in the following sequence: Firstly, the furnace heated to 980 C .then, silver (as small balls) was placed in the container in order to be put in the furnace under a air atmospheric condition till silver completely melted subsequently Cu (as small balls) is gradually added. The molten is kept in the furnace to be super-heated for ten minutes. Then, the inert atmosphere was made immediately by introducing the inert gas (Ar) tube in to the crucible subsequently Titanium (as powder after cover it by copper sheet with 0.1 mm is added at once.

The melt then poured in to crucible with an orifice of 1 mm in diameter at a distance of 2 mm from the spinning copper wheel from TOTSRIOS A TIMET Company rotating at 3200 rpm. The melt solidifies as ribbon of small thickness shown in figure (3-3). The high speed of solidification prevents the formation of long-range order instead short rang order is formed [90] .Figure 3-4 showed the Solidified Ribbons Produced. The second filler alloy prepare in same procedure but add Cobalt (as powder) with Titanium after cover them by copper sheet.

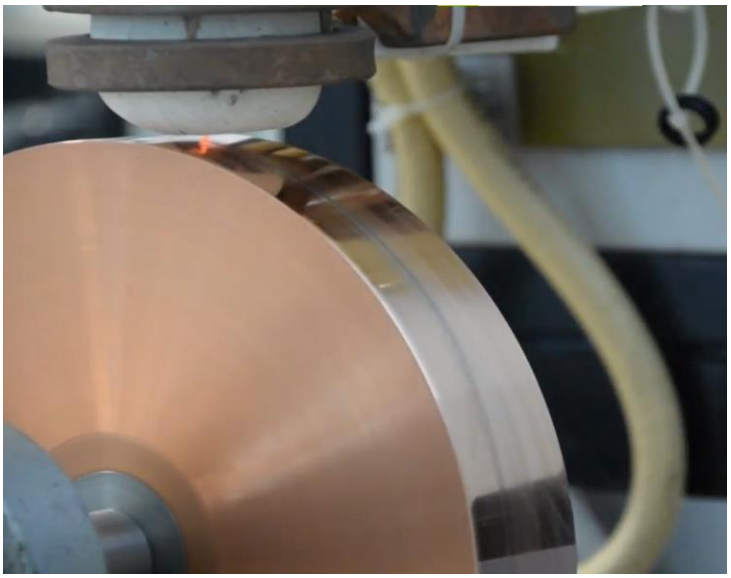

Figure 3-3. A: rotating copper disk, B:Schematic Melt Spinning Technique[90].

Figure 3.4 The Solidified Ribbons Produced.

The chemical analysis of initial materials and the resulting filler metal alloys were carried out by the device Niton XRF Analyzer device (Gun Spectro) at the Karbala Refinery Project Karbala. The device was made in 2013 in the United States of America (USA- NITONE instrument Model XL2 800). Table 3-2 illustrated chemical composition of initial metals and casted alloys. For each specimen, using 0.2 g of filler alloy after mix it with 0.05 cc glycerin.

Table 3-2 The chemical composing of initial materials and resulting fillers alloy from XRF test.

Material	Ag wt.%	Cu wt.%	Ti wt.	Co wt.	Other elements wt.%
Silver balls	99.5	-	-	-	0.5
Copper balls	-	99.2	-	-	0.8
Copper sheet	-	98			2
Titanium powder	-	-	99.9	-	0.1
Cobalt powder	-	-	-	99.9	0.1
Filler 1 alloy	68.6	26.5	4.1	-	0.8
Filler 2 alloy	68.7	25.7	4.2	0.5	0.9

3.3 Prepare Amorphas Alloy

Amorphous alloys (super cooled alloy) were used as brazing fillers. They have been stated to enhance atomic diffusion also develop the surface reactions throughout brazing procedure. Furthermore, they are also reported to reduce brazing temperature in order to diminish residual stress that generated in the brazed joint which in turn increases the strength of the brazed joint. They similarly have greater wettability as compared to atomized powders or paste formulations which necessitate large gaps within the joints for fillings[61]. Thus, to increase the amorphous structure in alloy added dry ice on the rotating disk. Dry ice used to accelerate the cooling rate of solidified brazing filler alloy. The rotating disk was immersed by dry ice (about -78 ^{0}C) for 3 hours and measured the disk temperature while it not rotated.

The minimum reached degree to the disk was (-3) measured by thermal imager (Fluke Ti300, USA) as shown in figure (3-5). Then follow the same procedure of

melt spinning technology to get the amorphous alloy. The produced alloy tested by X-ray diffraction test to show the amount of amorphous degree.

A B

Figure 3-5: a-The used thermal imager, B- the disk cooling degree

3.4 Furnace Brazing

An electrical furnace figure (3-6) was used in the present work for brazing zirconia to Ti6Al4V . The device model is VBF-1200X-H8 , USA. The furnace chamber has a quartz tube shape of a dimensions of (190mm inside diameter) and (300mm length) with set up as horizontally. It was designed to be used under vacuum or various other gas atmospheres with a temperature up to 1100˚C. The flow rate of argon gas is 5L/min. The process was carried out in the Metallurgical Laboratory, Mechanical Engineering Department, University of Karbala.

Figure 3-6 the used tube furnace in brazing process.

The specimen of Ti6Al4V with PSZ brazed by filler 1 and filler 2(as in table 3-2) alloys powders. The heating rate of the furnace was (25 deg\min) but cooling rate (3 deg\min) under argon gas through heating, holding and cooling step until 200 ^{0}C then close the gas and keep the specimens in the furnace to room temperature as shown in figure (3-7).

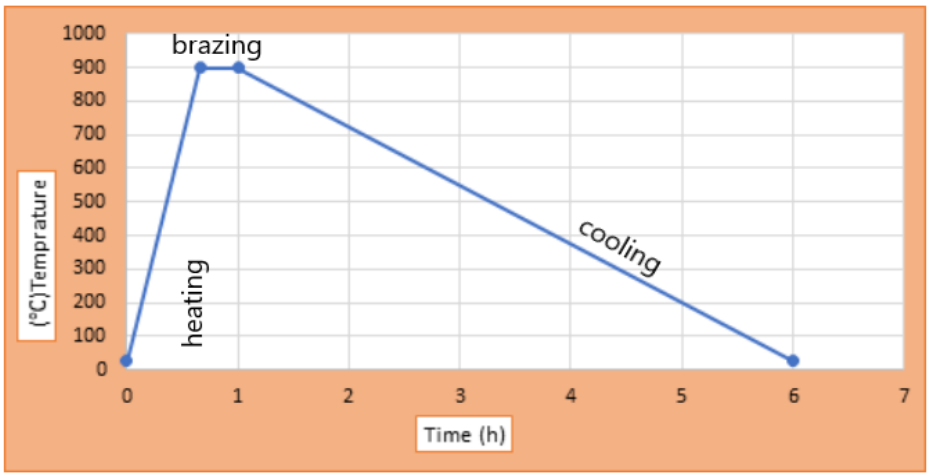

Figure (3-7) the thermal cycle for brazing process

3.5 specimen fixture

The used fixture was made from 2mm tool steel rectangular pieces and 2 screws with 10mm diameter. The specimen fixed in the fixture as shown in figure (3-8) while the ceramic part in bottom and metallic part in up with filler alloy powder between then. After put the parts in the fixture applied some load by screws just to fix the parts then placed in the furnace.

Firstly, chose time 10 and 15 minutes as brazing time but the joints were very weak and broke as some as them took out from the fixture. Then, chose time 20 minutes as brazing time. The brazing conditions included heating the specimens from room temperature to (850, 875, 900 and 925 ^{0}C) for 20 minutes to study the effect of temperature on the joint strength and diffusion of the filler alloys in ceramic

and metal parts. In addition to study the effect of brazing time on the joint properties (10 ,15,20 and 25 min) was used.

Figure 3-8: Fixture of single butt joint

Table 3-3 illustrated the prepared samples with all try and error cases .

3.6. Microstructure Characterization

3.6.1. X – Ray Diffraction Analysis

Both prepared alloys as well as brazed specimens have been tested individually by means of XRD techniques to examine the phases that presented in the alloys.

The XRD apparatus used to test specimens is of a model (SHIMADZU LabX XRD-6000), manufactured in Japan in ceramics and building materials department – university of Babylon as shown I Figure (3-9)**.** Cu was used as a target in XRD machine, Kα radiation with a wave length of (λ) 1.5406 A^o, and Ni filter. The scan rate of the diffractometer was selected to be (5^o/ minute) while the diffraction angle ($2\theta^o$) was chosen in a certain range of (30^o to 80^o).

Table 3-3 showed the prepared samples with try and error cases.

Sample No.	Sample Dimensions	Used Base Materials	Brazing Process Conditions (Temperature and Time)	Final Result of The Prepared Samples
1	15 mm ceramic 15 mm metal	ZrO2+ Ti6Al4V +Ag-Cu-Ti as filler alloy	850 C 10 min 850 C 15min 850 C 20 min 850 C 25 min 875 C 20 min 900 C 20 min 925 C 20 min	Failed Failed Success Success Success Success Success
2	15 mm ceramic 15 mm metal	ZrO2+ Ti6Al4V + (Ag-Cu-Ti – Co) as filler alloy	850 C 10 min 850 C 15 min 850 C 20 min 850 C 25 min 875 C 20 min 900 C 20 min 925 C 20 min	Failed Failed Success Success Success Success Success
3	7mm ceramic 7 mm metal	ZrO2+ Ti6Al4V +Ag-Cu-Ti as filler alloy	900 C 20 min	Success
4	7mm ceramic 7 mm metal	ZrO2+ Ti6Al4V + (Ag-Cu-Ti – Co) as filler alloy	900 C 20 min	Success

Figure 3-9 : XRD device.

3.5.2. Microstructure Observation

The brazed samples at each temperature (850, 875, 900 and 925 ^{0}C) at fixed time (20 min) and prepared filler alloy were selected to be tested with the aid of SEM to exam the microstructure and to identify each phase in the microstructure by the EDS equipped with the SEM image. Wet grinded was done firstly by a rotating Quartz disk, then grinding process with emery paper of fine grades(600, 800, 1000 ,1200, 1500, 2000, till 2500), polishing was done with the aid of diamond-paste. The polished specimens had been rinsed completely with distilled water then allowed to be dry in airflow, and kept for the minimum time possible before testing. Then examined under different magnification (500,1000,2000,4000 and 7000X for each specimen) using SEM that shown in figure (3-10). Scanning electron micrography was performed using SEM (TESCAN, Vega III/ Czech Republic)

Figure 3-10 The Scanning Electron Microscopy Used.

3.6 Single Shear Test

A universal tensile test machine (Microcomputer Controlled Electronic Universal Testing Machine) model (WDW-200E),2015, Germany, presented in the College of the Materials Engineering in Babylon University, with a cross-head speed of (1 mm per minute) has been set to carry out the test of Single Brazed Shear. The single shear test was done at room-temperature. The designed fixture was made-up from tool steel and costumed for converting the applied tensile stresses into a purely shear stress along the brazed line. All specimen surfaces have been ground also the edges were chamfered former to test so that stress concentrating would be avoided. Figure (3-11 A, B) displays the fixture diagram and the manufactured fixture respectively. Table 3-3 showed the mechanical properties of used base materials

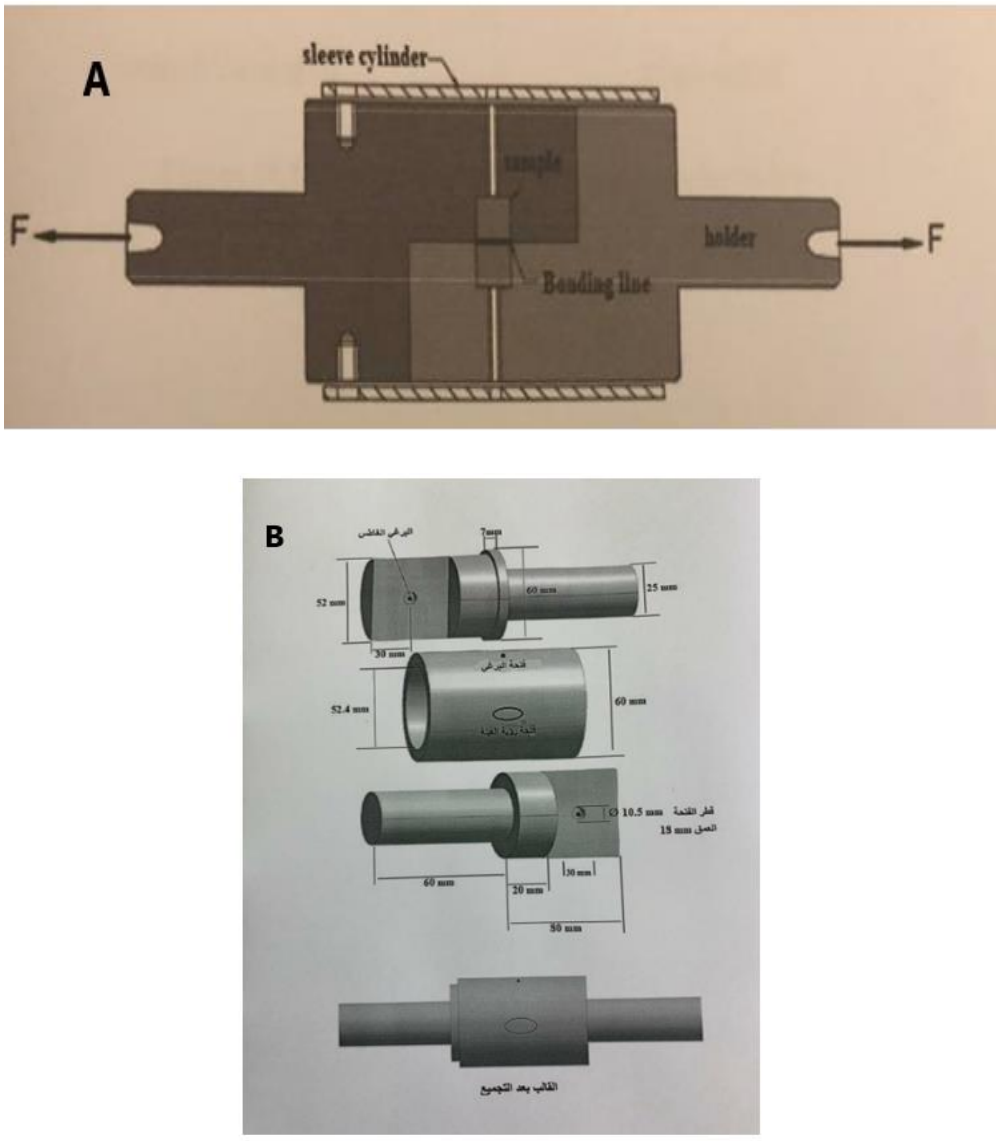

Figure 3-11: -Fixture schematic diagram,

3.7 Microhardness Test

Microhardness test was carried out according to ASTM E92 – 17, using Digital Vickers hardness tester of a model (HVS-1000), that presented in metals Laboratory/College of the Materials Engineering in Babylon University. The devise of Vickers hardness is shown in Figure(3-12). It has been used to estimate the hardness values of brazed specimens by applying load of 500 grams (10 N) and holding time of (15 seconds), with a square-base diamond pyramid. The hardness

readings were taken for the brazing area and adjacent areas (ceramic and metal) for each specimen. Hardness values (HV)were obtained by using the equation:

$$Hv = 1.8544 \frac{P}{d^2}$$

Were: p= applied load, Kg

d=average length of diagonal, mm

HV is the number of Vickers hardness in (kg/mm_2).

Figure 3-12: Vickers Hardness Tester

Table 3-4 illustrated the theoretical mechanical properties of the used base materials

Table (3-4) illustrated the mechanical properties of used base materials [66]

No.	Hardness	Shear strength
Ti6Al4V	36 **Rockwell**	40 GPa
Zro2 + 5% Y2o3	900 Mpa HV	33 GPa

3.8 Biocompatibility Test

Biocompatibility of the specimens and control materials was tested by animal implantation in vivo and blood test (systemic effect) .

3.8.1 Animal Models

A total of 30 males' adult Newsland rabbits weighing (1- 1.5 kg) were included in this study. All rabbits were examined by specialist, and kept under supervision for 14 days before testing to ensure that the animals were suitable for testing. The rabbits were housed bio technology research center, Al-Nahrain university in metallic cages, each cage for one rabbit, fed by pellets and green vegetables and supplied with water, kept at well-conditioned room temperature (25^0C) during the period of testing. The rabbits were grouped into 3 groups, 10 rabbits for each test as in table 3-4

Table 3-5 Rabbits grouping according to tested materials and times for biopsy.

Group	Time for biopsy taken	Filler 1 specimens	Group symbol	Filler 2 specimens	Group symbol
1	3 days	5 rabbits	G1F1	5 rabbits	G1F2
2	7 days	5 rabbits	G2F1	5 rabbits	G2F2
3	30 days	5 rabbits	G3F1	5 rabbits	G3F2

3.8.2 Sterilization

All instruments used in surgical procedure were sterilized in sterilizer at 150˚C for 2hours, using disposable instruments such as sutures, syringe and surgical blades, as shown in figure (3-13).

Figure 3-13 Surgical instruments

3.8.3Anesthesia

The anesthetic solution is ketamine HCL 1ml/kg mixed with xylazine hydrochloride 0.1ml/kg used an intramuscular injection. This dose was enough to keep the animal anesthetized during the surgical period, as shown in figure (3-14).

Figure 3-14 Intramuscular injection of anesthetic solution.

3.8.4 Implantation

The fur skin was shaved manually over the lower part of the back. This area was disinfected with a piece of cotton socked in Savelon disinfected solution. The shaved area was divided by vertebral column into right and left side. The

negative control case was in the right side, and on the left side the test specimen implanted and as showed in figure (3-15).

On the left side an incision of (1.5 cm) length was made through the skin of the rabbit with a blade No.10, as shown in figure (3-16 A). The subcutaneous supra muscular tissues were separated with blunt end instrument to create a pouch for the specimen as in figure (3-17B) .

Figure 3-15 the implantation areas after shaving process

A B

Figure 3-17: Surgical incision

The sample was held with a pair of tweezers and inserted in the pouch as shown in figure (3-18A), and the specimen pushed 5mm away from the incision line, as shown in figure (3-18 B). The control case on the right side of the rabbits back while the test specimen was implanted on the left side, each specimen was implanted away from the vertebral column about 2.5 cm.

A B

Figure 3-18: Specimen insertion.

The same procedure was repeated about 1.5cm anterior to the control sample, but without specimen implantation, which used as negative control. The incisions were sutured with a black silk suture. Then, the area was cleaned and disinfected with Savelon disinfectant solution, as shown in figure (3-19) ,and figure (3-20)

Figure 3-19 Suturing of the incision

Figure 3-20 Implantation the specimens, control on the right, test on the left, suturing incision and disinfection.

Antibiotic injection of 0.2ml/kg (oxytalin) was administrated intramuscularly after surgical procedure. The cage was sterilized by wiping the wall and floor of the cage with Savelon disinfectant solution then the rabbit kept in this sterilized isolated cage. Also, the weight of the rabbit was recorded for comparison with its weight during observation period.

3.8.5 Excisional Biopsy

At the end of the implantation periods the rabbit was anesthetized again. The site of the implantation was shaved if needed, cleaned and disinfected. The specimen was localized gently by palpation.

Then excisional biopsy was taken with sterile surgical blade No11.The biopsy involved the skin and included the embedded specimen with some of supra muscular tissue and (6±1mm) away from the specimen around each side, as shown in figure (3-21) and placed in 10% buffered formalin for 1day fixation. Then the biopsies were washed under tap water to remove the formalin for 20 minute after that the specimens were removed from the biopsies and continued the laboratory procedure, as shown in figure (3-22).

Figure 3-21: Biopsy of (6±1mm) away from the specimen around, include skin and seromuscular tissue

The second step was dehydration, in which the biopsies were socked in 70% ethanol alcohol for one day, and then, the biopsies passed through series of increasing concentrations of ethanol alcohol (80 ,90 and 100) % remaining in each concentration for two hours. Then, the biopsies transferred to xylol for 30 minute to get rid of any excess ethanol. Then, the biopsies were placed in small containers

containing melted paraffin wax and placed in an oven regulated at 60°C for 24hours. After that, the biopsies were placed in the center of metal molds. The molds were poured with melted paraffin to make blocks. The blocks were sectioned using microtome to get sections (5µm) thickness, were prepared from the

central part of the biopsies and surrounded tissues. For microscopical examination, three sections were taken from each biopsy and stained with Hematoxylin and Eosin (H&E) to prepare slides for histological examination under light microscope.

Figure 3-22 : Removal of the specimen from the biopsy

3.9 Blood Clinical Pathology

A blood samples of (10% of rabbit weight) [91] were taken from each rabbit before and after specimens implantation in order to estimate and compare (urea ,Creatinine , Albumin, ALT Alanine Aminotransferase enzyme , AST Aspartate Aminotransferase enzyme and ALP Alkaline Phosphatase enzyme) level before and after insertion of specimens. The blood sample was drowned from rabbit heart by syringe as shown in figure (3-23).

Figure 3-23 phlebotomy from rabbit heart.

The blood samples were kept in special blood collecting tubes (Vacutainer) so as to be tasted in centrifugal device in order to separate the blood plasma from other ingredients as shown in figure (3-24)

A B

Figure 3-24: A , blood samples in Vacutainer, B , centrifugal device.

Chapter four

Results and Discussion

4.1 Introduction

This chapter review in particular the results of the effect of cooling rate on the structure of prepared filler alloy. Also, estimate the effect of time and temperature on discoloration of PSZ. Microstructure and XRD results of the brazed joint have been exhibited. Then, explain the outcomes of conducted mechanical tests such as Microhardness and single shear strength. Biocompatibility results of the brazed joints have been reviewed.

4.2 Effect of Cooling Rate on Filler Alloy Structure

Figure (4-1A) illustrated the XRD patterns for slow cooling rate of crystalline eutectic Ag-Cu alloy. Figure (4-1B) showed XRD patterns for Ag-Cu alloy from crystal to amorphous then to nano scale crystal structure. Figure (4-2A) illustrated XRD patterns of filler 1(68.6Ag-26.5Cu4.1Ti) alloy prepared by rapid cooling. Figure (4-2B) shows the XRD patterns of eutectic Ag-Cu alloy prepared by supercooling (cooling the disk by dry ice).

Figure (4-2A) pattern shows wide peaks compared to the ordinary made Ag-Cu eutectic by casting and slow cooling rate Figure (4-1A) which is shows sharp peaks when the alloy is long range order (crystalline). The lake of sharp peaks in the test pattern reveals one meaning is that the alloy does not have a long rang order in the microstructure of the ordinary crystalline alloys. Supercooled alloy in figure(4-2B) demonstrates wider and shorted peaks than in rapid cooled alloys in figure (4-1B the gray line) which indicate that the alloy has short range order which is

approach to the nanomaterials as shown in Figure (4-1B) or amorphous materials (short range order) which is called metallic glas

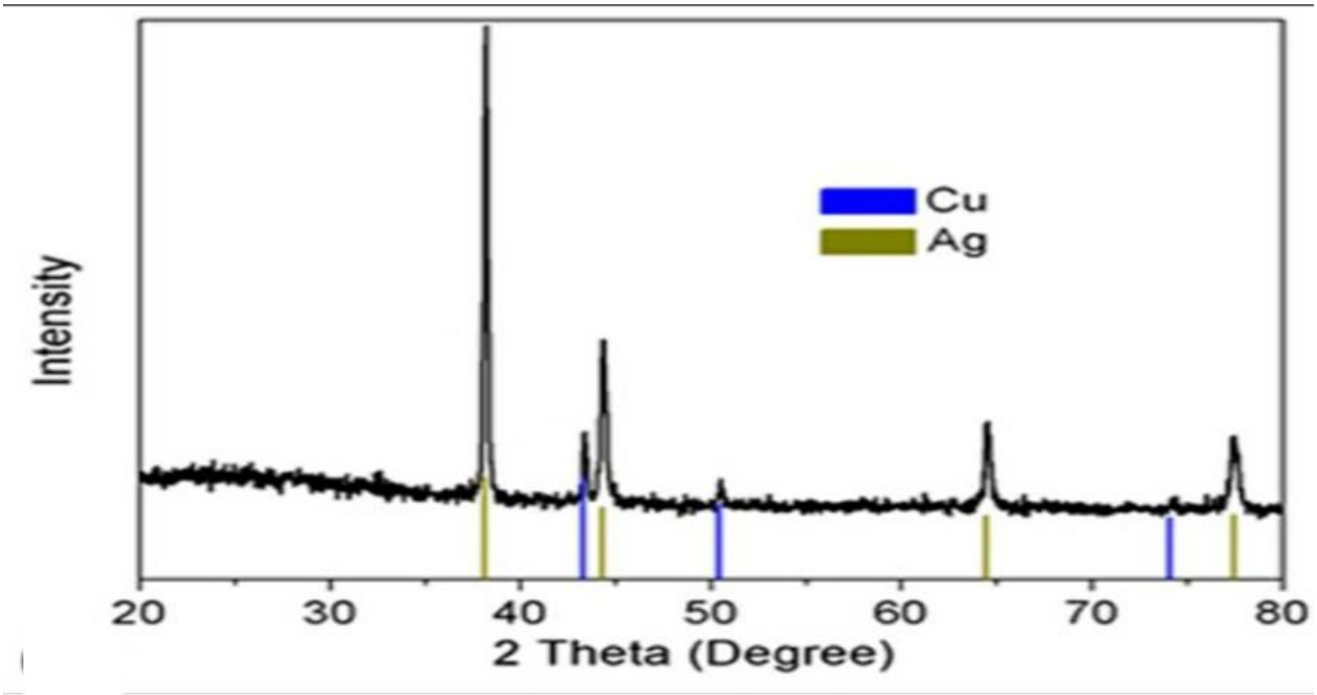

A

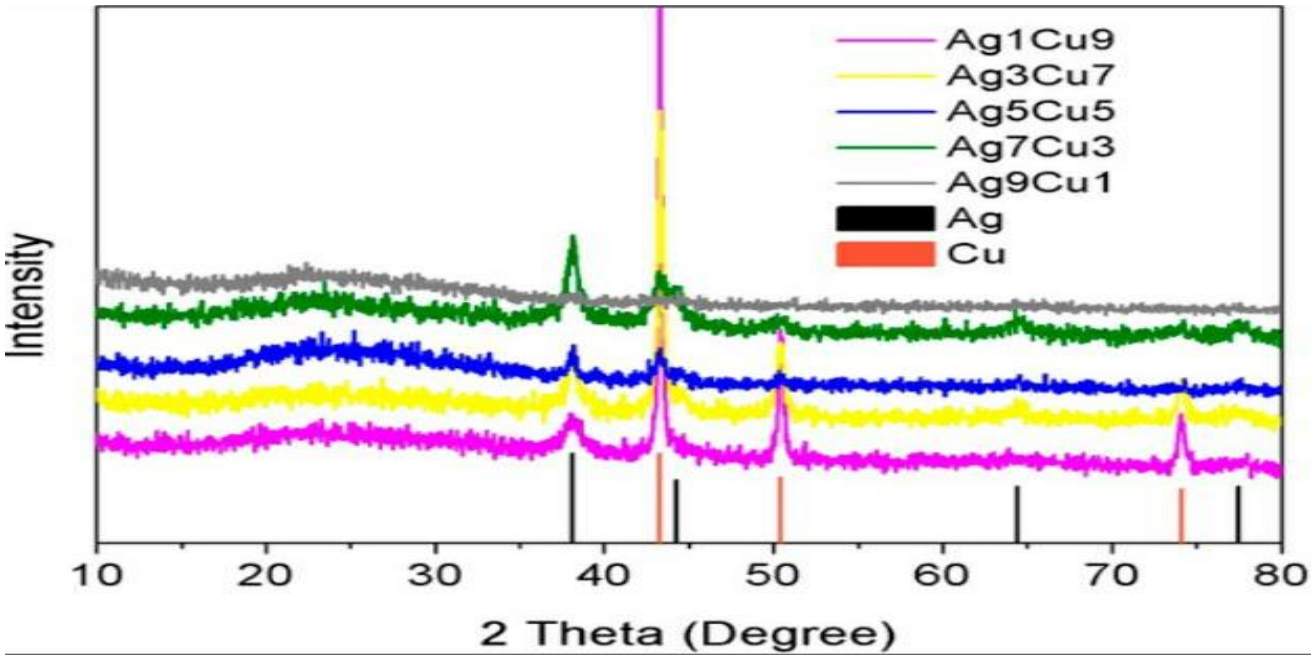

B

Figure (4-1) A-XRD patterns for Ag-Cu alloy prepared [92] , B- Ag-Cu alloy in nano scale [93]

A

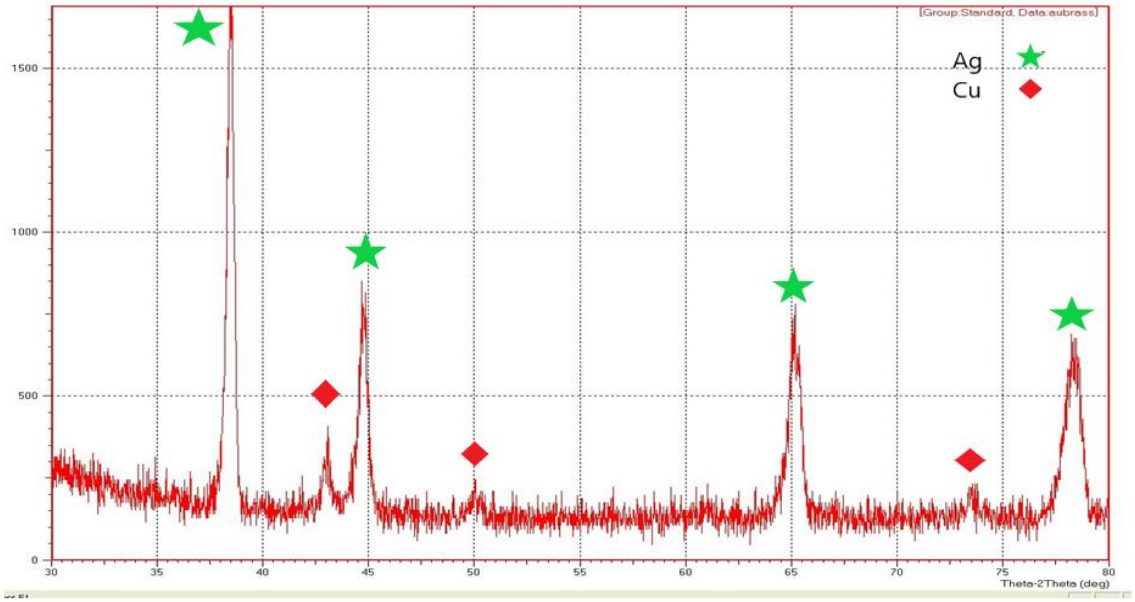

b

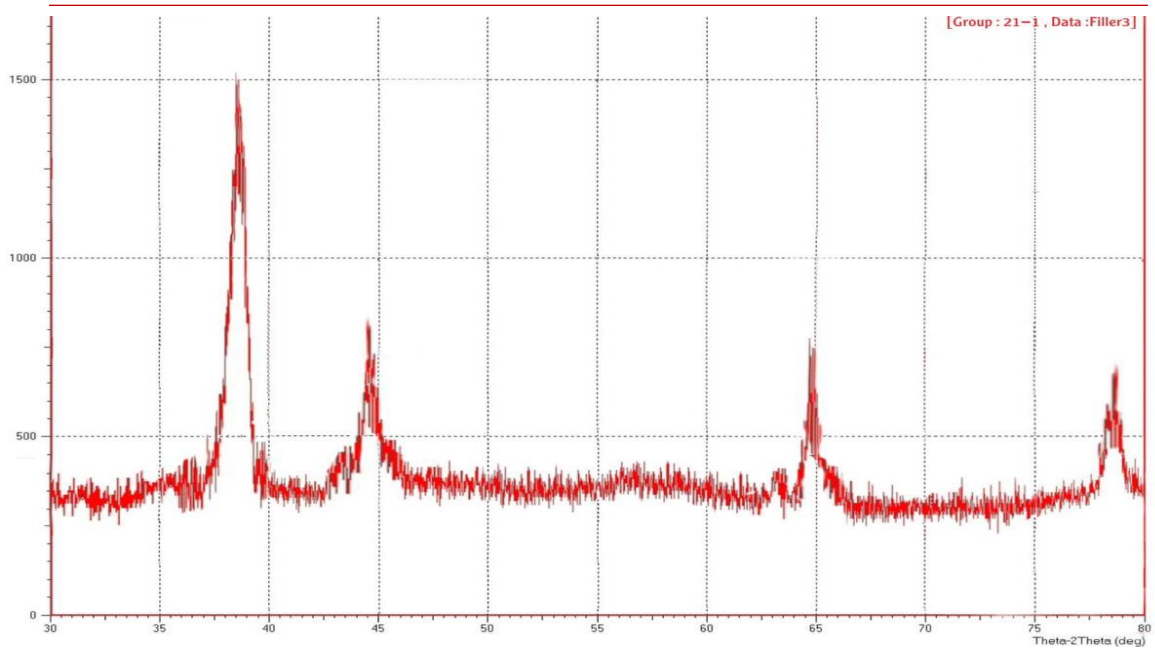

Figure (4-2) XRD patterns for filler 1 alloy: A-prepared by rapid cooling rate (melt spinning technology), B- prepared by super cooling rate (melt spinning technology with cooling the disk by dry ice)

These results are ascribed to influence of strain that leads to a slight expanding in the lattice parameters, then peaks are shifted to different diffraction angle. After crystal size is decreasing to nanometric-scale, the broadening in the diffraction peaks was noticed and the peak's width is straightly associated with the size of nano crystalline range which is agreeing with [94].

4.3 Effect of Temperature and Time on Discoloration of Partial Stabilizer Zirconia (PSZ)

At the interface between filler alloy with ceramic, the PSZ has undergone change in color from cream to black. The color is gradually becoming lighter with increasing the distance from the joint. The darkening phenomenon is affected by a number of factors including: temperature of brazing operation and time, the substrate to which the PSZ is being joined and the Ti amount in the brazing filler alloy [95].

Figure (4-3) illustrate the effect of temperature on discoloration of PSZ by Ti. As temperature increase the discoloration effect increase. Specimen brazed at temperature 925 ^{0}C as in figure (4-3D) exhibited the highest PSZ discoloration as compared with specimens that brazed at lower temperature 900, 875 and 850 ^{0}C which are shown in figure (4-3C) , (4-3B) and (4-3A) respectively .

The effect of time on the discoloration of PSZ illustrated in figure (4-4). With increasing the time of brazing the darkening effect had been increased, as can be noticed in figure (4-4D) which suffer the highest discoloration, while the discoloration becoming less gradually by reducing brazing time as in figure (4-4C), (4-4B) and (4-4A) respectively.

Zirconia is highly sensitive to changes in its stoichiometry (with the color changing detected when it being reduced), in which zirconia might lose oxygen because of the higher chemical affinity of active constituent in the filler alloy (Ti)

for oxygen, which causes Oxygen deficient region that looks dark. The consent that formation of TiO phase results in the reduction of PSZ from its stoichiometric composition on the interfacial region , thus causing the discoloration of PSZ ,this agree with [13].

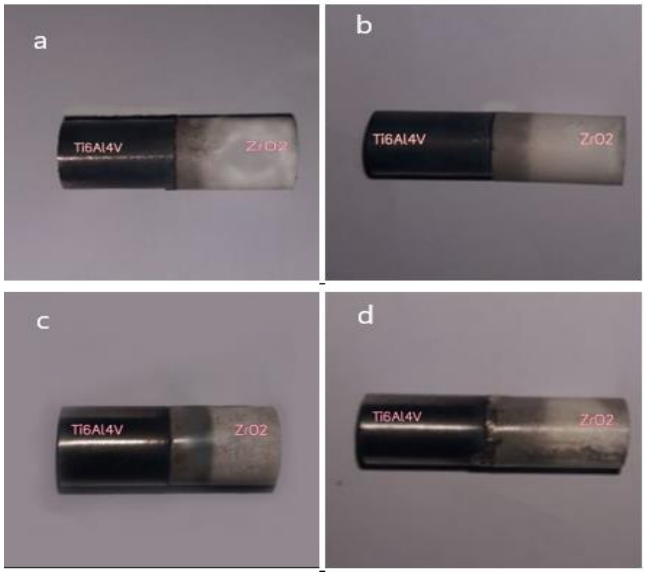

Figure 4-3: Discoloration of PSZ brazed for 20 min at temperatures of A-850 ,B875, C- 900 and d-925°C

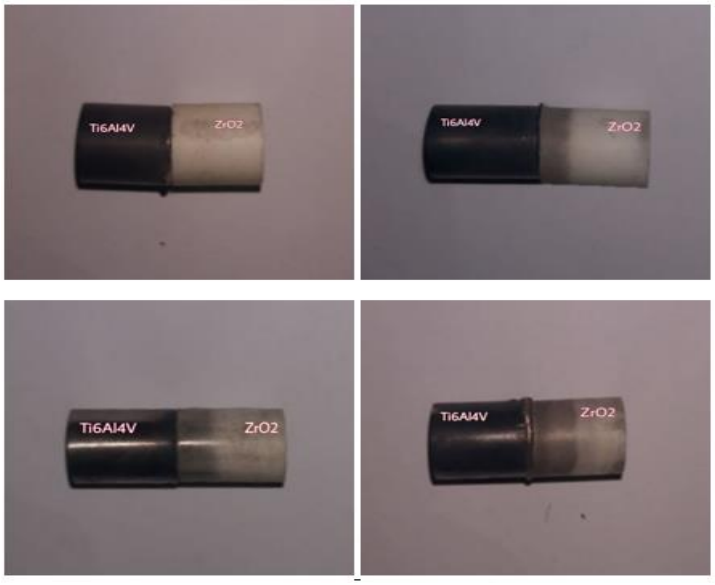

Figure 4-4: Discoloration of PSZ brazed for 900 C at time of : A- 10 , B-15, C- 20 , D- 25 min.

4.4 Microstructure Analysis

Figure (4-5) illustrated SEM image for Ti6Al4V / filler1 /ZrO_2 joint brazed at 900°C for 20 minutes. The SEM image illustrated two main regions: diffusion zone spot 1 (the region between Ti6Al4V and filler1 side) and the brazing region spot 2 and 3 (Zirconia to filler1 side). The EDS analysis results illustrated in Table (4-1) according to figure (4-5). According to figure1, the diffusion zone which show the region between Ti6Al4V/ filler1 there are white and black spots. EDS results (Table 4-1) showed high concentration of Cu-Ag and Ti in this region. In point A and B The Cu/Ti was about 1:2 (20.3 at. %Cu – 55.3 at. % Ti and 24.3 at. % Cu – 51.4 at. % Ti respectively) which represent as the black spots. While, the Ag concentrations (in the white spots) were 22.4 at. % in point A and 23.3 at. % in point B. this region called Zebra region.

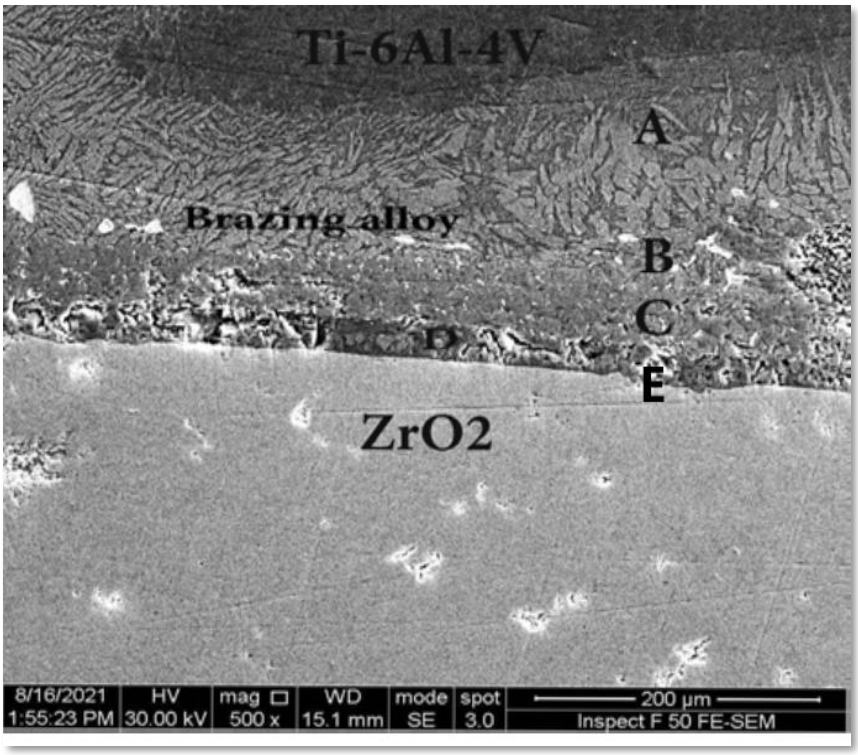

Figure 4-5 : SEM image of bond layer (Ti6Al4V / Ag-Cu-Ti filer/ZrO_2 joint brazed in 900°C for 20 min) .

Table (4-1): EDS chemical analysis (at%) of different positions of the joint in figure4-6.

	Ag	Cu	Ti	Al	V	Zr	Y	O
A	22.4	20.3	55.3	1.65	0.35	-	-	-
B	23.3	24.3	51.4	1.12	0.18	-	-	-
C	66.8	18.1	11.9	2.7	0.5	-	-	-
D	9.2	7.4	57.7	-	-	13.0	0.6	12.1
E	0.2	4	29.7	-	-	43.7	3.6	18.8

TiCu and $TiCu_2$ phases formed in black spots (see figure 4-6). While, the white spots were rich in Ag. It was recommended that copper has a high tendency to form an intermetallic compound with titanium, and silver has less activity than copper in of Ag-Cu filler alloys and low ability to diffuse in the TiCu and $TiCu_2$ films; since, the Ag concentration has unusually risen the active action of filler alloy to diffusive from higher concentration to low concentration of elements such as titanium, copper and others. The diffusive elements support interfacial reaction with officially constant ceramic. Zebra region play an important role in decreasing the residual stresses that produced as a results of cooling process. On the other hand, titanium is more active element and react with oxygen in ceramic to form reaction layers contain titanium oxides that have properties close to metal and enhance the wetting of ceramic. The present of other elements like V, Cr, Zr or Ta can increase the activity of the filler in brazing process of metals-ceramics this result agree with Feng , et al. [65].

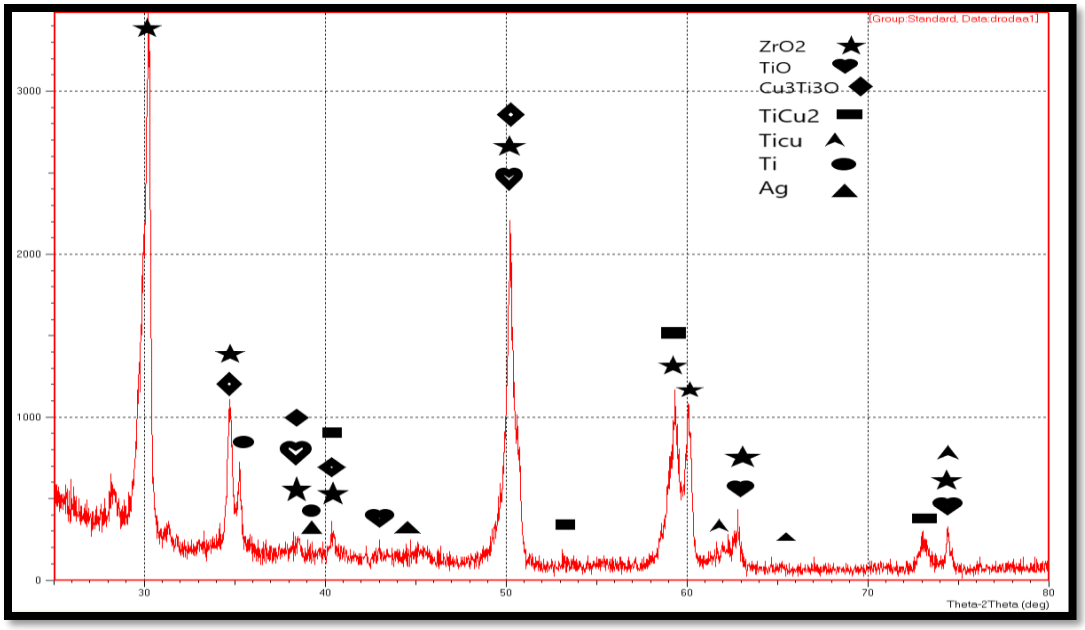

Figure 4-6 : XRD patterns for (Ti6Al4V/ Ag-Cu-Ti filer / ZrO_2) joint brazed in 900 ℃ and 20 minute.

Obviously, in the brazing zone (in point C) (see figure 4-7 the EDS results pointed to intelligible increase in Ag amount (66.8 at. %) on expense of Ti and Cu (11.9 and 18.1 at. %) which can be attributed to withdraw the copper from the filler alloy and react with Titanium to form TiCu and $TiCu_2$ phases. The reaction incomes in many steps. Through brazing, after the temperature is overhead solidus line of filler alloy, many elements might diffuse to both other sides across the interlayer. As, the filler dissolves, Ti is diffuse in the molten filler alloy then interacts with copper. Silver inhabits solid solution medium of the filler. The Cu-Ti phases at the boundaries formed and growth in path instantaneously between Ti and ZrO_2. ZrO_2 is attached under the effect of Ti that absorbed in surface apertures by the action of capillary action at ZrO_2 sides .This result agree with Smorygo , et al. [60].

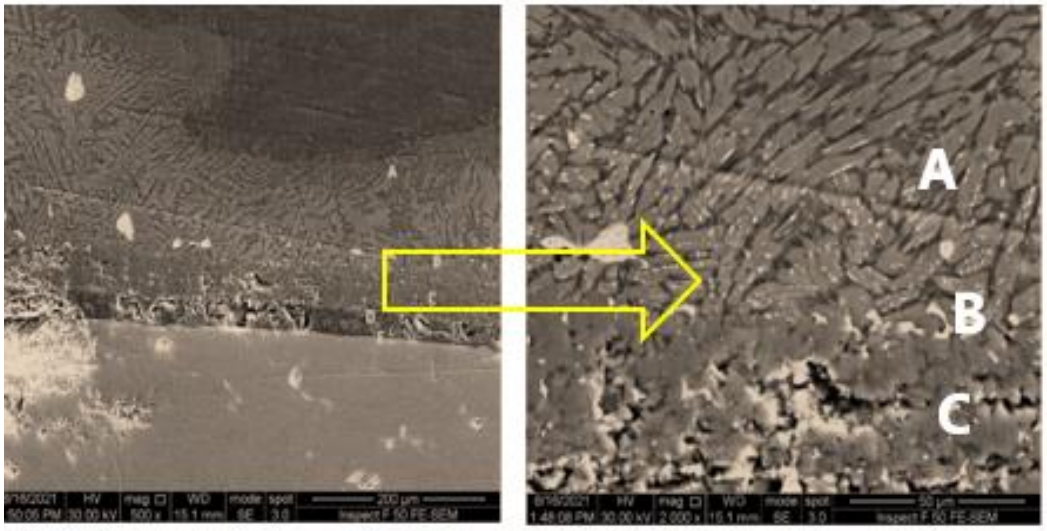

Figure 4-7 :- SEM image for Ti6Al4V / Filler interface .

Figure (4-8) showed SEM image for ceramic / filler 1 interface. In point D and E, titanium reacted with ZrO_2 and Y_2O_3 to form TiO phase which was required to improve the wettability of the filler alloy on ceramic side of the joint. TiO phase formation occurred due to diffusion of Ti in to ZrO_2 ceramic according to following equation;

$$ZrO_2 + Ti \rightarrow ZrO_{2-x} + TiO \quad \ldots \quad \text{eq 1 [66]}$$

TiO phase caused the darkening effect in ZrO2 side due to draining the oxygen from ZrO_2 and Y_2O_3 as in equation 1.this result agree with Dai , et al. [66].

It is observed from EDS analysis (Table 4-1) points D and E have different concentration of titanium and oxygen. Point D has rich in titanium and may be titanium react to oxygen to form titanium oxide rich in titanium, while point E has less titanium concentration and may be formed TiO in this region.

All SEM images for joined specimens showed the presence of vacancy , porosity and cracks in the joining line which may attributed to cooling process.

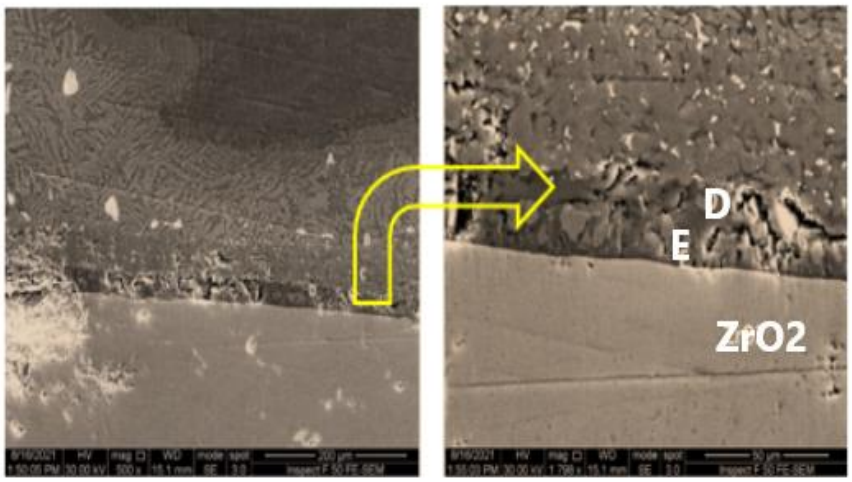

Figure 4-10 : SEM image for Ag-Cu-Ti filer / ZrO_2 joint brazed in 900 ℃ and 20 min.

4.5 Single Shear Strength Results

Table (4-2) showed the single shear strength for Ti6Al4V/ ZrO_2 joints brazed by filler 1and filler 2 alloys in different temperatures (850 ,875 ,900 and 925 ℃ at 20 minutes).

Table 4-2 : illustrated varied the shear strength with temperature for prepared joints .

No.	Temperature (℃)	Shear strength (MPa) Ti6Al4V/filler 1/ZrO_2 joints	Shear strength (MPa) Ti6Al4V/filler 2/ZrO_2 joints
1	850	18.3	19.4
2	875	20.04	22.1
3	900	18.7	18.9
4	925	17.5	18.4

Figure (4-11) showed the effect of temperature on the single shear strength for Ti6Al4V/ ZrO_2 joint brazed by Filler 1 alloy. From figure (4-11), the maximum shear

strength was 20.04 MPa at temperature 875 ℃. Where, it can be observed that there is an increasing in shear strength by increasing temperature till arrives to 875 ℃. Then, the shear strength becoming lower gradually with increasing temperature.

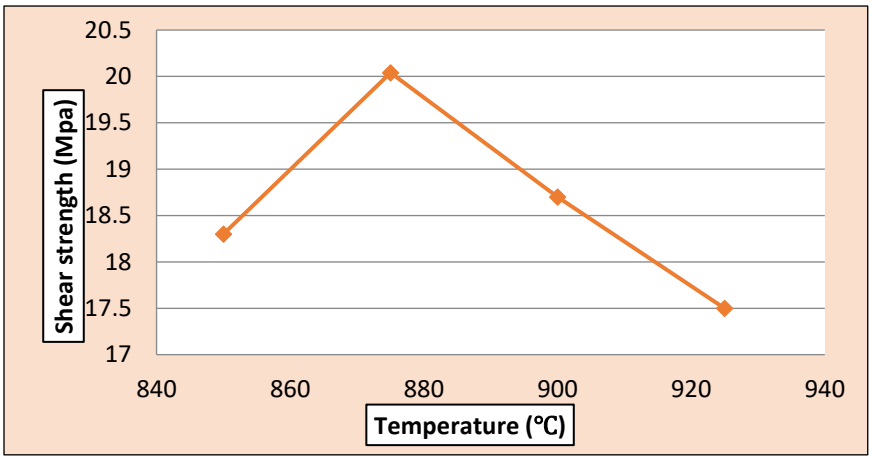

Figure 4-11: the effect of temperature on shear strength for Ti6Al4V/ Filler 1 /ZrO_2 joint brazed at 20 minutes.

Figure (4-12) illustrated the variation in shear strength with brazing temperature to Ti6Al4V/ Filler 2 (68.7Ag-25.7Cu-4.2Ti-0.5Co) /ZrO_2. from the figure it's can be notice that the maximum shear strength was 22.1 MPa at 875℃ . the shear strength increases with increasing brazing temperature until arrive to maximum value then start decrease with increasing temperature.

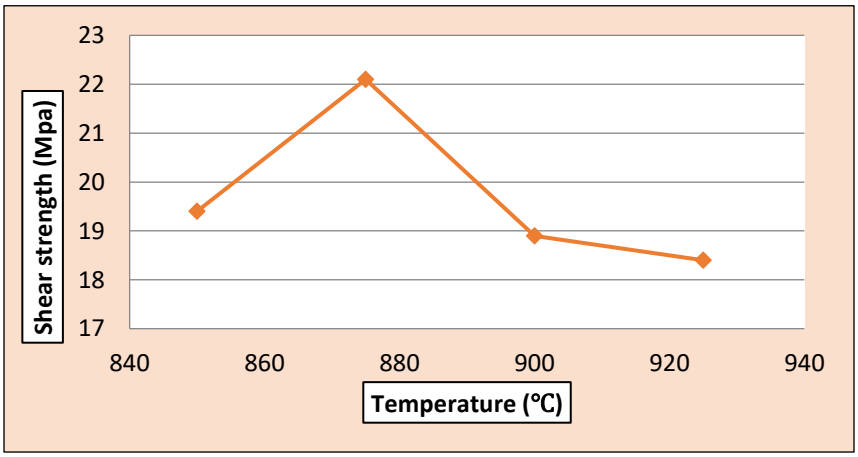

Figure 4-12: the effect of temperature on shear strength for Ti6Al4V/ Filler 2 /ZrO_2 joint brazed at 20 minutes.

Difference of the brazing temperatures affected the shear strength of the brazed joint in two facets. First and foremost, increasing temperature of the brazing improved the width Ti-Cu (TiCu and $TiCu_{2)}$ and TiO layers next to ZrO_2 ceramic, which directly affecting the shear strength of the bond. By decreasing temperature of brazing, the interfacial reaction was deficient and lead to reduce joint properties. As the temperature of brazing raise the growing of the reaction layer promoted next to ZrO_2 ceramic. Increasing the reacting layer thickness could result in high residual stress through the joint which dropping the joint shear strength. Secondly, the temperature of the brazing similarly influenced the magnitude of Ti–Cu phases. A high occurrence of brittle Ti-Cu through the joints might weaken the capability of silver based solid-solution to overcome the plastic distortion, that might result in an increase in the amount of residual stresses which in turn could reduce the joint shear strength [66].

From figure (4-11) and (4-12), it can be noticed that maximum shear strength of the brazed joints in the case of filler 2 was slightly higher than that in filler 1. It's can be attributed to additives of Cobalt element. The addition of Cobalt to Ag-Cu filler alloy play an important role in increasing the wettability of the filler alloy especially on the ceramic side .this result agree with KAIWA , et al. [97].

Figure (4-13) showed the SEM image of fracture surface for ZrO2/ Filler 1/Ti6Al4V joint brazed at 850℃ for 20 minutes. While, figure (4-14) illustrated the SEM image of fracture surface for ZrO2/ Filler 1/Ti6Al4V joint brazed at 925℃ for 20 minutes. Table (4-3) outline the EDS results for both specimens in different positions as installed on images. Figure (4-15) showed XRD patterns for fracture surface of ZrO2/ Filler 1/Ti6Al4V joint.

Noteworthy, there are two kinds of fracture surfaces resulted from single fracture test. First kind at low brazing temperature (850℃) as in figure (4-13). In this kind the fracture bath started from interlayer between ZrO_2 / filler 1 and progress with a flat fracture form. According to EDS Results, point a (area1) is mainly consists silver solid solution. While, points b and c contained high amounts of titanium, copper and oxygen then the possible phases in this area (area 2) are TiO and $TiCu_2$ (see figure (4-15)). These phases have an excellent plastic nature. While, at high brazing temperature (925℃) the fracture starts in the interlayer between ZrO_2 and Filler 1 then move toward the joint region with a fluctuating fracture form. According to EDS results, the possible phases appeared in d and e points (see figure 4-14) are $TiCu_2$ and ZrO_2 respectively. $TiCu_2$ phase played the main rule in initiation of the crack due to high plasticity then propagate toward the joint region. This result agree with Feng , et al. [65].

Table (4-3): EDS chemical analysis (at%) of different positions of the joint in figure (4-13) and (4-14)

	Ag	Cu	Ti	Al	V	Zr	Y	O
A	69.4	16.3	8.4	0.7	-	-	-	5.2
B	5.3	24.6	36.4	7.12	-	-	-	26.58
C	3.8	8.4	12.9	1.83	-	35.6	-	37.47
D	1.67	55.9	27.6	9.3	1.8	-	0.6	3.13
E	0.2	-	12.8	0.9	-	40.7	3.6	41.8

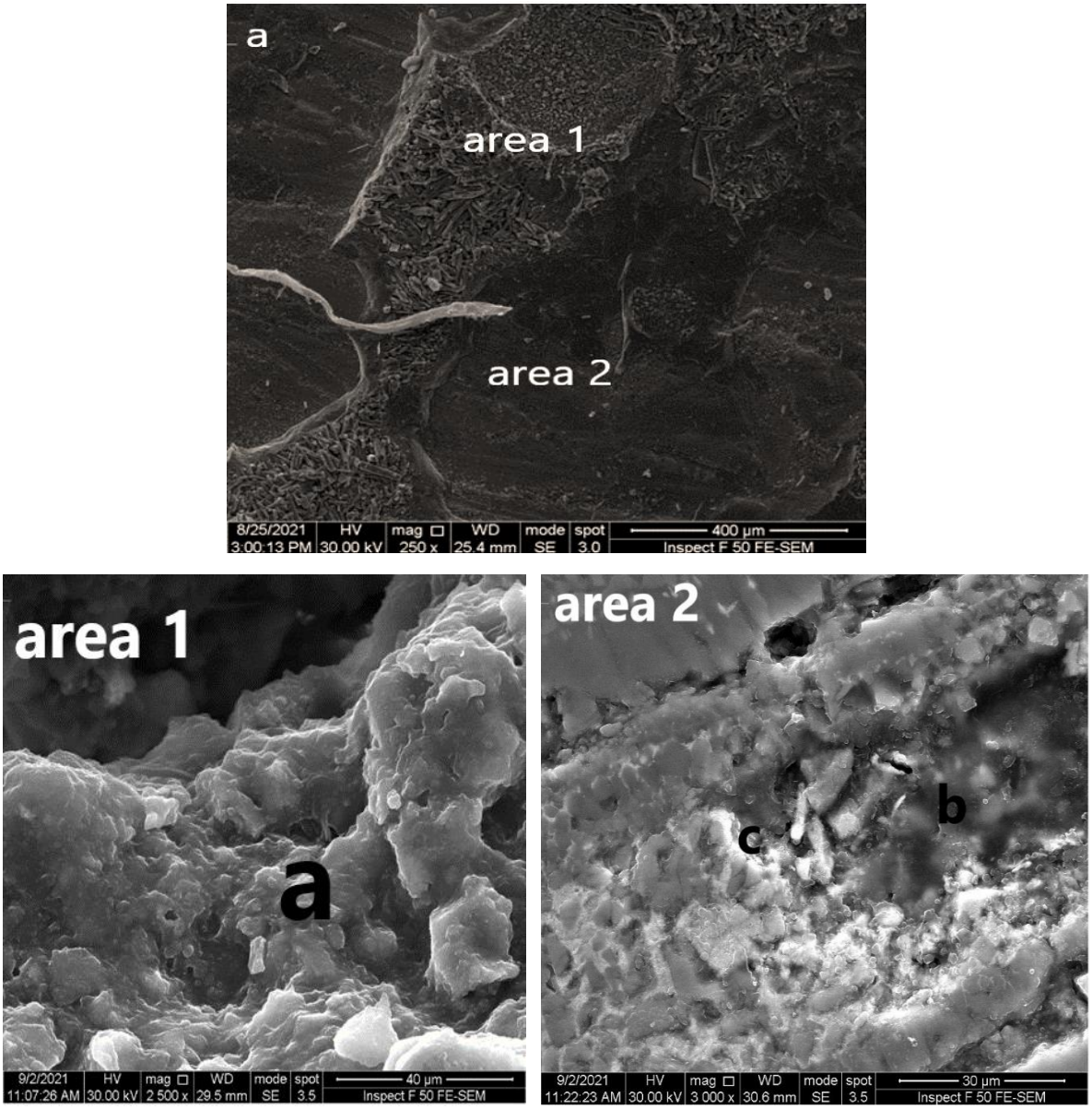

Figure 4-13 : SEM image for the fracture surface of ZrO2/ Filler 1/Ti6Al4V joint brazed at 850℃ for 20 minutes.

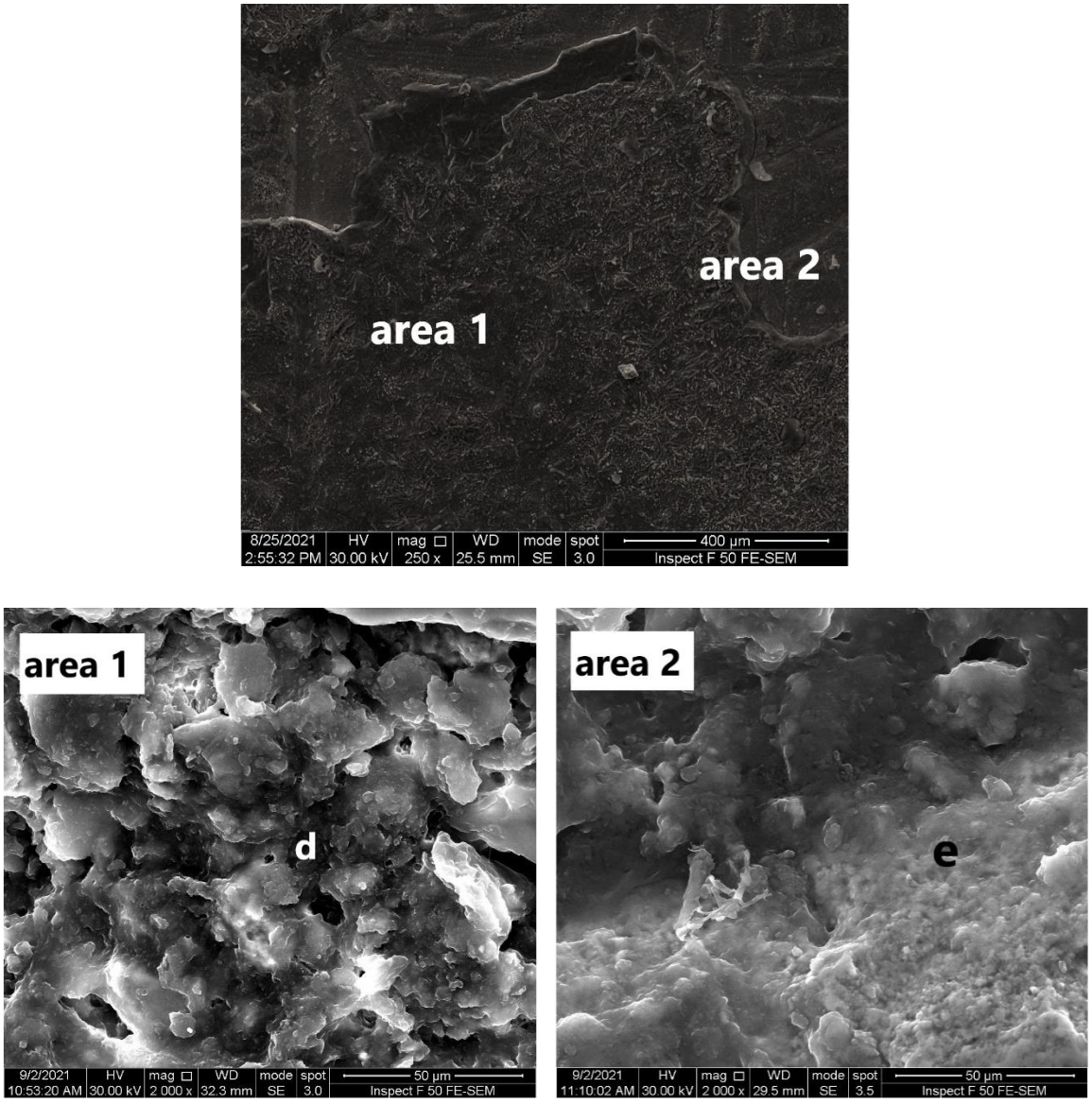

Figure 4 – 14 : : SEM image for the fracture surface of ZrO2/ Filler 1/Ti6Al4V joint brazed at 925℃ for 20 minutes

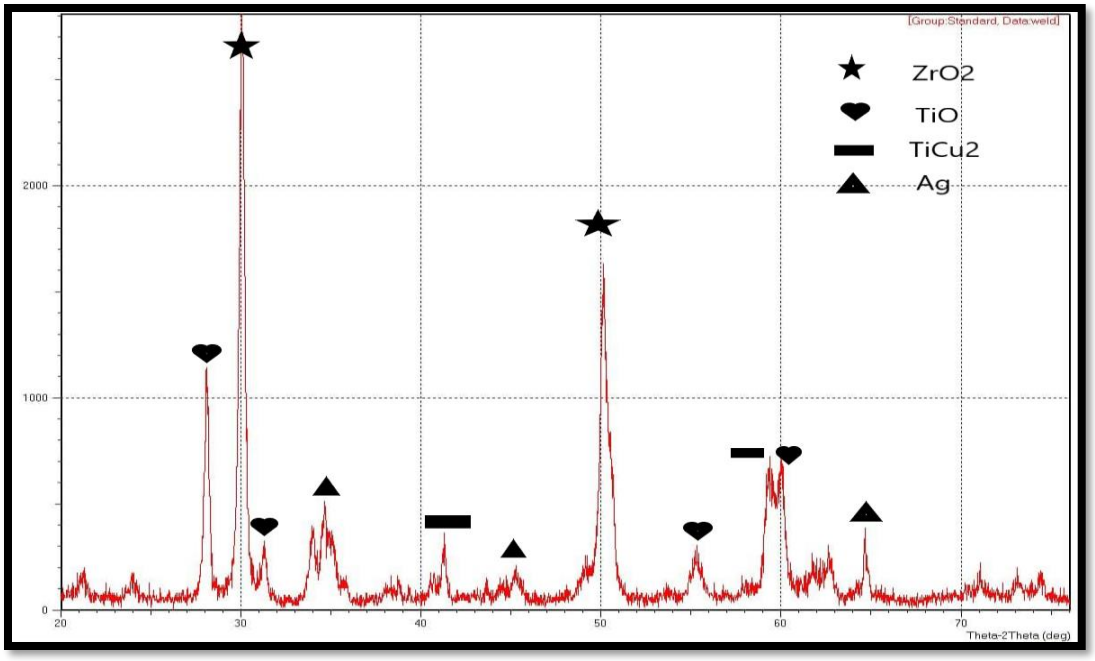

Figure 4-15: XRD pattern to the fracture surface of ZrO2/ Filler 1/Ti6Al4V joint .

4.6 Microhardness Results

Table (4-4) and figure (4-16) shown the Vickers microhardness of the prepared Ti6Al4V/ filler 1/ ZrO_2 joints in different brazing temperature along the joint line.

Table 4-4: illustrated the hardness of prepared joints (Ti6Al4V/ filler 1/ ZrO_2) brazed at different temperature along the joint.

No.	Point position	850℃	875℃	900℃	925℃
1	-5	1567	1570	1566	1550
2	-4	1555	1540	1551	1570
3	-3	1513	1516	1515	1517
4	-2	1480	1453	1510	1480
5	-1	1380	1430	1403	1420
6	0	189	195	203	220
7	1	222	252	259	271
8	2	280	300	340	300
9	3	310	324	352	367
10	4	340	355	377	370
11	5	351	372	380	390

Figure 4-16: hardness along the joint at defferent positions of (Ti6Al4V/ filler 1/ $ZrO_{2)}$ joint .

its obvious that the hardness of the joint parts are dissimilar .the dissimillarty in the hardness values could cause high resudual stresses in the joint after cooling. Figure (4-17) estimate the effect of brazing temperature on the hardness value of the (Ti6Al4V/ filler 1/ $ZrO_{2)}$ in the joints zone.

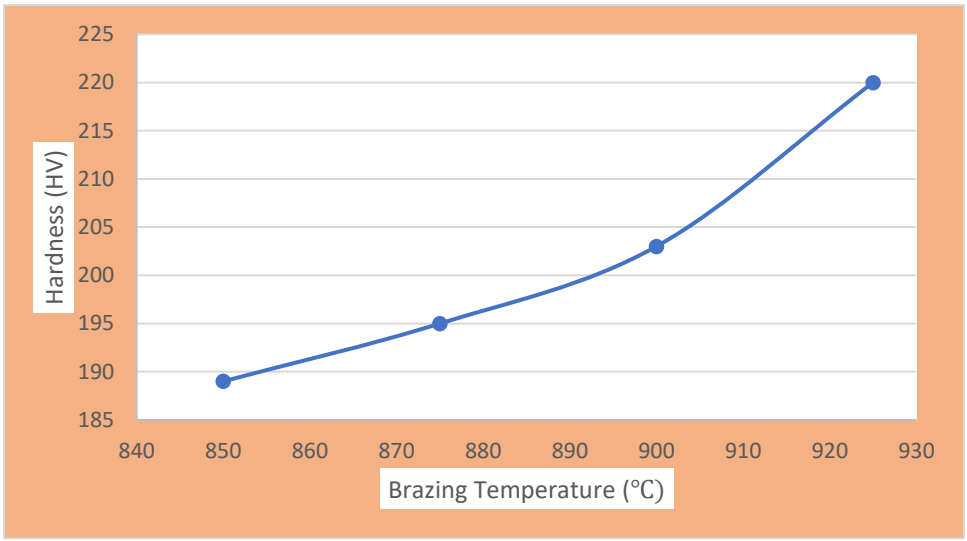

Figure 4-17: showed the effect of brazing temperature on the microhardness of (Ti6Al4V/ filler 1/ ZrO_2) brazed at different temperatures.

The microhardness of the joints increased gradually with increasing temperatures as in figure 4-17. This increment can be attributed to formation of TiO and $TiCu_2$ phases in the joint position. As the temperature rise, the amount of the intermetallic phases in the joint resultant in increasing the microhardness then the thickness of Ag-Cu base filler layer decrease (the hardness of Ag-Cu- Ti alloy is 115.1 Hv [54]). Table 4-5 and figure (4-18) showed hardness values of Ti6Al4V/ filler 2/ ZrO_2 brazed at different temperatures for 20 minutes.

Table 4-5 : illustrated the hardness of prepared joints(Ti6Al4V/ filler 2/ ZrO_2) brazed at different temperature along the joint.

No.	Point position	850°C	875°C	900°C	925°C
1	-5	1557	1567	1559	1561
2	-4	1549	1559	1552	1555
3	-3	1519	1516	1521	1530
4	-2	1475	1483	1498	1495
5	-1	1395	1401	1410	1390
6	0	219	226	230	245
7	1	233	251	247	263
8	2	271	298	342	314
9	3	344	358	397	377
10	4	375	376	401	381
11	5	392	399	409	390

From figure (4-18) it's can be noted that the hardness of the joint line is lower than that in Zirconia and Ti6Al4v base materials. Noteworthy, the hardness is gradually increased to word zirconia side and Ti6Al4V side due to formation the intermetallic phases which have hardness higher than that of filler alloy.

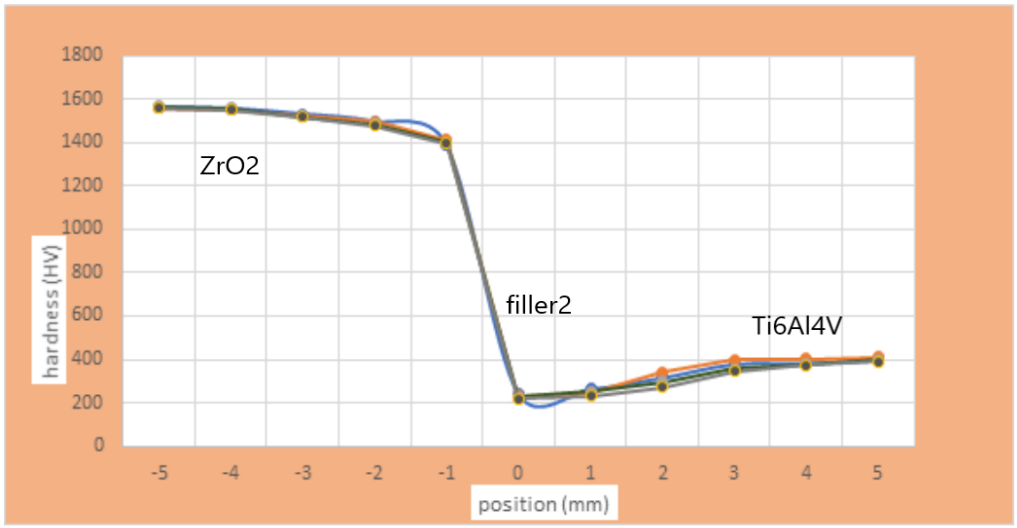

Figure 4-18: illustrated hardness values of Ti6Al4V/ filler 2/ ZrO_2 brazed at different temperatures for 20 minutes.

Figure (4-19) showed the effect of brazing temperature on the hardness in the joint at constant brazing time (20 minutes). The hardness increases as the brazing temperature increase due to formation of intermetallic. The hardness of the joints produced by using filler 2 have hardness higher than that brazed by filler 1. The addition of Cobalt element to Ag-Cu alloy increases the wettability of the filler then the hardness increased as the amount of Cobalt increased. This result agrees with KAIWA and et. al [97].

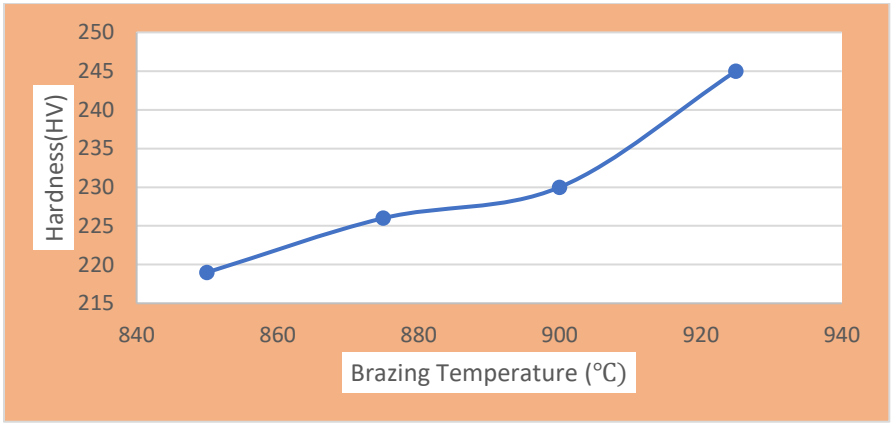

Figure 4-19: the effect of brazing temperature on the hardness of the joint line of Ti6Al4V/ filler 2/ ZrO_2 specimen.

4.7 Biocompatibility Tests Results

4.7.1 Histopathological Test Results

In figure (4-20) Group 1 (G1F1 see Table (3-3)) The sections of skin showed partial damage of epidermis which replace by remnant of necrotic cells and the dermis revealed degeneration of dermis, collagen bundles and sebaceous glands which due to incision during test specimen implantation. the signs of acute inflammation were clear during this period by the presence of dilated blood vessels and the presence of neutrophil cells.

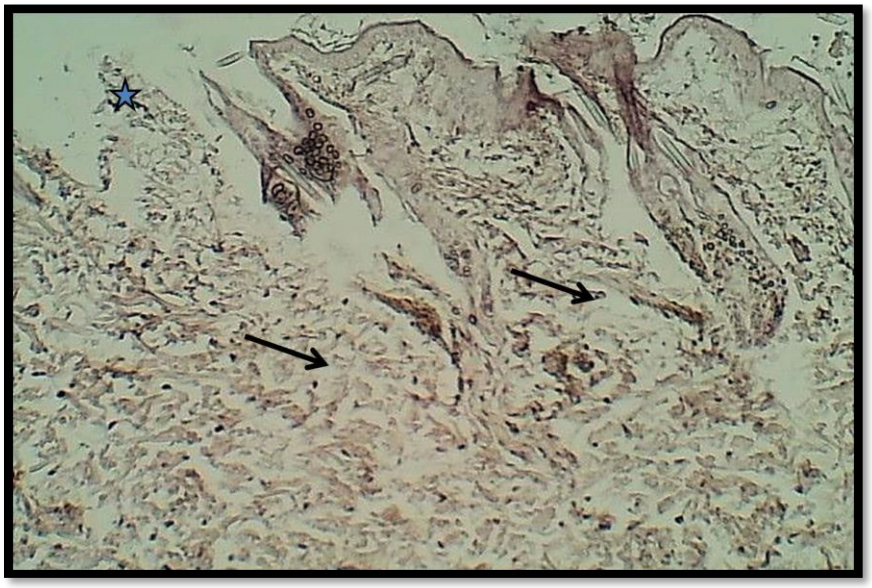

Figure 4-20: section of skin (G1F1) shows: necrosis of epidermis (Asterisk) and degeneration and necrosis od dermis collagen bundles and sebaceous glands (arrows) . H&E stain.100x.

In figure (4-21) and (4-22) Group (G1F2 and G1F2) after 3 days revealed the sections of skin showed damage of epidermis which was due to incision for sample implantation this damage was replace by ulcerative tissue composed of necrotic tissue and separated from underneath dermis by thick layer of acute inflammatory cells which are the neutrophil cells and dilated blood vessels, the dermis was

revealed no sweat and sebaceous glands and no hair follicles. Normal muscle fibers underneath the test specimen.

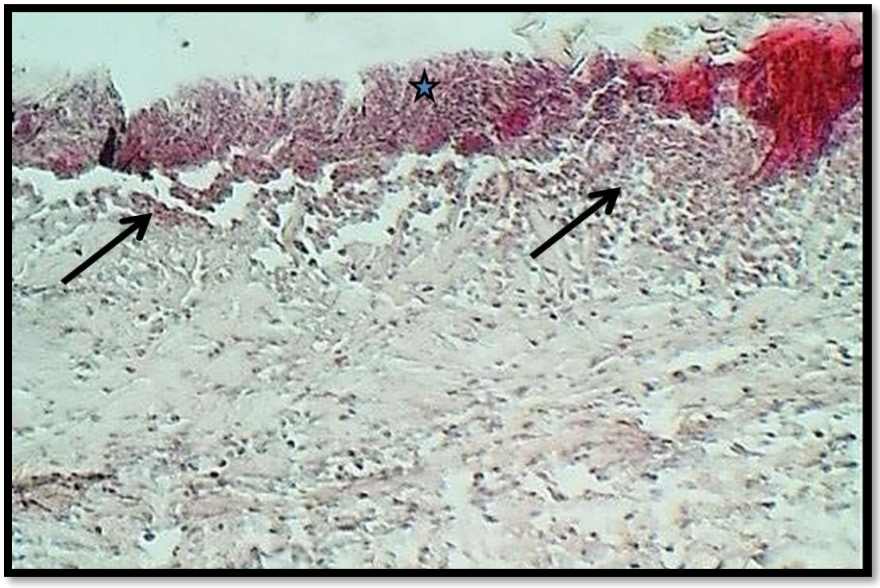

Figure 4-21: section of skin (G1F2) shows: ulcerative dermatitis with thick necrotic tissue (Asterisk) and inflammatory zone (arrows). H&E stain.100x.

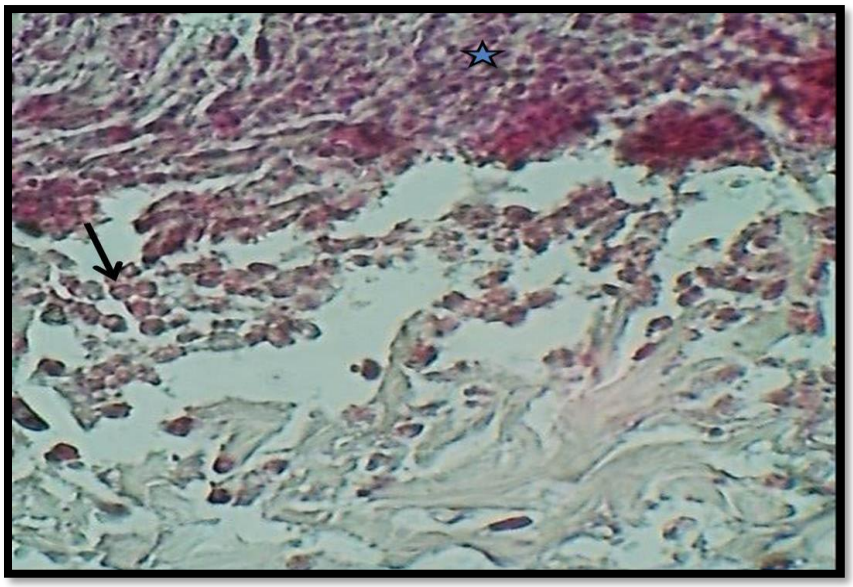

Figure 4-22: section of skin (G1F2) shows: thick necrotic tissue (Asterisk) and dead inflammatory cells (arrows). H&E stain.400x.

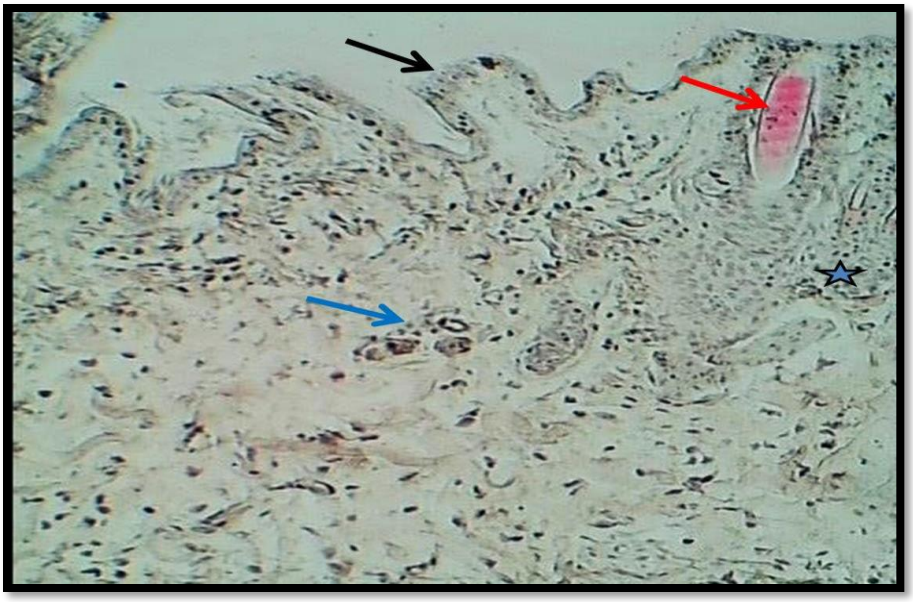

Figure 4-23: section of skin (G2F1 days) shows: normal epidermis (black arrow), well developed hair follicle (Red arrow), sebaceous gland (Asterisk) & normal dense irregular collagen bundles with sweat glands (Blue arrow) . H&E stain.100x.

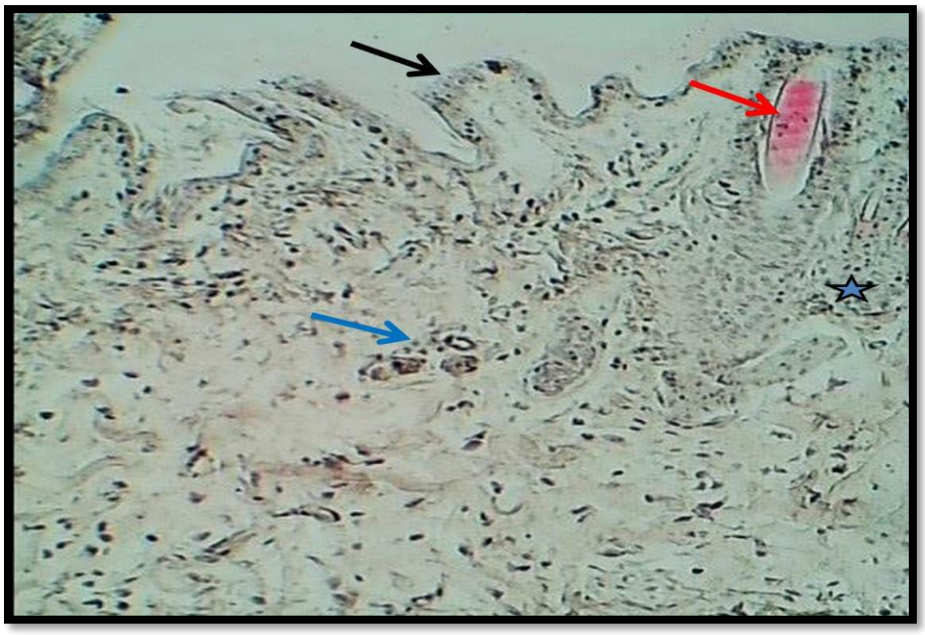

Figure 4-24: section of skin (G2F1) shows: normal epidermis (black arrow), well developed hair follicle (Red arrow), sebaceous gland (Asterisk) & normal dense irregular collagen bundles with sweat glands (Blue arrow) . H&E stain.100x.

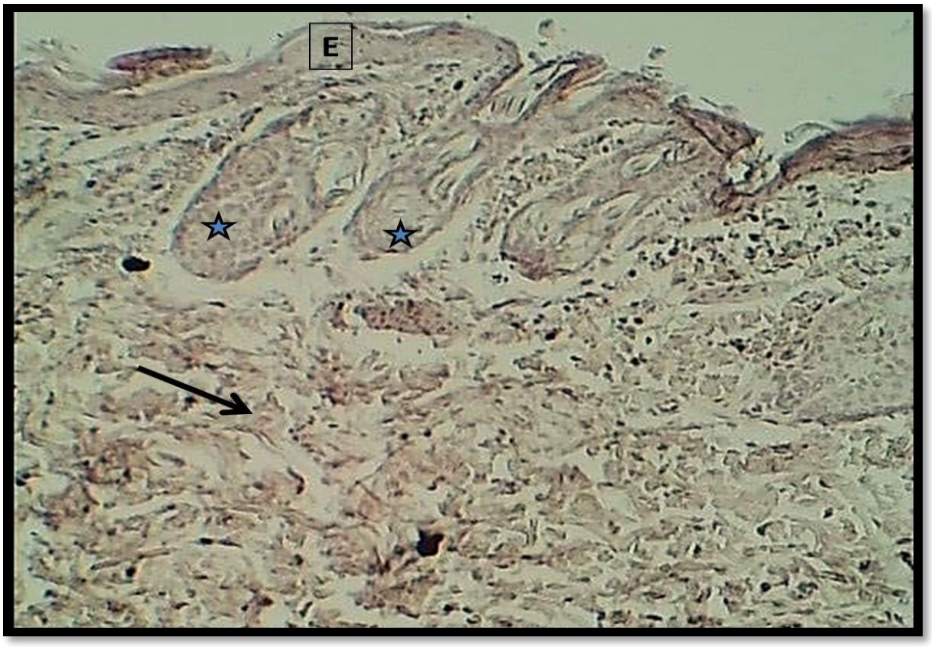

Figure 4-25: section of skin (G2F2 days) shows: normal epidermis (E) , well developed sebaceous glands (Asterisk) and normal dense irregular collagen bundles (arrow) . H&E stain.100x

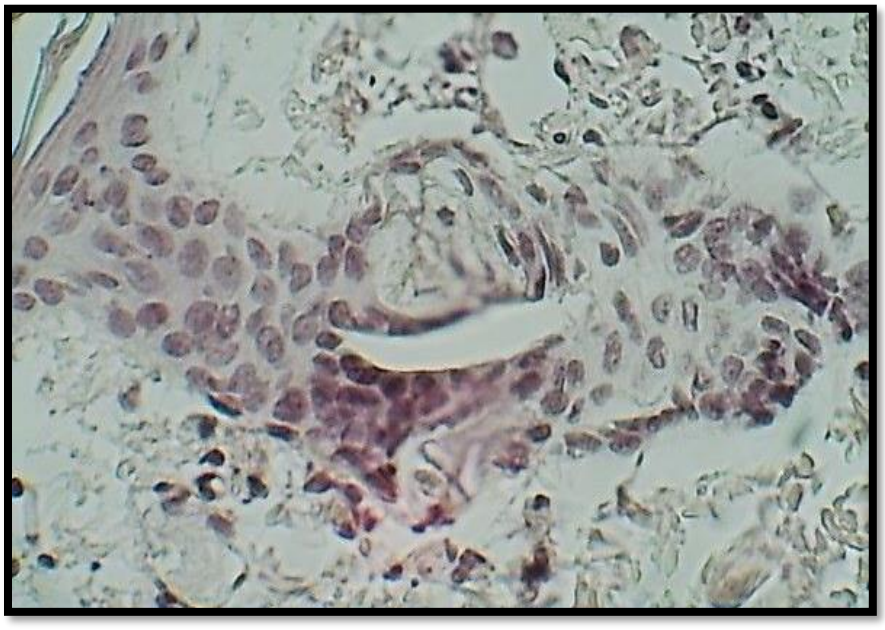

Figure 4-26: section of skin (G2F2 days) shows: normal epidermis and well developed sebaceous gland. H&E stain.400x.

In figure (4-23),(4-24), (4-25) and (4-26) showed Both Group 2 (R7 days) and Group 2 (L7 days) after 7 days the sections of skin showed signs of chronic inflammation by the presence of multinucleated giant cell with presence of fibroblast and collagen fiber formation normal epidermal non-keratinized stratified squamous epithelium. The dermis showed well developed sebaceous glands and normal dense irregular collagen bundles. This results normal healing sequence of the injured skin which agree with [98]

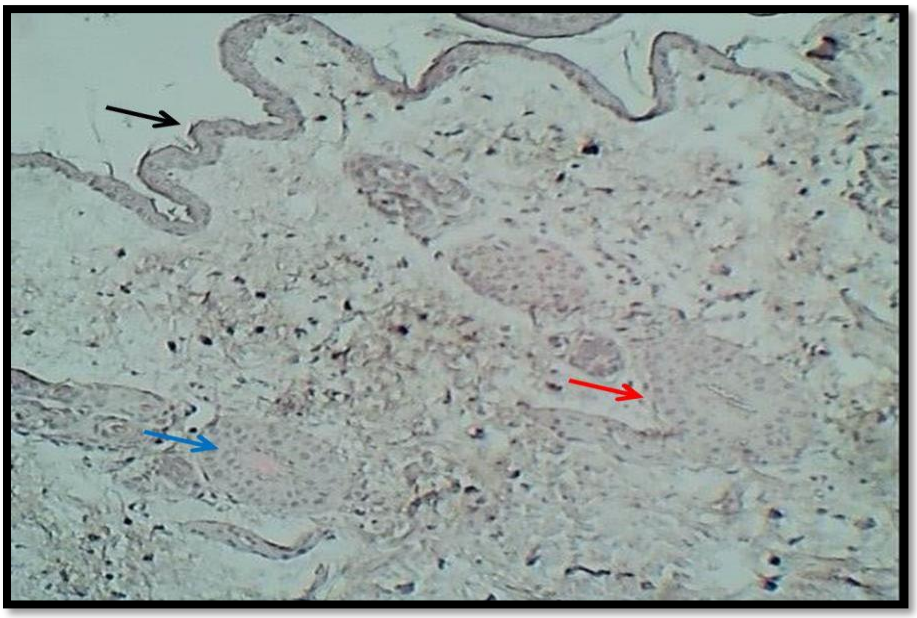

Figure 4-27: section of skin (G3F1) shows: normal epidermis (black arrow), with furthermore hair follicle (Blue arrow) and sebaceous gland (Red arrow) & mature dense irregular collagen bundles. H&E stain.100x.

Group 3 regarding the (G3F1 and G3F3) of test specimen implantation. The sections of skin showed normal epidermal non-keratinized stratified squamous epithelium. The dermis showed furthermore hair follicles and sebaceous glands within mature normal dense irregular collagen bundles. Normal muscle fibers underneath the test specimens as in figure (4-27), (4-28) and (4-29).

Figure 4-28: section of skin (G3F2) shows: normal epidermis (black arrow), with furthermore hair follicle (Blue arrow) and sebaceous gland (red arrow) & mature dense irregular collagen bundles of dermis. H&E stain.100x.

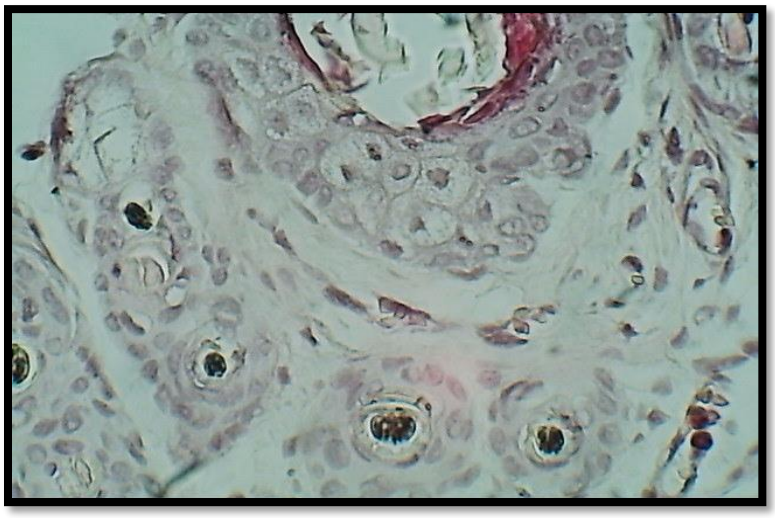

Figure 4-29: section of skin (G3F2) shows: normal epidermis (black arrow), with furthermore hair follicles . H&E stain.400x.

4.7.2 Blood test results

4.7.2.1 Urea Level in the Blood

The levels of Urea in rabbits' blood are depending on circadian rhythm, quantity as well as feature of proteins in food, nourishing ranks, functions of liver,

stomach absorption, urease's dynamic of the caeca a particular region plants and hydrating rank. Frequently, slight variations in urea amount are problematic to be interpreted [99]. Table (4-6) showed the urea levels in rabbits' blood before and after implantation process of specimens. The results of the test of both filler in the normal rang thus the presence of the joined specimens in the rabbit body have no reversible effect on the urea level.

4.7.2.2 Creatinine level

Creatinine is a protein catabolit which forms from the muscular-creatine and expelled by glomerulare purification at a continual rate. Creatinine is considered to be more dependable test to investigate renal performance than urea level in blood. In case of a rabbits, pre-renal azotemia may be produced by lake of hydration since rabbits acquire a partial capability to distillate urine. Creatinine level quickly come back to normal level when the dehydration problem is corrected. Stress may have similarly effect on creatinine level in rabbit body[100] .Table (4-7) exhibited that the amount of creatinine has slightly change after implantation process but as can be noticed the values of creatinine level remain in normal range.

Table 4-6 illustrated the Urea test results for Ti6Al4V/ filler 1 and filler2/ ZrO_2 at different times.

Test time	**Rabbit no.**	**Before test Filler 1**	**After test Filler 1**	**Before test** Filler 2	**After test Filler 2**	**Standard range (mg/dL)**
3 days	1	33	41	27	32	20-45
	2	29	27	23	30	
	3	35	32	34	33	
	4	23	30	40	41	
	5	30	43	42	39	
7 days	6	34	39	21	27	
	7	31	39	31	35	
	8	25	27	26	36	
	9	31	35	23	29	
	10	30	37	30	41	
30 days	11	41	50	44	46	
	12	23	22	23	21	
	13	35	31	25	31	
	14	30	33	33	32	
	15	31	29	32	34	

Table 4-7: illustrated the Creatinine test results of Ti6Al4V/ filler 1 and filler 2/ ZrO_2 for different times.

Test time	Rabbit no.	Before test Filler1	After test Filler1	Before test Filler2	After test Filler2	Standard range (mg/dL)
3 days	1	0.7	1.2	1.3	2.6	0.5-2.5
	2	0.5	0.9	2.3	1.5	
	3	1.6	1.8	1.0	2.0	
	4	0.8	1.3	1.3	1.6	
	5	0.8	1.4	0.8	1.2	
7 days	6	2.1	2.6	0.5	1.9	
	7	1.8	2.3	1.8	1.1	
	8	0.7	0.9	0.9	2.1	
	9	0.5	0.8	1.6	1.4	
	10	1.9	2.4	0.8	1.1	
30 days	11	0.9	1.1	0.8	1.5	
	12	0.7	0.9	1.3	1.5	
	13	1.5	1.7	1.5	1.2	
	14	2.3	2.1	1	1.0	
	15	1.6	1.6	0.7	0.8	

4.7.2.3 Albumin level results

Albumin is the first portion to form by electrophoresis and is the major serum protein. Albumin is created in the liver and aids keep osmotic pressure in the interior the intravascular compartment[101]. The findings of the Albumin level in the rabbit's blood are shown in table (4-8). These results indicate that the Albumin level remain in normal level through implantation period.

Table 4-8: illustrated Albumin range in rabbits' blood before and after implantation process for Ti6Al4V/ filler 1/ ZrO_2 at different times

Test time	Rabbit no.	Before test Filler 1	After test Filler 1	Before test Filler 2	After test Filler 2	Standard range (g/d)
3 days	1	3	3.4	2.4	2.7	2.4-4.6
	2	2.6	2.6	2.7	2.9	
	3	4.2	4.5	3.2	3.7	
	4	3.4	3.5	2.8	3.1	
	5	3.4	3.7	3.1	3.2	
7 days	6	2.7	3.1	3	3.5	
	7	3.1	3.6	3.3	3.7	
	8	4.1	4.6	4	4.4	
	9	4	4.5	3.5	4	
	10	3.8	4.2	3.1	3.8	
30 days	11	2.6	2.7	3	3.1	
	12	2.6	2.9	2.5	2.9	
	13	2.9	3	2.6	2.9	
	14	4	4	3	3.2	
	15	3.9	4.1	3.2	3.3	

4.7.2.4 ALT (Alanine Aminotransferase enzyme)

The ALT enzyme isn't specific in the liver of herbivores, such as the rabbit. The ALT possesses a small half-life of around (5 h) in the rabbit's blood, therefore it isn't a quite suitable diagnostic tool of liver damage. Though, ALT enzyme isn't raised by limit in the rabbits, therefore a high ALT values is expected of tissue harm. The ALT is present at high amounts in cardiac muscle of rabbit body. The ALT may be slightly raised in rabbit with good health later to be exposed to small level of lead, mycotoxins or even to halothane anesthesia. ALT can also be raised in rabbit with progressive hepatic neoplasia[102]. ALT enzyme concentration levels in tested rabbits are recorded in Table (4- 9). since all tested results are in normal range then

the presents of the implanted specimens have no reversible consequences on rabbit body.

Table 4-9: illustrated ALT (Alanine Aminotransferase enzyme(IU/l)) range in rabbits blood before and after implantation process for Ti6Al4V/ filler 1 and filler 2/ ZrO_2 in different times

Test time	**Rabbit no.**	**Before test Filler 1**	**After test Filler 1**	**Before test Filler 1**	**After test Filler 2**	**Standard range** (lU/l)
3 days	1	20	24	30	32	14-80
	2	45	46	27	30	
	3	36	38	32	36	
	4	28	29	49	51	
	5	22	27	25	29	
7 days	6	50	54	36	39	
	7	33	36	31	34	
	8	49	51	24	27	
	9	39	42	42	45	
	10	25	27	33	37	
30 days	11	35	36	41	44	
	12	37	39	34	36	
	13	56	59	29	32	
	14	45	49	36	39	
	15	40	44	27	31	

4.7.2.5 **Aspartate Aminotransferase enzyme (AST)**

AST is broadly presented in numerous tissues of rabbit. It's existing in cardiac tissues and muscles, besides the liver. It has a shot half-life (5 h). Even though greater AST levels might be measured in cases diagnosed with liver disease, striving to collect the sample of blood because of hemolysis that raises AST levels. Levels of AST might be raised owing to disease, environmental factors, or technical reasons [103]. Table (4-10) illustrated the results of AST test for both filler in different times (3, 7 and 30 days). After tests all specimens of both fillers, the results

refer to a normal level in rabbit after implantation process, therefore the implants didn't cause any harmful effect to the rabbit body.

Table 4-10: illustrated AST range in rabbits' blood before and after implantation process for Ti6Al4V/ filler 1 and filler 2/ ZrO_2 in different times

Test time	**Rabbit no.**	**Before test filler1**	**After test filler 1**	**Before test filler2**	**After test filler 2**	**Standard range** (lU/l)
3 days	1	51	55	45	49	14-113
	2	72	78	54	61	
	3	63	68	78	83	
	4	50	55	58	62	
	5	69	73	49	53	
7 days	6	79	81	73	77	
	7	45	48	47	51	
	8	58	61	37	42	
	9	53	55	53	55	
	10	61	64	72	75	
30 days	11	52	54	45	46	
	12	67	69	57	59	
	13	34	35	44	48	
	14	49	51	38	41	
	15	30	31	73	75	

4.7.2.6 Alkaline Phosphatase enzyme (ALP)

ALP is a broadly spread enzyme. Bone and liver containing the maximum concentration, nonetheless it is correspondingly existed in bowel-epithelium, kidney, as well as placenta. A biological reason of higher serum ALP amounts are osteoblastic activities of the growing animals. The animals that have bone injuries will demonstrate elevated ALP level. like a liver enzyme ALP show no increasing as a result of hepatocellular harm nevertheless is revealing of bile stasis for example, hepatic coccidiosis, liver swellings, neoplasia, lipidosis.

Extrahepatically reasons, for instance abscesses otherwise neoplasia, may lead to a bile stasis via sealing the bile duct. ALP has a diagnostical value since it isn't changed by restraint and therefore is recorded to be a decent indicator of actual tissue harm[91]. table (4-11) showed the ALP results in different times (3, 7 and 30 days) for both fillers. Since all data results for both fillers haven't shown any abnormality in ALP concentration therefor specimen presence in the rabbit's body have no negative effect.

Table 4-11: illustrated ALP range in rabbits' blood before and after implantation process for Ti6Al4V/ filler 1 and filler 2/ ZrO_2 in different times

Test time	**Rabbit no.**	**Before test filler 1**	**After test filler1**	**Before test filler 2**	**After test filler2**	**Standard range** (lU/l)
3 days	1	75	79	85	90	10-140
	2	96	101	68	72	
	3	74	82	97	103	
	4	59	63	86	92	
	5	41	47	43	46	
7 days	6	110	113	52	55	
	7	85	87	119	122	
	8	37	39	83	85	
	9	93	96	47	50	
	10	46	48	84	85	
30 days	11	45	47	99	102	
	12	59	61	39	42	
	13	42	45	87	90	
	14	88	90	32	35	
	15	53	55	62	64	

Chapter five

(Conclusion and Recommendations)

5.1 Conclusions

The conclusions obtained in this work can be summarized as follows:

1- melt spinning technology process was effective to produce an alloy with some amorphous structure which in order led to improve the properties . Increasing the rotating speed of the disk or decrease its temperature will increase the alloys amorphously. The obtained XRD patterns support this result.

2- The joining process of metal to ceramic was successful by using filler alloys which contain active element (titanium)

3- The present of Titanium element in the filler alloy will discolorize the ZrO_2 part. As the brazing temperature or brazing time increase the discoloration phenomena increase.

4- SEM images and XRD patterns exhibited 7 phases along the brazed specimens which include ZrO_2, TiO, Cu_2Ti_3O , $TiCu_2$, TiCu , Ti and Ag phases. These images also exhibit the Zebra structure throughout the region between filler alloy and Ti6Al4V part. Zebra structure presence decrease the residual stresses which in tearing protect the joint from cracking.

5- The presence of some inter midrate phases such as TiO, Cu_2Ti_3O , $TiCu_2$ and TiCu act an important role in decreasing the mismatch between the metal and ceramic.

6- As the brazing temperature increased the shear strength of the Ti6Al4V/ filler 1 / ZrO_2 and Ti6Al4V/ filler 2 / ZrO_2 strength increase until arrive to 875℃ then decreased gradually with increasing brazing temperature. the shear strength of Ti6Al4V/ filler 2 / ZrO_2 joints are higher than that for Ti6Al4V/ filler 1 / ZrO_2 due to present of Cobalt in the filler alloy.

7- There are two kinds of fracture forms seen in the prepared specimens after shear test (flat and fluctuating form).

8- The microhardness of Ti6Al4V/ filler 2 / ZrO_2 joints are higher than that for Ti6Al4V/ filler 1 / ZrO_2 joints.

9- Histopathological Test Results showed that normal muscle fibers underneath the test specimen after the implantation process

10- The blood rest for urea ,Creatinine , Albumin, ALT Alanine Aminotransferase enzyme , AST Aspartate Aminotransferase enzyme and ALP Alkaline Phosphatase enzymes confirm they were in normal level

11- The biocompatibility tests (histopathological and blood tests) in the vivo (rabbit body) showed that the both types of prepared specimens are biocompatible.

5.2 Recommendations for Future Work

1- Add another alloying element to Ag-Cu alloy like Chromium or Nikal to improve the wettability and biocompatibility of the filler alloy.

2- Using filler alloys with chemical composition contain anther active elements such as Zr and Hf etc.

3- Prepare a tubular specimen from ZrO_2 / Ti6Al4V parts in order to estimate the amount of leakage in the joint.

4- Add alloying elements with Nano particle size to the filler alloy and study the effect of these additives on mechanical and physical properties of the filler alloy.

5- Using anther biocompatible filler alloy like CoCrNi etc.

References

1. Soldering, A.W.S.A.C.C.o.B.a., *Brazing Handbook*. Fifth Edition ed. Brazing Handbook, ed. A.W. Society. Vol. 1. 2011, USA: American Welding Society.
2. Sekulić, D.P., *Advances in brazing: science, technology and applications*. 2013: Elsevier.
3. Lewinsohn, C.A., M. Singh, and R. Loehman, *Advances in Joining of Ceramics*. 2012: Wiley.
4. Way, M., J. Willingham, and R. Goodall, *Brazing filler metals.* International Materials Reviews, 2020. **65**(5): p. 257-285.
5. Uday, M., et al., *Current issues and problems in the joining of ceramic to metal*, in *Joining Technologies*. 2016, IntechOpen.
6. Martinelli, A. and A. Buschinelli, *Review Article: recent advances in metal-ceramic brazing.* Cerâmica, 2003. **49**(312): p. 178-198.
7. Zhou, Y. and M.D. Breyen, *Joining and assembly of medical materials and devices*. 2013: Elsevier.
8. Zhou, D. and E. Greenbaum, *Implantable neural prostheses 2: techniques and engineering approaches*. 2010: Springer Science & Business Media.
9. Jiang, G. and D.D. Zhou, *Technology advances and challenges in hermetic packaging for implantable medical devices*, in *Implantable Neural Prostheses 2*. 2009, Springer. p. 27-61.
10. Mills, J., A. Jalil, and P. Stanga, *Electronic retinal implants and artificial vision: journey and present.* Eye, 2017. **31**(10): p. 1383-1398.
11. Kane, M.J., et al., *BION microstimulators: A case study in the engineering of an electronic implantable medical device.* Medical engineering & physics, 2011. **33**(1): p. 7-16.

12. Park, J.B. and J.D. Bronzino, *Biomaterials: principles and applications.* 2002.
13. Hanson, W., K. Ironside, and J. Fernie, *Active metal brazing of zirconia.* Acta materialia, 2000. **48**(18-19): p. 4673-4676.
14. Smallman, R.E. and A. Ngan, *Physical metallurgy and advanced materials*. 2011: Elsevier.
15. Niinomi, M., *Mechanical properties of biomedical titanium alloys.* Materials Science and Engineering: A, 1998. **243**(1-2): p. 231-236.
16. Suganuma, K., T. Okamoto, and K. Kamachi, *Influence of shape and size on residual stress in ceramic/metal joining.* Journal of materials science, 1987. **22**(8): p. 2702-2706.
17. Atabaki, M.M., *Recent progress in joining of ceramic powder metallurgy products to metals.* Metalurgija-J. Metallurgy (MJoM), 2010. **16**(4): p. 255-268.
18. Nicholas, M. and D. Mortimer, *Ceramic/metal joining for structural applications.* Materials Science and Technology, 1985. **1**(9): p. 657-665.
19. Intrater, J., *Review of some processes for ceramic-to-metal joining.* MATERIAL AND MANUFACTURING PROCESS, 1993. **8**(3): p. 353-373.
20. Weman, K., *Welding processes handbook*. 2011: Elsevier.
21. Suganuma, K., *Recent advances in joining technology of ceramics to metals.* Isij International, 1990. **30**(12): p. 1046-1058.
22. Savage, W., *Joining of Advanced Materials*. 2013: Elsevier Science.
23. Walker, C. and V. Hodges, *Comparing metal-ceramic brazing methods.* Welding Journal, 2008. **87**(10): p. 43-50.

24. Siddiqui, M.S., *Vacuum brazing of alumina ceramic to titanium for biomedical implants using pure gold as the filler metal*. 2011, Florida International University.
25. Schwartz, M.M., *Brazing*. 2003: ASM international.
26. Kah, P., M. Shrestha, and J. Martikainen. *Trends in joining dissimilar metals by welding*. in *Applied Mechanics and Materials*. 2014. Trans Tech Publ.
27. Society, A.W., *Welding handbook*. 1982: American welding society.
28. Fedorov, V., et al. *Interfacial microstructure and mechanical properties of brazed aluminum/stainless steel-joints*. in *IOP Conference Series: Materials Science and Engineering*. 2017. IOP Publishing.
29. Gibson, S.W., *Advanced welding*. 1997: Macmillan.
30. Thwaites, C.J., *Capillary joining: Brazing and soft-soldering*. 1982: John Wiley & Sons.
31. Singh, M., et al., *Ceramic integration and joining technologies: from macro to nanoscale*. 2011: John Wiley & Sons.
32. Jacobson, D.M. and G. Humpston, *Principles of brazing*. 2005: Asm International.
33. Lancaster, J.F., *Metallurgy of welding*. 1999: Elsevier.
34. Milner, D.R. and R.L. Apps, *CHAPTER 8 - Soldering and brazing*, in *Introduction to Welding and Brazing*, D.R. Milner and R.L. Apps, Editors. 1968, Pergamon. p. 178-195.
35. Mclean, M., *Encyclopedia of materials science and engineering*. 1986, Taylor & Francis.
36. Metco, S., *An Introduction to Brazing: Fundamentals, Materials, Processing.* no, 2011. **3**: p. 10-24.
37. Rao, P.N., *Manufacturing technology*. Vol. 1. 2013: Tata McGraw-Hill Education.

38. Lippold, J.C. and D.J. Kotecki, *Welding metallurgy and weldability of stainless steels*. 2005.
39. Mittemeijer, E.J., *Fundamentals of materials science: the microstructure–property relationship using metals as model systems*. 2010: Springer Science & Business Media.
40. Zhang, G., et al., *Influence of copper on amorphous nickel based brazing alloy.* Science and technology of welding and joining, 2001. **6**(2): p. 103-107.
41. Eskin, D., L. Katgerman, and J. Mooney, *Contraction of aluminum alloys during and after solidification.* Metallurgical and Materials Transactions A, 2004. **35**(4): p. 1325-1335.
42. Niinomi, M., T. Narushima, and M. Nakai, *Advances in Metallic Biomaterials: Tissues, Materials and Biological Reactions*. Vol. 3. 2015: Springer.
43. Bian, H., et al., *Microstructure evolution and mechanical properties of titanium/alumina brazed joints for medical implants.* Metals, 2019. **9**(6): p. 644.
44. Niinomi, M., et al., *Development of low rigidity β-type titanium alloy for biomedical applications.* Materials Transactions, 2002. **43**(12): p. 2970-2977.
45. Jardini, A.L., et al., *Customised titanium implant fabricated in additive manufacturing for craniomaxillofacial surgery: This paper discusses the design and fabrication of a metallic implant for the reconstruction of a large cranial defect.* Virtual and physical prototyping, 2014. **9**(2): p. 115-125.
46. Ganjeh, E., et al., *Increasing Ti–6Al–4V brazed joint strength equal to the base metal by Ti and Zr amorphous filler alloys.* Materials characterization, 2012. **71**: p. 31-40.

47. Hémery, S., P. Villechaise, and D. Banerjee, *Microplasticity at Room Temperature in α/β Titanium Alloys.* Metallurgical and Materials Transactions A, 2020. **51**(10): p. 4931-4969.
48. Zhang, J., et al., *Complexion-mediated martensitic phase transformation in Titanium.* Nature Communications, 2017. **8**(1): p. 14210.
49. Bahraminasab, M. and F. Farahmand, *State of the art review on design and manufacture of hybrid biomedical materials: hip and knee prostheses.* Proceedings of the Institution of Mechanical Engineers, Part H: Journal of Engineering in Medicine, 2017. **231**(9): p. 785-813.
50. Fischman, G., *1.3.4B - Structural Ceramic Oxides*, in *Biomaterials Science (Fourth Edition)*, W.R. Wagner, et al., Editors. 2020, Academic Press. p. 319-326.
51. Bollen, C., *Zirconia: the material of choice in implant dentistry? An update.* J. Dent. Heal. Oral. Disord. Ther, 2017. **6**(6): p. 1-4.
52. Muñoz, M., et al., *Adhesion at metal–ZrO2 interfaces.* Surface Science Reports, 2006. **61**(7): p. 303-344.
53. Terki, R., et al., *Structural and electronic properties of zirconia phases: A FP-LAPW investigations.* Materials Science in Semiconductor Processing, 2006. **9**: p. 1006-1013.
54. Sharma, A. and B. Ahn, *Brazeability, Microstructure, and Joint Characteristics of ZrO2/Ti-6Al-4V Brazed by Ag-Cu-Ti Filler Reinforced with Cerium Oxide Nanoparticles.* Advances in Materials Science and Engineering, 2019. **2019**.
55. Subramanian, P.R. and J.H. Perepezko, *The ag-cu (silver-copper) system.* Journal of Phase Equilibria, 1993. **14**(1): p. 62-75.

56. Chuang, T., M. Yeh, and Y. Chai, *Brazing of zirconia with AgCuTi and SnAgTi active filler metals.* Metallurgical and Materials Transactions A, 2000. **31**(6): p. 1591-1597.

57. Peytour, C., et al., *Interface microstructure and mechanical behaviour of brazed TA6V/zirconia joints.* Journal of materials science letters, 1990. **9**(10): p. 1129-1131.

58. Correia, R., J. Emiliano, and P. Moretto, *Microstructure of diffusional zirconia–titanium and zirconia–(Ti–6 wt% Al–4 wt% V) alloy joints.* Journal of materials science, 1998. **33**(1): p. 215-221.

59. Jiang, G., et al., *Zirconia to Ti-6Al-4V braze joint for implantable biomedical device.* Journal of Biomedical Materials Research Part B: Applied Biomaterials: An Official Journal of The Society for Biomaterials, The Japanese Society for Biomaterials, and The Australian Society for Biomaterials and the Korean Society for Biomaterials, 2005. **72**(2): p. 316-321.

60. Smorygo, O., et al., *Evolution of the interlayer microstructure and the fracture modes of the zirconia/Cu–Ag–Ti filler/Ti active brazing joints.* Materials letters, 2007. **61**(2): p. 613-616.

61. Liu, Y., et al., *Joining of zirconia and Ti-6A1-4V using a Ti-based amorphous filler.* Journal of Materials Science & Technology, 2011. **27**(7): p. 653-658.

62. Liu, Y., et al., *Microstructural and mechanical properties of jointed ZrO2/Ti–6Al–4V alloy using Ti33Zr17Cu50 amorphous brazing filler.* Materials & Design, 2013. **47**: p. 281-286.

63. Cao, J., et al., *Brazing ZrO2 ceramic to Ti–6Al–4V alloy using NiCrSiB amorphous filler foil: Interfacial microstructure and joint properties.* Materials characterization, 2013. **81**: p. 85-91.

64. Pimenta, J.S., et al., *Brazing of zirconia to titanium using Ag-Cu and Au-Ni filler alloys.* Soldagem & Inspeção, 2013. **18**(4): p. 349-357.
65. Feng, J., et al., *Microstructure evolution and mechanical properties of ZrO2/TiAl joints vacuum brazed by Ag–Cu filler metal.* Materials Science and Engineering: A, 2015. **639**: p. 739-746.
66. Dai, X., et al., *Interfacial reaction behavior and mechanical characterization of ZrO2/TC4 joint brazed by Ag–Cu filler metal.* Materials Science and Engineering: A, 2015. **646**: p. 182-189.
67. Sharma, A., et al., *Compressive strength evaluation in brazed ZrO 2/Ti6Al4V joints using finite element analysis.* Journal of Materials Engineering and Performance, 2016. **25**(5): p. 1722-1728.
68. Li, C., et al., *Joining of yttria stabilised zirconia to Ti6Al4V alloy using novel CuO nanostructure reinforced Cu foam interlayer.* Materials Letters, 2019. **253**: p. 105-108.
69. Zhang, C., et al., *Interfacial microstructure and mechanical properties of ultrasonic-assisted brazing joints between Ti–6Al–4V and ZrO2.* Ceramics International, 2020. **46**(6): p. 7733-7740.
70. Guo, W., et al., *Study on the interfacial properties of active Ti element/ZrO2 by using first principle calculation.* International Journal of Applied Ceramic Technology, 2020. **17**(3): p. 1286-1292.
71. Lei, Y., et al., *Evaluation of Biomedical Ti/ZrO2 Joint Brazed with Pure Au Filler: Microstructure and Mechanical Properties.* Metals, 2020. **10**(4): p. 526.
72. Park, S.W., et al., *Effect of Interface Microstructure on Joint Strength of Zirconia/Titanium Alloy Brazed with Amorphous Zr-Ti-Ni-Cu Active Filler Metal.* Metals, 2020. **10**(6): p. 718.

73. Xian, Y., et al., *Enhancing interface bonding strength of Ti-ZrO2 joints using graphene as brazing materials.* Materials Letters, 2020. **264**: p. 127360.
74. Ibrahim, T.K. and A.S. Humod, *Rapid Solidification Processing of Al-3wt% Mg Alloy.* Journal of Engineering and Technology, 2007. **25**(10).
75. Basu, J. and S. Ranganathan, *Bulk metallic glasses: A new class of engineering materials.* Sadhana, 2003. **28**(3-4): p. 783-798.
76. Busch, R., *The thermophysical properties of bulk metallic glass-forming liquids.* Jom, 2000. **52**(7): p. 39-42.
77. Greer, A.L., *Metallic glasses.* Science, 1995. **267**(5206): p. 1947-1953.
78. Wang, W.-H., C. Dong, and C. Shek, *Bulk metallic glasses.* Materials Science and Engineering: R: Reports, 2004. **44**(2-3): p. 45-89.
79. Miller, M. and P. Liaw, *Bulk metallic glasses: an overview.* 2007.
80. Shen, K. and M.M. Maharbiz, *Ceramic packaging for neural implants.* Journal of neural engineering, 2020.
81. Koch, J., et al., *Electrical connectors for neural implants: design, state of the art and future challenges of an underestimated component.* Journal of neural engineering, 2019. **16**(6): p. 061002.
82. Mallela, V.S., V. Ilankumaran, and N.S. Rao, *Trends in cardiac pacemaker batteries.* Indian pacing and electrophysiology journal, 2004. **4**(4): p. 201.
83. Ouyang, H., et al., *Symbiotic cardiac pacemaker.* Nature communications, 2019. **10**(1): p. 1-10.
84. Zeng, F.-G., et al., *Cochlear implants: system design, integration, and evaluation.* IEEE reviews in biomedical engineering, 2008. **1**: p. 115-142.
85. Dagnelie, G., *Retinal implants: emergence of a multidisciplinary field.* Current opinion in neurology, 2012. **25**(1): p. 67-75.

86. Weiland, J.D., W. Liu, and M.S. Humayun, *Retinal prosthesis.* Annu. Rev. Biomed. Eng., 2005. **7**: p. 361-401.

87. Zeng, Q., et al., *Micro/nano technologies for high-density retinal implant.* Micromachines, 2019. **10**(6): p. 419.

88. Loeb, G.E., F.J. Richmond, and L.L. Baker, *The BION devices: injectable interfaces with peripheral nerves and muscles.* Neurosurgical focus, 2006. **20**(5): p. 1-9.

89. van Bloemendaal, M., et al., *Gait training assisted by multi-channel functional electrical stimulation early after stroke: study protocol for a randomized controlled trial.* Trials, 2016. **17**(1): p. 1-8.

90. Tuma, M.S., *A Study of Mechanical and Electrochemical Properties of Gallium Restorative Alloys*, in *Department of Metallurgical Engineering - Collage of Materials Engineering*. 2020, University of Babylon: Iraq p. 156.

91. Melillo, A., *Rabbit clinical pathology.* Journal of exotic pet medicine, 2007. **16**(3): p. 135-145.

92. Delsante, S., et al., *Synthesis and thermodynamics of Ag–Cu nanoparticles.* Physical Chemistry Chemical Physics, 2015. **17**(42): p. 28387-28393.

93. Song, X., et al., *Effect of Si3N4-particles addition in Ag–Cu–Ti filler alloy on Si3N4/TiAl brazed joint.* Materials Science and Engineering: A, 2011. **528**(15): p. 5135-5140.

94. Nayef, U.M., H.T. Hussein, and A.M.A. Hussien, *Study of photoluminescence quenching in porous silicon layers that using for chemical solvents vapor sensor.* Optik, 2018. **172**: p. 1134-1139.

95. Pimenta, J.S., et al., *Brazing of zirconia to titanium using Ag-Cu and Au-Ni filler alloys.* Soldagem & Inspeção, 2013. **18**: p. 349-357.

96. Murray, J., *The Cu− Ti (copper-titanium) system.* Bulletin of alloy phase diagrams, 1983. **4**(1): p. 81-95.

97. Kaiwa, K., et al. *Effects of Ni and Co additions to filler metals on Ag-brazed joints of cemented carbide and martensitic stainless steel*. in *Advanced Materials Research*. 2014. Trans Tech Publ.

98. Jassim, R.K. and A.A. Radhi, *Evaluation the biological effect of two types of denture base materials reinforced with silanated glass fiber.* Journal of baghdad college of dentistry, 2011. **23**(2).

99. Quesenberry, K. and J.W. Carpenter, *Ferrets, Rabbits and Rodents-E-Book: Clinical Medicine and Surgery*. 2011: Elsevier Health Sciences.

100. De la Fuente, J., et al., *Physiological response of rabbits to heat, cold, noise and mixing in the context of transport.* Animal Welfare, 2007. **16**(1): p. 41-47.

101. Umemoto, T., et al., *Chemotaxis of oral treponemes toward sera and albumin of rabbit.* Microbiology and immunology, 2001. **45**(8): p. 571-577.

102. Gil, A.G., G. Silván, and J.C. Illera, *Pituitary–adrenocortical axis, serum serotonin and biochemical response after halothane or isoflurane anaesthesia in rabbits.* Laboratory animals, 2007. **41**(4): p. 411-419.

103. Washington, I.M. and G. Van Hoosier, *Clinical biochemistry and hematology*, in *The laboratory rabbit, guinea pig, hamster, and other rodents*. 2012, Elsevier. p. 57-116.